DOE/PC/79853--T1

DE90 013757

A NOVEL LIQUID MEMBRANE TECHNIQUE FOR REMOVAL OF SO_2/NO_X FROM FLUE GAS

FINAL REPORT

DOE Project no.: DE-AC22-87PC79853

Contract Period: 4/15/87 - 2/28/90

Prepared by:

Stevens Institute of Technology
Department of Chemistry and Chemical Engineering
Center for Membranes and Separation Technologies
Castle Point, Hoboken, NJ 07030

for

Department of Energy
Pittsburgh Energy Technology Center
Project Manager: S. S. Kim

Contributors: K. K. Sirkar
A. Sengupta
S. Majumdar
B. Raghuraman
J. S. Cha
S. Karoor
T. H. Papadopoulos
S. Khare
Y. T. Lee

Contents

List of Tables

List of Figures

EXECUTIVE SUMMARY

Membrane gas separation is appealing due to several reasons e.g., high energy efficiency, simplicity, modular nature and lower capital and operating cost. A membrane-based regenerable flue gas clean up process has the potential of becoming a highly efficient alternative to conventional scrubbing and throwaway processes. Polymeric membranes in such an application suffer from low values of permeabilities and selectivities between SO_2/CO_2 and SO_2/N_2. Although liquid membranes are highly attractive due to very high selectivities and permeabilities, they have not been industrially adopted yet due to the problems of membrane instability, flooding, low operating life and poor operational flexibility. A hollow-fiber-contained liquid membrane (HFCLM) process, proposed recently, appears to be able to overcome all of the above shortcomings present in the traditional immobilized liquid membrane (ILM) techniques.

The HFCLM technique uses two sets of hydrophobic, microporous hollow fibers, packed tightly in a shell. The remaining void space in the shell is filled with an aqueous liquid to be utilized as a membrane. The feed gas mixture is separated by selective permeation of a species through the liquid from one fiber set to the other. Vacuum may be pulled or a sweep fluid may be introduced in the second set of fibers to maintain the driving force for permeation of SO_2/NO.

The objectives of this project are as follows:

1. To measure the permeability coefficients of different gas components present in a flue gas mixture (e.g., SO_2, CO_2, NO, O_2 and N_2) through

several liquid membranes utilizing ILM technique.

2. To select and identify attractive liquid membranes from the above.
3. To study the extent of flue gas purification with selected liquid membranes in a HFCLM permeator.
4. To determine the stability and reliability of the HFCLM under sweep and vacuum modes of operation.

A feed gas mixture having a composition of 5000 ppm SO_2, 12% CO_2, 1.8% O_2 and balance N_2 was used primarily for permeability studies through ILMs. Excellent SO_2 permeabilities and selectivities for SO_2/CO_2 (70-200) and SO_2/N_2 (1500-3000) were obtained at 25°C when water, aqueous solutions of 1N $NaHSO_3$ and 1N Na_2SO_3 were used as membranes. The permeability values for SO_2 and selectivities between SO_2/CO_2 were slightly lower (50-200) for aqueous 0.02M Fe^{2+}EDTA or 0.02M Fe^{3+}EDTA liquid membranes. A high selectivity between NO and N_2 was obtained when a feed gas containing 450 ppm NO and balance N_2 was tested with an aqueous membrane of 0.01M Fe^{2+}EDTA solution. The selectivity of 0.01M Fe^{3+}EDTA solution was significantly lower.

The better liquid membranes identified through ILM studies were then utilized in HFCLM permeators for purification of a simulated flue gas mixture. Permeators having different effective lengths (43.2 to 157.5 cm) and different fiber dimensions (100 μm and 240 μm ID) were tested, mostly at around 25°C and a few at 70°C. The total number of fibers in these permeators varied from 180 to 600 and the active membrane surface area to equipment volume ratio varied between 2420 to 4850 m^2/m^3. Depending on the feed gas flow rate, 60 to 95%+ SO_2 was removed under vacuum or sweep gas modes of operation from a simulated flue gas mixture containing 5000 ppm SO_2. The liquid membranes tested include

pure water and 1N $NaHSO_3$ solution. The permeate in vacuum mode was highly enriched in SO_2.

Utilizing aqueous solutions of either Fe^{2+}EDTA or Fe^{3+}EDTA as liquid membranes, about 50-85% of NO was removed from 250-500 ppm NO containing feed gas. For a feed gas mixture containing both SO_2 and NO, 70-90% of the feed SO_2 and 50-75% of the feed NO were removed simultaneously in a small permeator (length: 43.2 cm) having 0.01M Fe^{2+}EDTA solution as a liquid membrane. At 70°C, the same experiment showed only slightly reduced performance. For simulated flue gas mixture containing O_2, the performance of Fe^{2+}EDTA membrane progressively decreased with increasing time. However, no such deterioration was observed when Fe^{3+}EDTA membrane was used under identical conditions. For permeators with larger diameter fibers, the axial gas flow pressure drop remained within the acceptable limit. The highest SO_2 flux observed in some experiments was around 1.1×10^{-4} $cm^3/sec\text{-}cm^2\text{-}cm$ Hg.

Theoretical models have been developed for both ILM permeability measurements and HFCLM permeator operations. Facilitated transport of SO_2 through pure water ILM and SO_2 selectivity over CO_2 can be described adequately by equilibrium approximation model as well as by nonequilibrium boundary layer approximation model. Additional efforts are needed to develop a better model for EDTA facilitated transport of NO. For HFCLM operation, model calculations suggest that gas phase boundary layer resistances are insignificant for SO_2 permeation through pure water membrane.

Section 1

Introduction

1.1 Significance of the problem

Stack or flue gases released from coal fired electric utility steam generating units contain significant amounts of SO_2 and NO_X pollutants. Unless these pollutants are removed substantially, they will pose a serious threat to our environment. A typical untreated flue gas produced by coal burning consists of 0.1-0.5% SO_2, 10-15% CO_2, 1-5% O_2, 70-75% N_2, 10-15% H_2O and 0.01-0.05% NO. Reduction of such emissions of SO_2 and NO to achieve mandated environmental standards (New Stationary Sources Performance Standards of 1979) is a DOE mission.

In a conventional flue gas treatment process, the separation of SO_2 is achieved by contacting the flue gas mixture with an aqueous alkaline solution or limestone slurry (Walker et al., 1985; Drummond and Gyorke, 1986). The spent liquor is most often discarded. However, these scrubbing solutions are not very effective in removing NO due to its very low solubility in alkaline solutions or limestone slurry. Further, the processes are expensive.

Therefore, there is a search for advanced separation technologies that do not impose undue economic burden on coal-burning utilities. The present project is directed toward accomplishing such a goal. The work described in this report focuses on a new hollow-fiber-contained liquid membrane process (Majumdar et al., 1988; 1989) for flue gas separation. In this one-step

process, the pollutants can be withdrawn through the liquid membrane as a concentrated permeate stream while the feed gas is purified. If successful, the process could become a highly efficient alternative to scrubbing and throwaway processes. The volumetric efficiency of membrane processes based on hollow-fiber devices is well known. Much smaller cleanup devices are possible. Scrubbing liquor regeneration problem is essentially eliminated. The SO_2 enriched permeate may be processed by a variety of processes to liquefied SO_2, elemental sulfur or sulfuric acid. A throwaway $CaSO_4$ based product may be replaced by a heavy chemical needed as a raw material in the chemical industry. Further, retrofitting of existing utilities is easily possible using such modular membrane devices.

1.2 Project objectives and overall approach

The objective of this project is to (i) measure the permeability coefficients of SO_2, CO_2, NO, O_2 and N_2 through a variety of immobilized liquid membranes using simulated flue gas mixtures, (ii) select the promising liquid membranes, (iii) study the extent of flue gas purification achieved in a novel microporous hollow-fiber-contained liquid membrane (HFCLM) permeator using selected membrane liquids, and (iv) determine the stability and reliability of this novel permeator for different operational modes.

These objectives are to be achieved by pursuing the following tasks identified in the STATEMENT OF WORK:

TASK I PROJECT WORK PLAN

TASK II MODIFICATION OF PERMEABILITY APPARATUS FOR SO_2/NO

TASK III PREPARATION OF EXCHANGED ILM (IMMOBILIZED LIQUID MEMBRANE) IN

	CELGARD 2400 AND SCREENING OF VARIOUS LIQUID MEMBRANES FOR SO_2 SEPARATION
TASK IV	DETAILED MEASUREMENT OF SO_2, CO_2, AND N_2 PERMEABILITY COEFFICIENTS THROUGH SELECTED LIQUID MEMBRANES
TASK V	PREPARATION OF EXCHANGED ILM-S IN CELGARD 2400 AND SCREENING OF VARIOUS LIQUID MEMBRANES FOR NO SEPARATION
TASK VI	DETAILED MEASUREMENT OF NO, N_2, AND CO_2 PERMEABILITY COEFFICIENTS THROUGH SELECTED LIQUID MEMBRANES
TASK VII	MEASUREMENT OF PERMEABILITIES OF SO_2, NO, CO_2, AND N_2 THROUGH AN OPTIMUM LIQUID MEMBRANE
TASK VIII	PURIFICATION STUDIES FOR SO_2/CO_2 SEPARATION IN A HFCLM PERMEATOR
TASK IX	PURIFICATION STUDIES FOR NO SEPARATION IN A HFCLM PERMEATOR
TASK X	PURIFICATION STUDIES FOR SO_2/NO SEPARATION IN A HFCLM PERMEATOR

The simulated flue gas mixture to be used for the project should have a composition of around CO_2 12%, N_2 74%, O_2 1.8%, H_2O 12%, NO 0.045% and SO_2 0.5%. The ultimate target for purification is simultaneous 90% reduction of SO_2 and NO. A SO_2/CO_2 selectivity in the range of 50-200 is desirable along with high SO_2 and NO flux. Measurements are to be made primarily at 25°C with one measurement at 70°C for the selected liquid membranes.

The ultimate goal of this work would be to have a hollow-fiber-contained liquid membrane (HFCLM) permeator purify flue gas containing SO_2/NO to the extent of about 90% using liquid membranes with a high selectivity of SO_2/NO over CO_2, N_2 and O_2 and having high flux levels for the preferentially permeating species.

Section 2

Background

2.1 Membrane gas separation

Various efforts are currently under way to develop regenerable flue gas cleanup (FGC) processes using advanced separation technologies. Membrane gas separation is one of them. It is an appealing process for a number of reasons including higher energy efficiency, simplicity of operation, modular nature, and lower capital and operating cost (Sengupta and Sirkar, 1986). The membranes used as the semipermeable barrier can be solid or liquid. Solid membranes (polymeric or inorganic, generally nonporous) usually have rather low selectivity between SO_2 and CO_2 and between SO_2 and N_2, and also low permeabilities, to be economically feasible at this point in time. Liquid membranes on the other hand can exhibit excellent selectivities and permeabilities. Traditionally, the liquid is immobilized in the pores of a microporous film spontaneously wetted by the liquid. The liquid is held in the pores by capillary forces. Such a membrane is known as the immobilized liquid membrane (ILM) (Ward and Robb, 1967). However, conventional immobilized liquid membranes suffer from one or more of the following problems: instability, low operating life, flooding, limited pressure capabilities, and low surface area per equipment volume.

2.2 Hollow-fiber-contained liquid membrane for gas separation

We- have recently proposed a new liquid membrane structure which appears

to be able to overcome most of the shortcomings of the conventional ILMs. It is called the hollow-fiber-contained liquid membrane, or HFCLM (Majumdar, 1986; Majumdar et al., 1988). This liquid membrane has been used quite successfully for separating gas mixtures of CO_2-N_2 and CO_2-CH_4 (Majumdar et al., 1988; Guha, 1989). It is logical to explore the efficacy of this gas separating liquid membrane structure in FGC. Not only can a membrane-based FGC be an efficient SO_2 removal technique (along with all the advantages of a membrane process), but it can also produce a SO_2-rich product which can be used separately to produce byproducts like liquefied SO_2, elemental sulfur or sulfuric acid.

The new technique, illustrated in Figure 2.2-1, uses two sets of hydrophobic, microporous hollow fine fibers, packed tightly in a permeator shell. The inter-fiber space is filled with an aqueous liquid acting as the membrane. The first fiber set (marked 'F') carries the feed gas in their lumen while the second fiber set (marked 'S') carries a sweep stream, gas or liquid, or simply the permeated gas stream. The feed gas mixture comes in contact with the membrane liquid, through the pores of the feed fibers, at the fiber outside surface. Various solute species dissolve at this feed gas - membrane liquid interface, diffuse through the liquid membrane at their respective rates to arrive at the pores of the nearest sweep fiber where they desorb.

The aqueous membrane liquid is introduced to the permeator shell through an opening from a membrane liquid reservoir at a pressure slightly higher than the feed gas and sweep (or permeate) gas pressures. For a pure liquid membrane, the system can be operated without proper humidification of the gas streams. The liquid lost by evaporation is automatically replenished by a

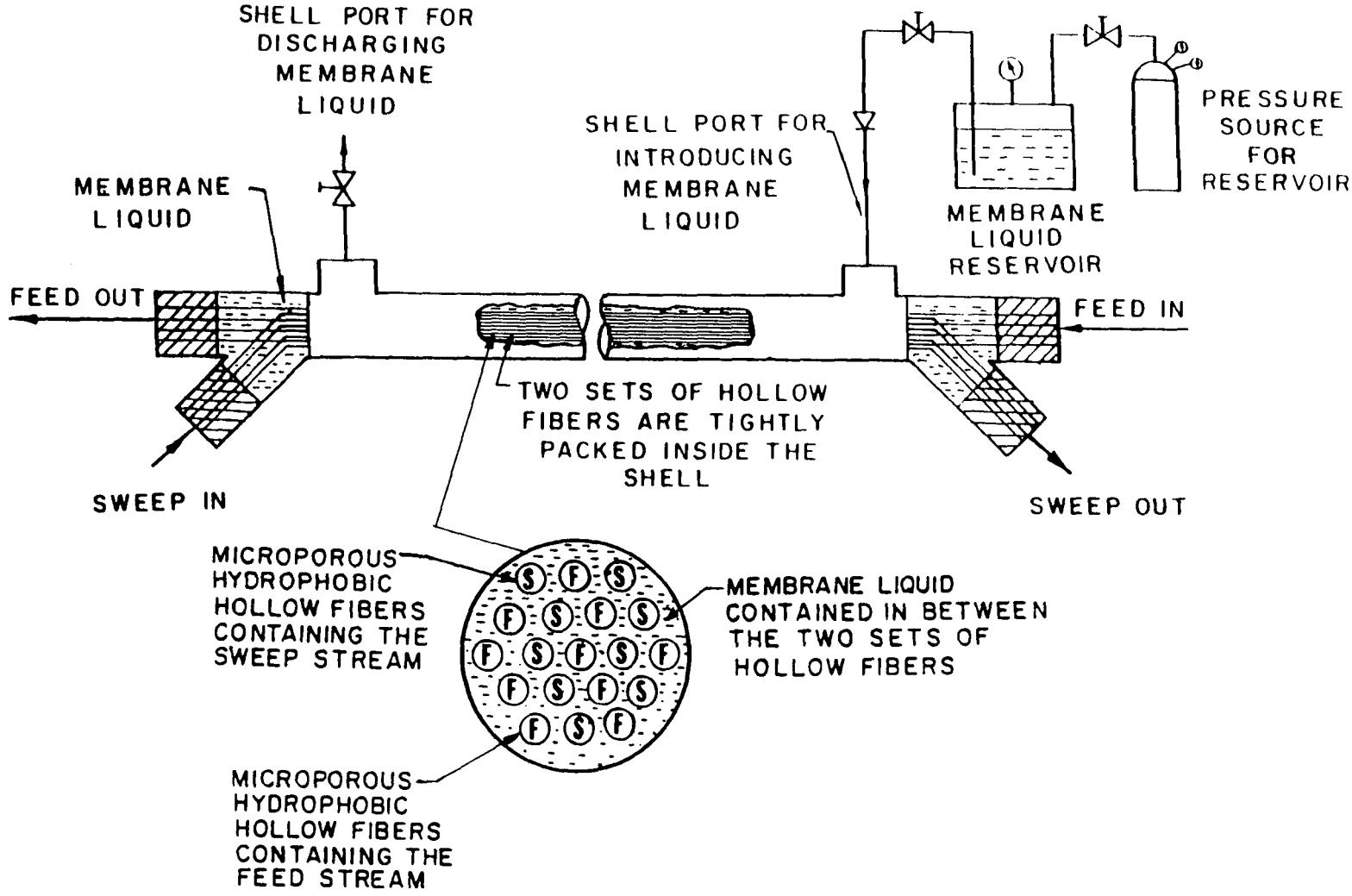

Figure 2.2-1: Configuration of the Hollow-Fiber-Contained Liquid Membrane

continuous supply of the membrane liquid from the reservoir due to its higher pressure. Should the membrane liquid get poisoned or deactivated, it could be automatically replaced by opening the shell port for discharging membrane liquid. These are unique features of this technique.

Some of the advantages of this process are: i) humidification of the gas streams is not necessary for a pure liquid membrane; ii) unlike other membrane processes, defects in the fiber wall do not lead to physical mixing of the feed and the permeate gas; iii) membrane is stable and replacement of membrane liquid is easy; iv) membrane flooding problem is eliminated due to the hydrophobic nature of the fibers; v) high pressure capabilities; and vi) high surface area per equipment volume.

Walker et al. (1985) had made an economic evaluation of membrane gas separation process for SO_2 removal under a variety of conditions. Their calculations suggested that operation of a permeator with a condensable vapor as a sweep gas on the permeate side was quite economical. They had found that operating the permeate side under vacuum was economically only slightly inferior to the sweep mode of operation. In this project, therefore, the two modes of operation adopted were sweep mode and the vacuum mode. For simplicity, helium was chosen as the sweep gas instead of a condensable vapor.

Section 3

Experimental Methods

3.1 Preparation of immobilized liquid membranes

The immobilized liquid membrane (ILM) used for permeability measurement is represented in Figure 3.1-1. The liquids were impregnated in thin microporous polypropylene (Celgard 2400, Hoechst Celanese, Charlotte, NC) films, cut in circular pieces about 2.5 cm in diameter. The properties of this support are listed in Table 3.1-1. These films are hydrophobic as received, and are not wet by water or most aqueous solutions. A solvent exchange technique similar to that used in Bhave and Sirkar (1986) was used to create the ILMs. The films were first wet by a 40 vol% solution of ethanol in water. They were then transferred to a large volume of distilled water, and kept there under stirred conditions for at least 48 hours, so that ethanol was extracted out from inside the pores of the film. The water was replaced usually at least twice during this time. The resulting films were the water ILM-s. To create salt solution ILM-s, a similar exchange process was carried out to replace the pure water in the film pores by the corresponding salt solution.

The Celgard 2400 microporous films used to immobilize the liquid membranes occasionally varied in quality. This became evident from the appearance of the wet films in terms of texture and transparency. This sometimes affected the quality of the experimental data. A visual screening was therefore essential before the film was used in the test cell.

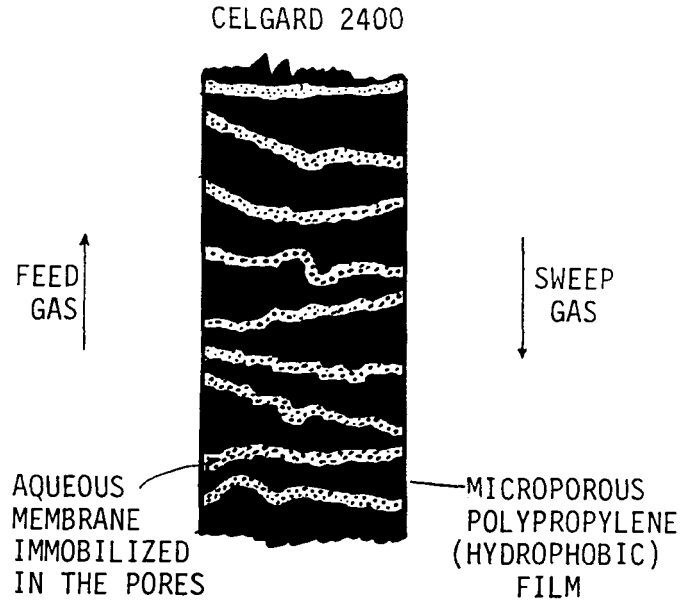

Figure 3.1-1: Supported Liquid Membrane for Permeability Measurement

Table 3.1-1 : Substrate Properties

Substrate : Microporous hydrophobic polypropylene film, Celgard 2400
Substrate film thickness : 25.4×10^{-4} cm.
Substrate porosity : 0.38
Average pore size : 0.02 microns
Estimated tortuosity factor : 7.0 *

* based on pure gas permeation measurement; under condition of atmospheric pressure and with no backing.

3.2 Test cell for permeability measurement

One of the test cells used to measure the permeability of any species through the immobilized liquid membrane film is shown in Figure 3.2-1. Just prior to mounting the film, each film was placed on a hard flat surface, and a clean glass rod was used to roll out all the extraneous water from the film surface. In the test cell, both feed and sweep gases were maintained at atmospheric pressure. No backing of any kind was used on either side of the film. Since both sides of the film were at essentially atmospheric pressure, use of backing was not necessary. For SO_2 permeability measurements, the smaller test cell was used (inner O-ring ID: 1.27 cm, active permeation area: 1.27 cm^2). For NO permeability measurements, a larger cell was used (inner O-ring ID: 3.81 cm, active permeation area: 11.4 cm^2).

3.3 Experimental procedure for permeability measurement

The SO_2 permeation experiments at 25°C were carried out in an apparatus whose general schematic is shown in Figure 3.3-1. The feed and the sweep gases flowed countercurrent through the cell at known flow rates. The flow rates were monitored and controlled by electronic mass flow transducers and flow control valves (models 8100 and 8200, Matheson Gas Products, East Rutherford, NJ). The pressures on the two sides of the film were atmospheric, and monitored by Matheson test gauges. Proper humidification of the feed and the sweep gases entering the cell were very important to prevent the film from drying up. The humidification of the feed stream was carried out using either two stainless steel humidifiers or a hollow fiber humidifier module having a

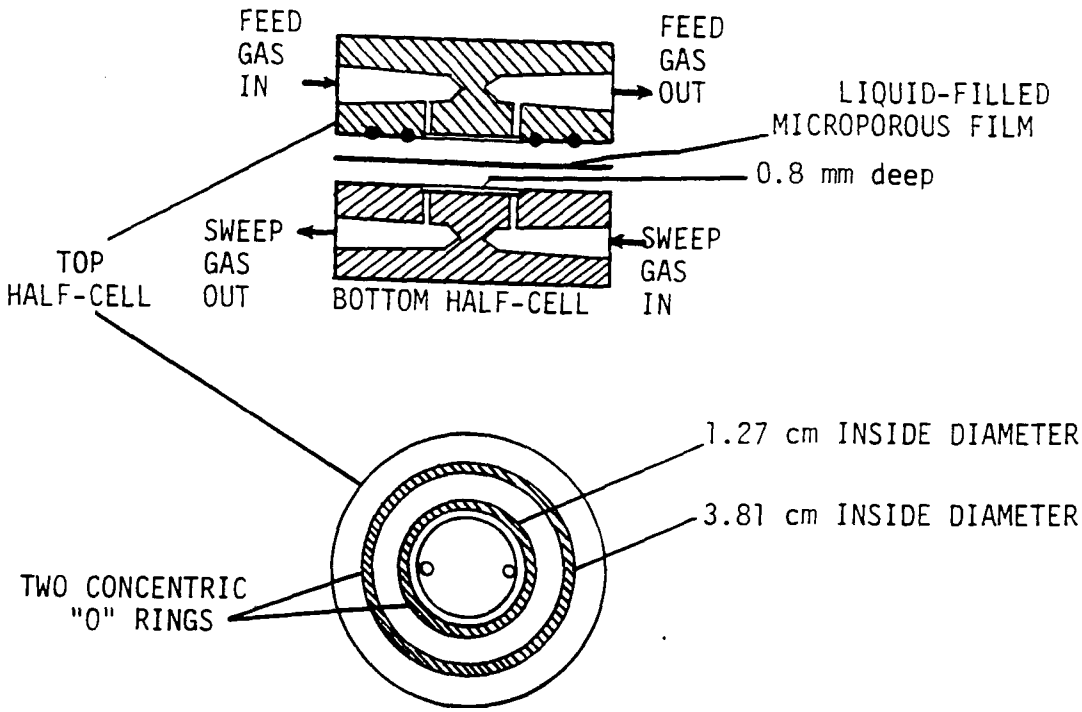

Figure 3.2-1: Test Cell Construction

BPR : BACK PRESSURE REGULATOR; CV : CHECK VALVE; FC : FLOW CONTROLLER
FM : FLOW METER; GC : GAS CHROMATOGRAPH; GH : GAS HUMIDIFIER
HP : HUMIDITY PROBE; OLF : ON LINE FILTER; PG : PRESSURE GAUGE; SV : SHUT-OFF VALVE

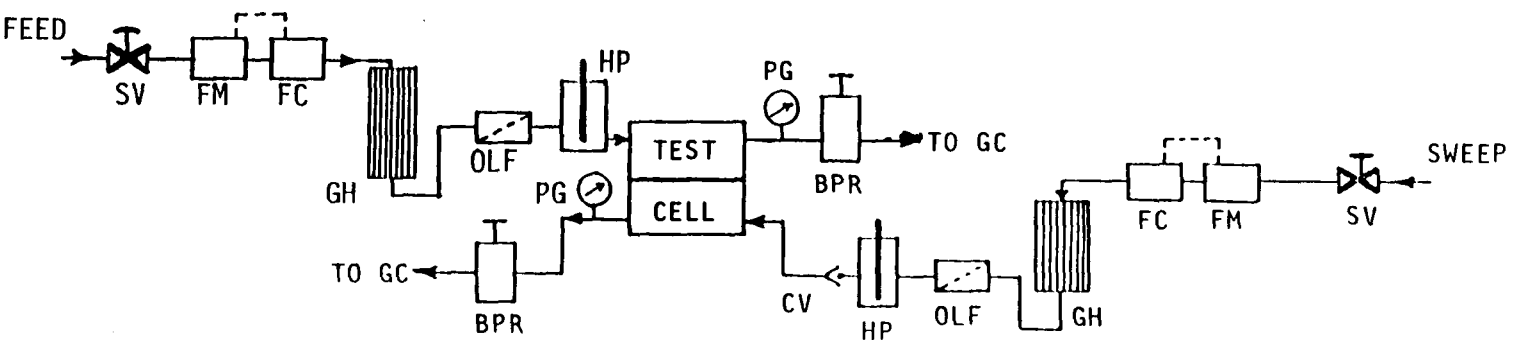

Figure 3.3-1: Permeability Measurement Setup

gas-water contact area of 2500 cm^2 (shown schematically in Figure 3.3-2). The sweep stream was always humidified by bubbling helium through a series of two bubblers, holding about 450 ml water in each.

Prior to making any SO_2 permeation measurement, quite a few experiments were carried out to determine the tortuosity factor of the substrate Celgard 2400. In these experiments the permeation rate of an inert gas such as N_2 or CO_2 through an ILM containing water was measured. The permeability of these gases through water are already known. One can therefore estimate the tortuosity factor from the experimental permeation rate. The experiments were mainly carried out at a feed pressure of 1 atm. For one experiment feed N_2 pressure was maintained at 10 psig.

For SO_2 permeability studies, a primary standard gas mixture was used for the feed. The composition was 5000 ppm SO_2, 12% CO_2, 1.8% O_2 and balance N_2. Three different feed gas concentrations were used. The purpose in changing the feed gas concentration was to study the effect, if any, of concentration on the species permeabilities. This was particularly important for SO_2 which undergoes chemical reactions in water, and aqueous salt solutions. Because of reaction, its rate of permeation is facilitated (Roberts and Friedlander, 1980a; 1980b). The degree of facilitation depends on the nonlinear reaction equilibrium, and hence on the feed and sweep side gas phase concentrations of SO_2.

In the first concentration level, the above primary standard gas mixture itself was used as the feed. The other two concentration levels were prepared by blending the above primary standard gas mixture with pure helium, in (i)

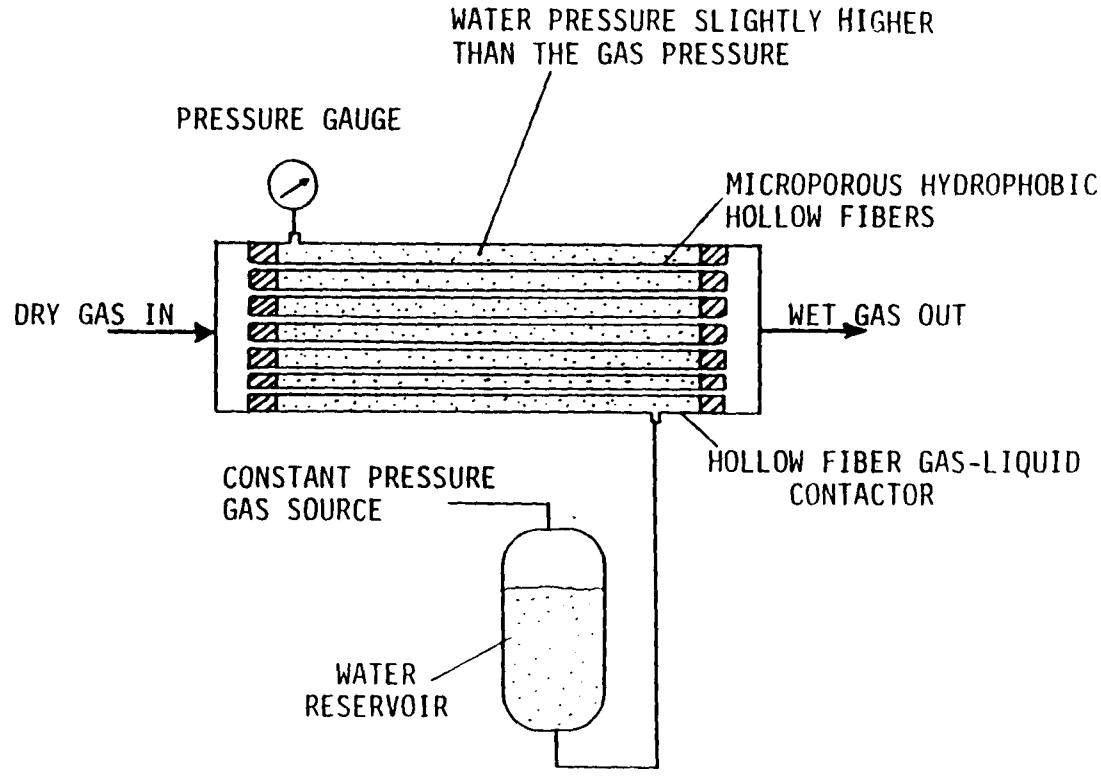

Figure 3.3-2: Hollow Fiber Humidifier

1:1 volume ratio, and (ii) in 1:9 volume ratio. Thus the nominal SO_2 concentrations in levels 2 and 3 were 2500 ppm, and 500 ppm, respectively. However, the relative concentrations of the active permeants remained same in all three levels. This was thought to be the proper basis to change the feed concentration levels.

Upon humidification, the feed gas naturally picked up moisture, which suppressed the concentration of each species to some extent. Based on water vapor pressure data, the moisture concentration in the humidified gas stream should typically be 3-4 vol%. Also, the SO_2 concentration in the humid feed gas was found to be dependent somewhat on the room temperature, gas flow rate, etc. since SO_2 is highly soluble in water and its solubility is a function of temperature. Thus it was essential to monitor the actual feed gas composition entering the test cell. The gas stream composition in the feed bypass line was routinely measured, under steady flow conditions, before and after each experiment. This would give the true feed inlet composition that would be used in calculating permeabilities. In a single data set, the actual composition varied around the nominal value from day to day. The maximum extent of variation around the nominal value was around 10-15%.

The compositions of the feed inlet, the feed outlet, and the sweep outlet streams were measured by a Hewlett-Packard 5890A Gas Chromatograph using a thermal conductivity detector. This analysis was crucial and demanding. The samples, which contained SO_2, CO_2, O_2, N_2, moisture and sometimes helium, were extremely corrosive in nature. It was essential to completely separate all of the first five of the above components in the GC, and quantitatively measure the first four components. A two-column system was

used in the GC along with a column sequence reversal technique.

The sampling and column reversal were accomplished by a two-valve valve system containing a four-port two-stream selection valve, and a ten-port gas sampling valve, as shown in Figure 3.3-3. Two packed GC columns were used : a 6′ x 1/8" Chromosorb 108, 80/100 mesh (Chrompack Inc., Bridgewater, NJ) as column 1, and a 10′ x 1/8" Molecular Sieve 13X, 80/100 mesh (Alltech Associates, Deerfield, Il) as column 2. The column sequence was reversed at 1.9 mins after the sample injection. The main purpose in this method is to have O_2 and N_2 separated by the molecular sieve column, without allowing CO_2, SO_2 and moisture to enter the molecular sieve column, since its performance is adversely affected by these species. With this arrangement and a sweep helium gas flow rate of 42.4 cc/min, the retention time for different gas species were obtained as follows: CO_2 - 4 mins, O_2 - 5.4 mins, N_2 - 6.3 mins, SO_2 - 10.7 mins and moisture - 12 mins. The valve system in the GC had to be kept at high temperature (> 125°C) to prevent moisture condensation. The gas lines out of the test cell were also heated with heating tapes to prevent any line condensation.

The experimental setup for the nitric oxide (NO) permeability measurement at 25°C is shown schematically in Figure 3.3-4. The gas stream composition for components other than NO were measured in the gas chromatograph. The NO composition in the sweep outlet was measured in an on-line NO-analyzer (Interscan Corp., Chatsworth, CA, model LD-54), which employs an electrochemical voltametric sensor, with a direct ppm NO readout. The NO concentration in the feed outlet was determined by a MSA nitric oxide analyzer (Mine Safety Appliances, Pittsburgh, PA, model LIRA 202).

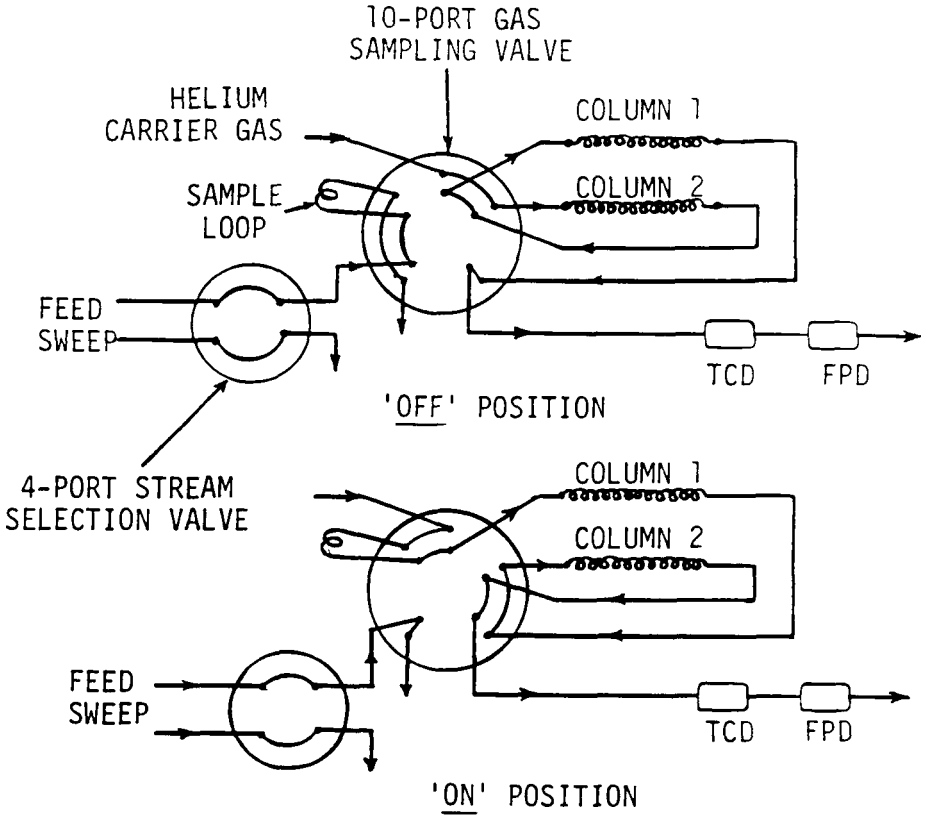

Figure 3.3-3: GC Sampling Method

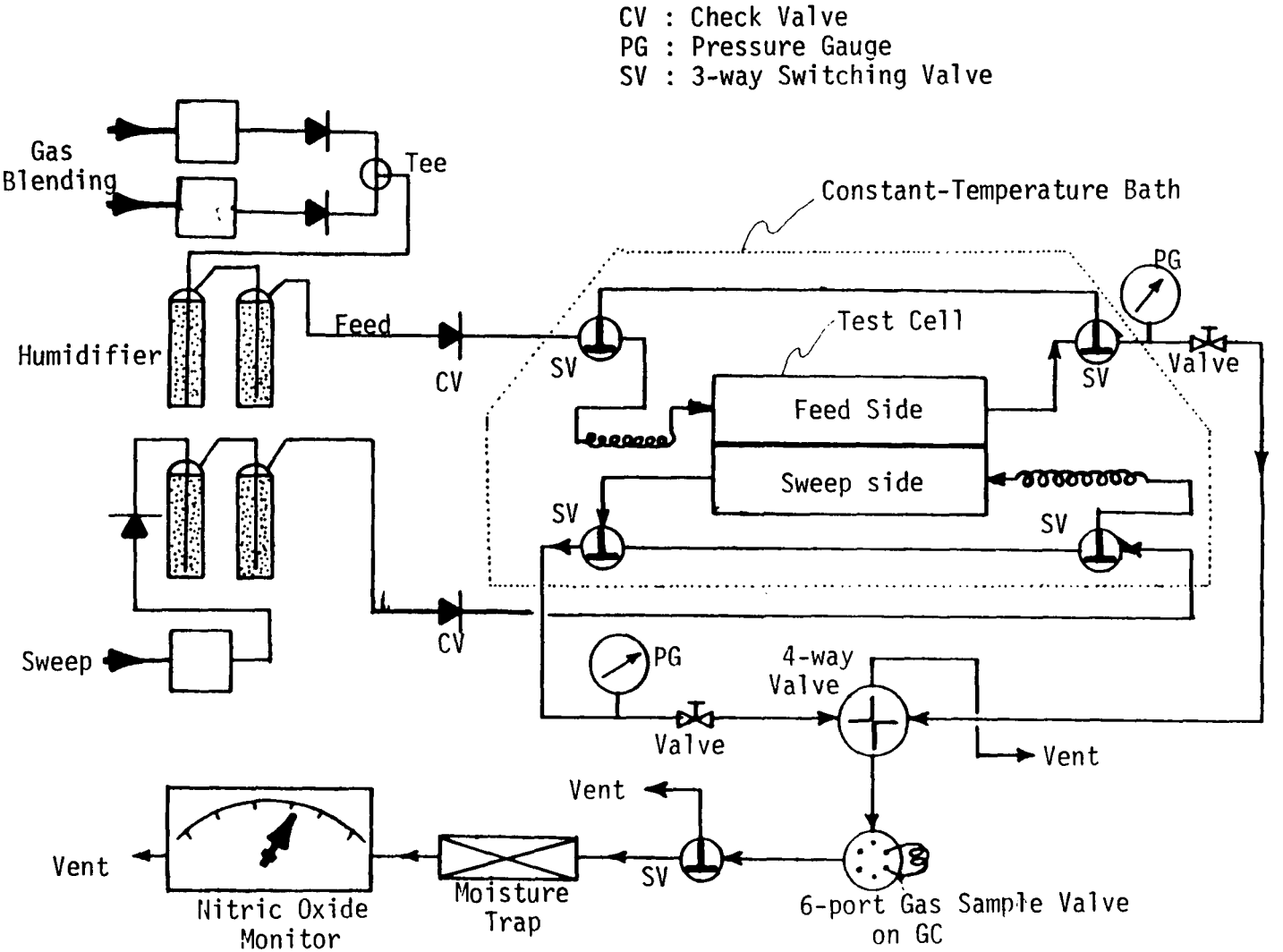

Figure 3.3-4: Schematic of Nitric Oxide Permeability Measurement Setup

The concentration of NO in the feed gas for permeability measurement was generally less than 500 ppm. For this low concentration, the rate of transfer across the immobilized liquid membrane was expected to be very low. Therefore, we had to use very low sweep gas flow rate in the test cell in order to achieve comparatively high and measurable NO concentration in the sweep outlet. Besides, we used the larger test cell (with an active area of 11.4 cm^2) as opposed to the small test cell (area 1.27 cm^2) which was used for the highly permeable SO_2.

3.4 High temperature permeability measurement experiments

For higher temperature ILM permeability experiments (at around 75^oC), a continuously smooth control of feed and sweep stream temperatures was more difficult than what we had initially anticipated. For each gas line we tried to use initially a relay type temperature controller in conjunction with a temperature probe, and a heating tape, which was wrapped around the gas flow tubes and supplied the necessary heat. In the absence of water in the system, the temperature control was excellent, but raising the gas stream temperature and maintaining complete humidification at the same time proved difficult. The problem was that one could not heat the gas streams after humidification since that made the gas stream unsaturated, and the liquid membrane tended to run dry. On the other hand, if the heating was done before and during saturation, unless proper post-humidification heating and/or insulation was maintained, significant amount of moisture tended to condense in the flow lines, preventing proper experimentation.

Finally, after several trials, the following arrangement was found to be successful in raising the temperature and humidity simultaneously to the desired level. The whole setup was put in the constant temperature bath. Two teflon coated 316 stainless steel humidifiers for the feed and the sweep gas lines were placed in the constant temperature bath adjacent to the permeability cell. A sparging arrangement was installed in those vessels whereby the incoming gas stream was broken into small size bubbles. This arrangement improved and ensured that the gas streams entering the cell were properly humidified at the operating temperature. Many of the 304 stainless steel 1/8 inch tubes used to connect the cell and the humidifiers and other section of the apparatus were replaced by the tubes made of Impolene, a plastic material (Imperial Eastman, Chicago, IL), in order to reduce the chance of any chemical attack in the tubes by the corrosive gas mixture containing SO_2, NO_x and moisture at high temperatures. Tubes made of 304 stainless steel were found to be unsuitable for long term use in the corrosive environment.

Both gas streams need to be dried before they enter the GC or analyzers. Previously, packed drierite-based columns were used for this purpose. They were changed to miniature tubular membrane dryers (Perma Pure Products, Farmingdale, NJ, model MD-125-12P or MD-125-12S) to selectively remove moisture from gas streams. These dryers employ tubular ion exchange membranes, which are highly and selectively permeable to water vapor, in a shell and tube type arrangement. The wet gas passes through the inside of the tube, while a dry purge gas like N_2 passes countercurrently through the shell side, and removes the moisture form the feed gas.

The experimental setup for nitric oxide permeability measurement through

ILMs at higher temperatures is shown in Figure 3.4-1. The same apparatus with the exception of the nitric oxide monitor was also utilized for SO_2 permeability measurement at higher temperatures. The smaller diameter test cell was, however, used for SO_2.

It should be mentioned here that we faced a tremendous corrosion problem whenever moist SO_2 was present. After being used over a long period for the humidification of SO_2-containing gases, especially at elevated temperatures, the water inside the humidifier was found to have turned dark, and the 304-SS stainless steel tube insert and the humidifier vessel were coated with a black deposit. This phenomenon also caused large fluctuations in the SO_2 composition in the humidified gas stream. Corrosion resistant materials which were later introduced reduced the problem significantly but could not eliminate it entirely. We had also encountered corrosion in the test cell, GC sampling valve, membrane humidifier etc. It was anticipated that slow and irreversible chemical reactions were taking place in humidifiers and test cell etc. during the permeation experiments.

Therefore, during the permeability measurement of SO_2 (especially at high temperatures), the composition of the feed gas mixture containing SO_2 was measured frequently after the gas stream exited the humidifiers. The results showed that the SO_2 composition decreased progressively with increasing time. A steady value of SO_2 composition was never realized. Therefore, to analyze the experimental data under such conditions, one has to consider a pair of feed and sweep compositions at a given time.

3.5 Details of liquid membrane solutions used for ILM studies

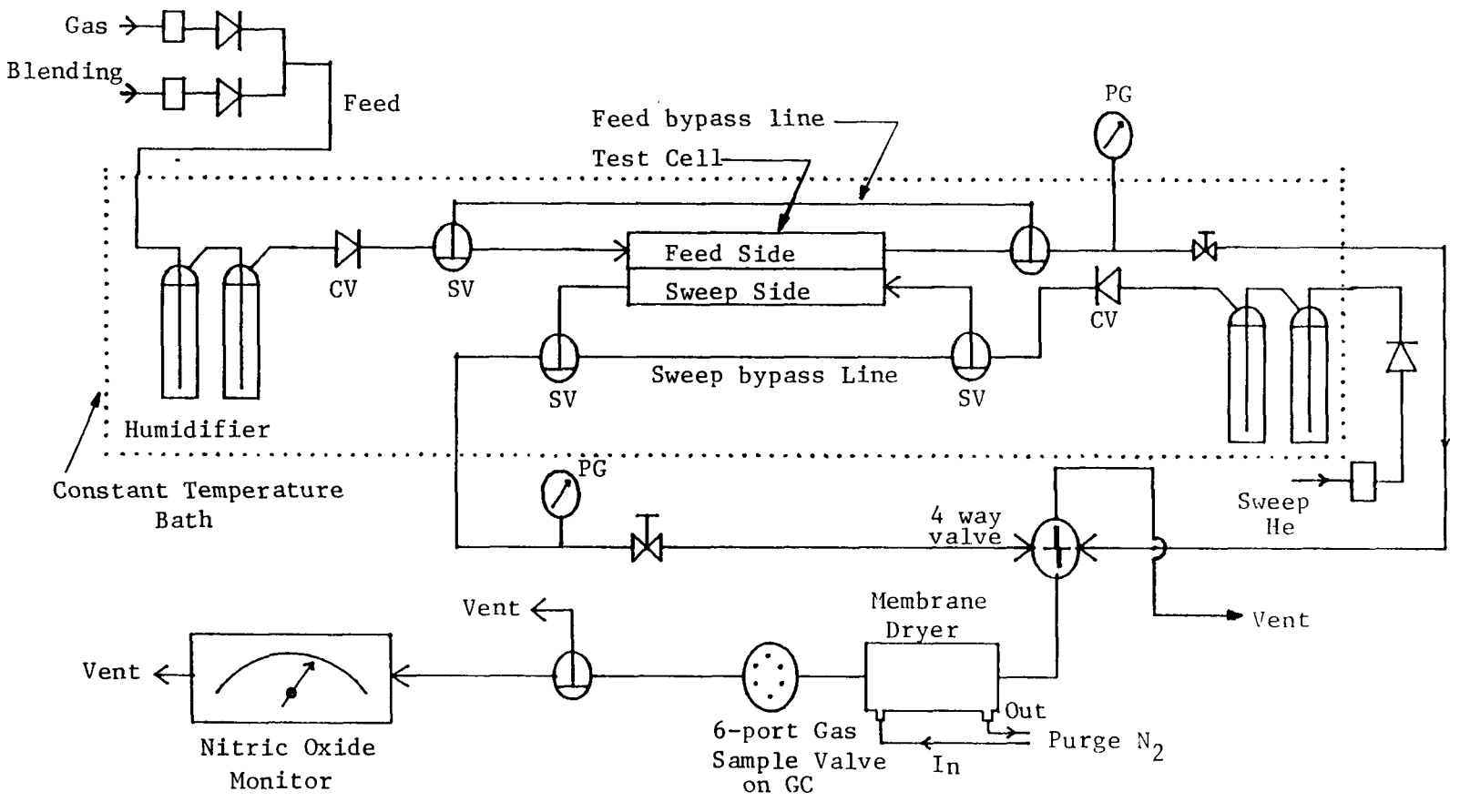

Figure 3.4-1: Schematic of Nitric Oxide Permeability Measurement Setup at High Temperature

The liquid membranes used were prepared from the following chemicals: Sodium bisulfite (99-100% as anhydrous Sodium metabisulfite), Ethylenediaminetetraacetic acid (EDTA) disodium salt dihydrate, 99%, and Sulfolane (tetramethylene sulfone), from Sigma Chemical Co.; Sodium sulfite anhydrous 98+ % and Sulfolene (butadiene sulfone) 98%, from Aldrich Chemical Co.; Ferrous sulfate 7-Hydrate 99.7% from J.T. Baker Chemical Co.; Ferric sulfate (+ Aq) analytical reagent, Mallinckrodt Chemical Works. The following solution compositions were used as membranes : 1N concentration for $NaHSO_3$ and Na_2SO_3, 7.5 and 15 wt/vol% sulfolene, 12 wt/vol% sulfolane, and 0.02M or 0.01M concentration for Fe^{2+}EDTA and Fe^{3+}EDTA. The reason for using low EDTA concentrations is its low solubility at room temperature.

Preparation of chemically stable EDTA complexes (Fe^{2+}EDTA and Fe^{3+}EDTA) posed many problems. The most difficult problem was precipitation from the solution. The method of preparation we used follows that of Sada et al. (1980; 1981). The chelate to metal ion molar ratio was 1:1. Different chelate solubility levels were tested. At 25°C, the chelate solubility is rather low. Besides, even if the metal-chelate solution was clear to start with, pH adjustment and concurrent stirring produced dark brown precipitates from the solution. Sometimes the precipitation occurred gradually with time. Note that, the solution pH of the chelates as prepared were usually less than 2.0. Concentrated NaOH solution was added to adjust the pH when needed.

The chemical stability and permeation data reproducibility of the EDTA complexes used for NO separation were extremely uneven. The permeation through the EDTA membranes were found to be very sensitive to (i) the solution

preparation method, and (ii) the age of the aqueous solution used as the liquid membrane. Besides, the solution seemed to denature with time, and white suspended solids were formed. This is most probably because of occasional exposure of the solution and the films to atmospheric oxygen.

In order to minimize the contact with atmospheric oxygen, the EDTA chelate solutions were therefore prepared in the following careful steps. Freshly prepared double-distilled water was filtered through a 0.5 micron membrane filter (Millipore Corporation, Bedford, MA) to remove any suspended solids. The water was thoroughly degassed under vacuum for about 5-7 mins in a 1000 ml volumetric flask. EDTA disodium dihydrate crystals were weighed into the flask first, followed by addition of $FeSO_4$, $7H_2O$ crystals. Subsequently, the flask was purged with helium, and the liquid was stirred with a teflon-coated magnetic stirrer for at least 12 hours.

The salts were weighed in such a way that the solution would be 0.02M in EDTA, and 0.01M in Fe^{2+}. Excess EDTA was added in order to minimize the oxidation of Fe^{2+} to Fe^{3+} by dissolved oxygen during subsequent use. Upon stirring, a small fraction of EDTA was found to have remained undissolved. We did not undertake an exact analysis of the amount of undissolved EDTA, since the chelate concentration can be assumed to be 0.01M, as $FeSO_4$ was found to dissolve completely.

After the stirring of solution was stopped, helium pressure was used to transfer the solution from the flask into small bottles. An online membrane filter (0.22 micron, Gelman Sciences, Ann Arbor, MI)) was used to remove any solid particle. The transfer was carried out wholly under helium atmosphere to

prevent any contact with air.

3.6 Fabrication of hollow-fiber-contained liquid membrane permeators

Seven HFCLM permeators were used for flue gas cleanup experiments. Of these, permeator modules A, B and G were specifically fabricated for this project. Modules C, D, E and F were available from another project. The detailed geometrical characteristics of each permeator used in this study are given in Section 5. The hollow-fiber surface area on the feed fiber side was equal to that of the permeate fiber side in all permeators.

The fabrication procedures of HFCLM permeators are described in detail in literature (Majumdar, 1986; Guha, 1989; NYSERDA Report 87-10). However, a brief account of the same is given here. Fabrication of a permeator involved preparation of a fiber bundle, inserting it in a shell and finally potting the different ends of each fiber set with a resin mixture to form a tube sheet.

A mat of fibers (type: X-10; OD: 150 or 290 micron; number: varied from module to module) was first prepared on a polyethylene sheet over a laboratory bench top taking out six fibers at a time from a bobbin containing the fibers. They were cut to the desired length using scissors and both ends of the fibers were attached to a strip of scotch tape. Thus fibers were placed close to one another. Once such a mat was ready, the mat ends were covered by two polyethylene sheets. The polyethylene sheets were kept in place by scotch tape outside the region of the mat. Two new pieces of scotch tape were placed on the polyethylene sheets to put another set of fibers having the same dimensions. These fibers were placed in between the fibers of the previous mat

to ensure close proximity between the two sets of fibers. Thus, two sets of fibers were well mixed in the middle section but were separated completely at the end by the upper polyethylene sheets.

The integrated mat was then rolled to prepare the fiber bundle. Distilled water was sprayed over the mat for easy handling of the fibers. Cotton threads (wetted) were tied loosely in the middle section as well as at the four separated ends to keep the fibers together. They were removed slowly as the fiber bundle was inserted into a specially constructed permeator shell. A 1/8-inch teflon pipe (I.D. 0.240 inch, O.D. 0.406 inch; Cole Parmer, Chicago, IL) was inserted into a 1/2-inch schedule 40 stainless steel pipe to make the shell. Epoxy resin was used to fill the annular space between the two concentric pipes. The pipe was fitted with either a 1/2-inch stainless steel Cross (Cajon) or a 1/2-inch stainless steel 45^{o} Y-fitting (NJ Engineering & Supply Co., Passaic, NJ) at each end.

Two openings of the Cross or Y-fitting were needed to separate the two sets of fibers. Y-fittings have a distinct advantage over cross connection (Majumdar, 1986) as they require less bending of fibers. To each of these ends, a 2-inch-long hexagonal nipple (Cajon) connection was attached. The shell was completely immersed in water when the fiber bundle was gently pulled through the shell assembly by using a cotton thread tied at one end of the bundle. Once the bundle was through at both the ends, two sets of fibers were separated and each set was then introduced through one of the hexagonal nipple connections. The assembly was air dried. The fibers were potted on each nipple either with a polyurethane resin mixture prepared with a 58:42 ratio of Polycin - 1670 to Vorite 1701 (Caschem Inc., Bayonne, NJ) or with a epoxy resin

(resin: C4; activator: D; ratio: 4:1; Beacon Chemical Co., Mt. Vernon, NY) mixture.

3.7 Experimental procedure for CLM studies

The apparatus used for CLM studies essentially consists of three different segments: feed gas line, permeate or sweep gas line and membrane liquid line. The setup used for NO separation is described schematically in Figure 3.7-1. The feed gas mixture of desired composition was generated by carefully controlled mixing of three different primary standard gas mixtures using three electronic mass flow transducer controllers, FC (Matheson model 8141). The gas flow rate readings of all the transducers were monitored centrally by a Matheson digital readout and control module (model 8249). The feed gas mixture was then sent to a humidifier (a 20 liter stainless steel vessel, Millipore Corporation, Bedford, MA; equipped with a small pressure gauge of range, 0 - 160 psig and a safety valve). The pressure of the feed gas was measured by a Matheson test gauge (range: 0-220 psig) before it entered the HFCLM module.

The purified feed gas stream from the permeator was then passed through a water (or liquid) separator. This device prevented carryover of the liquid droplets which appeared at the permeator tube sheet (from condensation or fiber leakage through the damaged fibers of the permeator, or both). The separator used a Celgard 2400 hydrophobic microporous film to separate the gas from the liquid.

The nature of the instrumentation in the sweep gas line was essentially

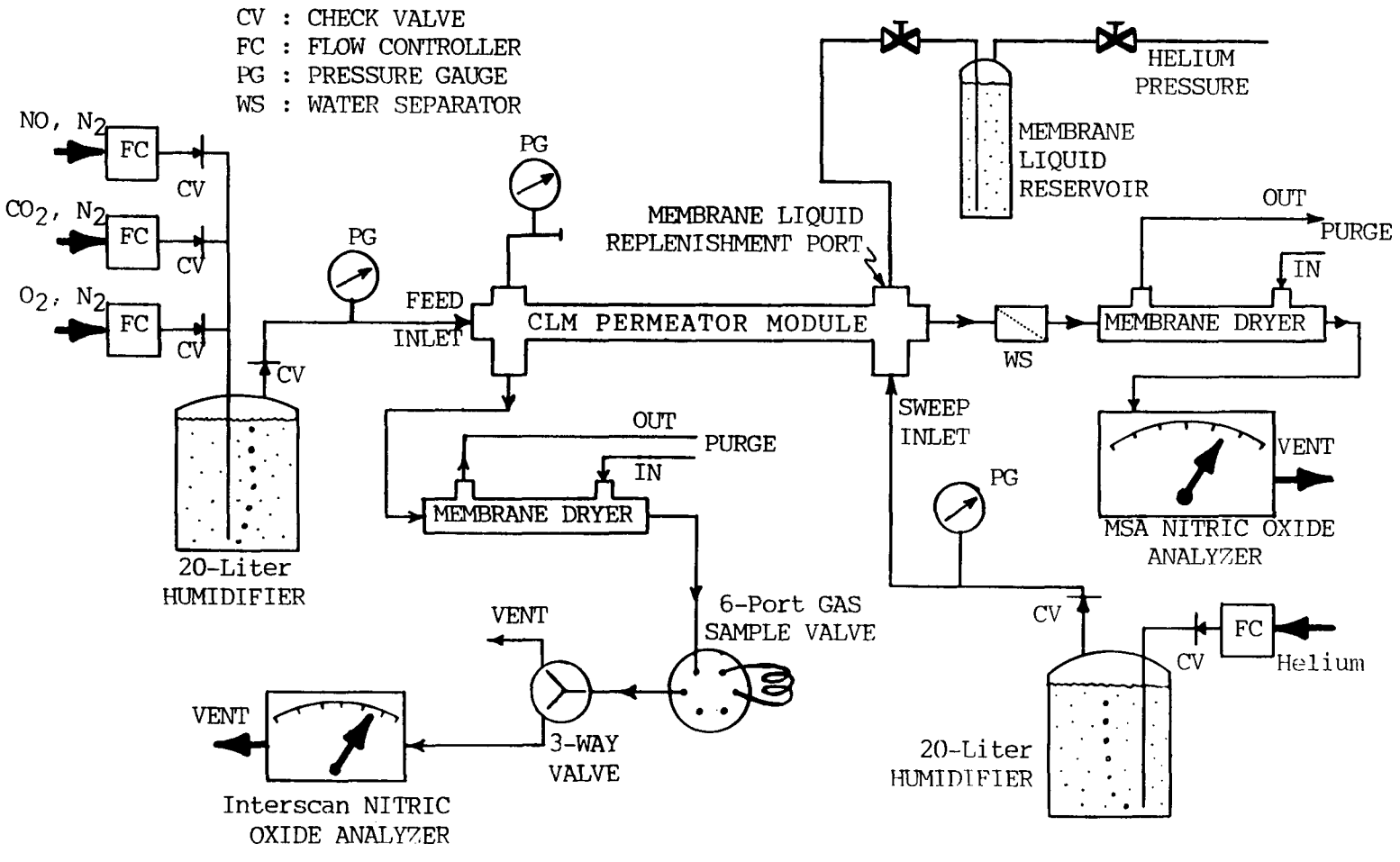

Figure 3.7-1: Experimental Setup for Nitric Oxide Separation Using Contained Liquid Membrane Permeators

identical to that in the feed gas line. Pure helium was used as a sweep gas. The permeator shell side inlet was connected to a membrane liquid storage tank (a 500 ml. Hoke stainless steel cylinder) through an on-off ball valve on each side of the cylinder. The liquid storage tank was pressurized by a helium gas cylinder. The pressure of the liquid line connecting to the permeator was indicated by a Matheson test gauge (0-15 psig) at the other end of the permeator. This pressure was always maintained at a level higher than those of both the feed and the sweep gas streams. The feed and the sweep gas stream pressures were maintained slightly above the atmospheric pressure. The pressure of the liquid reservoir could be independently changed if necessary. The shell side outlet was kept closed by a plug. It was opened to drain the membrane liquid from the permeator when the system was shut down and the permeator was not operational.

Both the feed and sweep gas streams were dried before they entered the NO analyzers. Packed drierite-based columns were tried at first for this purpose. However, they posed a serious problem especially at high nitric oxide concentrations. The color of the packing changed to a very unusual reddish brown, and the packed bed took the look of a sintered monolithic structure. Because of these problems, we switched to miniature tubular membrane dryers (Perma Pure Products, Farmingdale, NJ, model MD-125-12P or MD-125-12S) to selectively remove moisture from gas streams. The nitric oxide concentration in the feed gas exiting the module was measured by the MSA nitric oxide analyzer (range 0-500 ppm NO), whereas the sweep outlet NO concentration was measured in an Interscan NO analyzer (range 0-50 ppm).

The composition of the gas streams was measured periodically by a Varian

3700 Gas Chromatograph (6 ft x 1/4" CTR column) to measure the concentration of the other components, e.g. CO_2, N_2 and O_2. The GC operation had been automated for gas sampling at regular intervals. The 6-port gas sampling valve was driven by a solenoid-operated actuator, which was electronically controlled by a four-interval digital valve sequence programmer (Valco Instrunents, Houston, Texas), with preset time intervals.

For simultaneous separation of SO_2 and NO, the arrangement was as shown in Figure 3.7-2. This arrangement was similar to the previous one with minor variation. The 20-liter stainless steel vessel previously used for feed gas humidification in HFCLM runs had been replaced by a series of two 500 ml capacity teflon coated 316-SS cylinders (Hoke Inc., Cresskill, NJ). This was done to prevent any chemical attack on the humidifier by the highly corrosive gas mixture containing SO_2, NO_x and moisture. A sparger arrangement was adopted in each cylinder to enhance humidification. Two primary standard gas mixtures were blended, one with a nominal dry composition of 5000 ppm SO_2, 12% CO_2, 1.8% O_2, balance N_2, and the other with a nominal dry composition of 1000 ppm NO, balance N_2. The blend was bubbled through the humidifiers before entering the HFCLM permeator module. The steady state feed inlet composition was measured first. Then the permeator was connected. The feed outlet stream was dried using a membrane dryer, and was then introduced to the sample line of a Varian 3700 GC. The gas stream coming out of the GC sample line was next introduced to the MSA nitric oxide analyzer before being vented to fume hood. This series arrangement allowed for simultaneous measurement of SO_2 and NO concentration. In some experiments, the sweep outlet stream was analyzed in the MSA analyzer instead of in the Interscan analyzer, since the nitric oxide concentration was beyond the range of the Interscan analyzer (0-50 ppm NO).

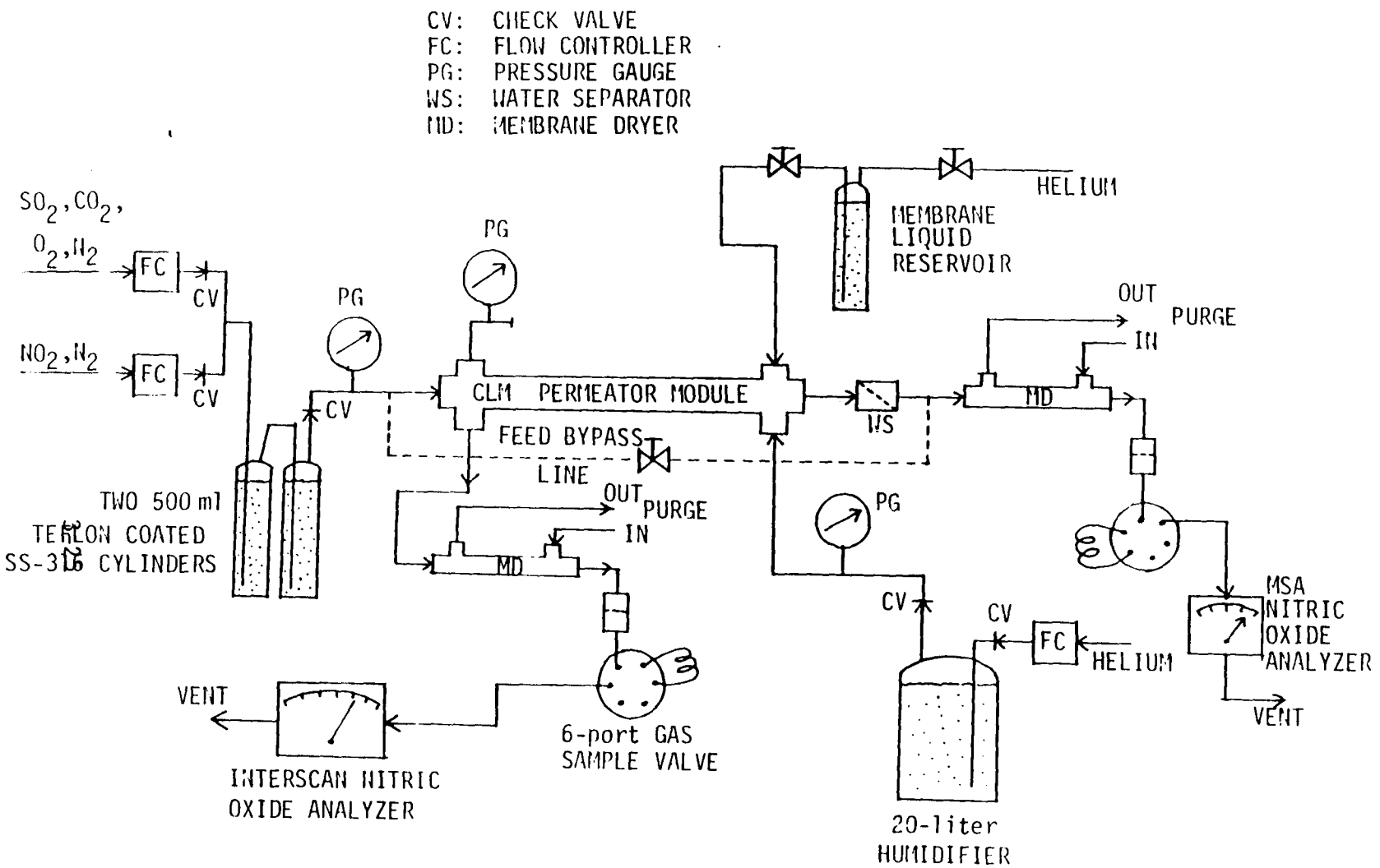

Figure 3.7-2: Experimental Setup for Simultaneous SO_2/NO Separation Using Contained Liquid Membrane Permeators

The GC column previously used in the gas chromatograph Varian 3700 (6 ft x 1/4" CTR column) had been replaced by a 6 ft x 1/8" Chromosorb 108 column, since the former was unsuitable for analyzing SO_2-containing samples. Unfortunately, Chromosorb 108 can not separate O_2 from N_2 (both elute at the same time from the column). Since it was more important to monitor SO_2 concentration than the O_2 and N_2 concentrations separately, we kept on using the Chromosorb column.

The same apparatus with the exception of the nitric oxide monitors was utilized for SO_2 separation. For high temperature experiments, the permeator was kept immersed in a water bath. The water temperature was maintained by a constant temperature circulator (Haake Inc., Saddle Brook, NJ, model E 52).

To carry out purification studies in the vacuum mode, a few modifications were made only in the permeate line. In the absence of a sweep gas, one end of the permeator (previously inlet end) was kept closed. A Heise vacuum gauge (range 0-30 inch vac) was used to monitor the pressure at the permeate outlet through which vacuum had been pulled. An oilless diaphragm vacuum pump (KNF Neuberger Inc., Princeton, NJ, model N026.3 SVP) was used to create and maintain the vacuum. Moisture from the permeate stream was eliminated by a drierite column (W. A. Hammond Drierite Co., Xenia, OH, model L68GP). The vacuum exhaust stream was sent directly to the fume hood.

For water CLM separation runs, the humidification of the feed and/or the sweep gas stream(s) was unnecessary. Therefore, the stainless steel humidifiers were removed from the system for sweep and vacuum modes of

operation. At the module outlets, however, they had generally been found to be fully saturated.

At the end of every CLM separation run employing aqueous salt solutions, it was extremely important to clean the modules thoroughly. We adopted the following procedure for cleaning : (i) immediately after the end of the run, water was passed through the shell side of the CLM module for a few hours at a rate of 10-20 ml/min; (ii) hot water at about 60°C was passed through the shell side at a flow rate of 10-20 ml/min for 10-12 hours; (iii) hot water was passed through the inside of both the sets of fibers at about the same flow rate and for about the same time; (iv) the module was dried under vacuum.

For a HFCLM permeator there is a total of five possible variations in mode of operation. They are presented in Figure 3.7-3. For sweep mode of operation we have always used countercurrent flow as it is more efficient. For vacuum mode of operation, one can apply the vacuum from both ends of the module [vacuum (2)], or one can pull vacuum from one side keeping the other side plugged [vacuum (1)]. In the former situation, the feed-permeate flow pattern inside the permeator is partly cocurrent and partly countercurrent, whereas in the latter, it will be either completely countercurrent or completely cocurrent. All three variations of the vacuum mode have been studied in the present work.

3.8 Calibration

The calibration curves for the GC columns for both Hewlett-Packard 5890A and Varian 3700 gas chromatographs were developed for SO_2, CO_2, O_2 and N_2 by

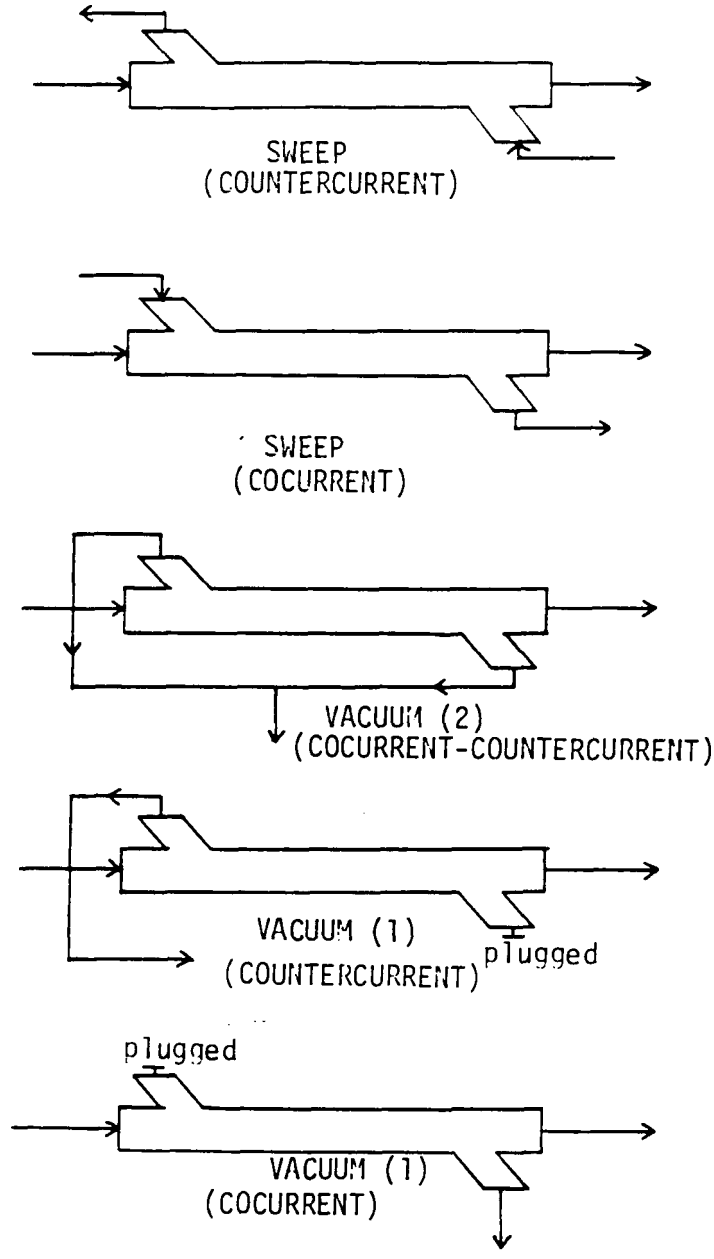

Figure 3.7-3: Different Modes of Operation Possible in HFCLM Permeator

utilizing primary standard gas mixture and/or gas mixtures obtained by carefully controlled mixing of separate gases in different proportions using Matheson flow transducer controllers. The thermal conductivity detector was used in both the GCs. The response from the detector was recorded by a digital reporting integrator (Hewlett Packard, Paramus, NJ, model 3390A or 3392A). Since helium was used as a carrier gas, the thermal conductivity detector could not detect He. Feed and sweep outlet streams would contain helium in varying proportions. If necessary, the helium content could be determined by subtracting the combined percentage of gas species from 100.

Section 4

Theoretical Considerations

4.1 Determination of permeability coefficient and separation factor

The steady state rate of permeation of any species i from the feed gas through the immobilized liquid film into the sweep gas is obtained experimentally according to the following equation:

$$R_i = V_S \times y_i^{SO} \qquad (4.1\text{-}1)$$

where R_i = permeation rate, Std cc/sec

V_S = sweep flow rate, Std cc/sec

y_i^{SO} = mole fraction of species i in sweep outlet

The species permeability, $(Q_i)_{expt}$, is related to R_i by

$$R_i = N_i A_M = (Q_i)_{expt} (\varepsilon_M / t_M \tau_M) A_M \Delta p_{i,LM} \qquad (4.1\text{-}2)$$

where $(Q_i)_{expt}$ = permeability of species i, (Std cc) (cm)/(sec)(cm^2)(cm Hg)

t_M = film thickness, cm

ε_M = substrate porosity

τ_M = substrate tortuosity factor

$\Delta p_{i,LM}$ = log mean partial pressure difference of species i across the film, cm Hg

A_M = membrane area, cm^2

N_i = flux of species i, (Std cc)/(cm^2)(sec)

For countercurrent flow pattern inside the test cell,

$$\Delta p_{i,LM} = \frac{[(P_F y_i^{FI} - P_S y_i^{SO}) - (P_F y_i^{FO} - P_S y_i^{SI})}{\ln[(P_F y_i^{FI} - P_S y_i^{SO})/(P_F y_i^{FO} - P_S y_i^{SI})]} \qquad (4.1\text{-}3)$$

Here y_i^{FI}, y_i^{FO} and y_i^{SI}, y_i^{SO} are the mole fraction of species i at feed inlet, outlet and sweep inlet and outlet, respectively. The quantities ε_M, t_M and τ_M are known properties of the microporous support, A_M is known from test cell dimensions, and R_i and $\Delta p_{i,LM}$ are known from experimental measurement of pressures, flow rate and compositions. The permeability can therefore be obtained from eqn. (4.1-2).

Equation (4.1-2) is strictly valid only locally across the ILM with local partial pressure differential between the feed and the sweep. In the present case (e.g., for SO_2) the feed and sweep cencentrations do change between inlets and outlets because of permeation. It is therefore important to use a very small permeation area to minimize the composition change in each stream, so that a cell-average partial pressure difference can be used without incurring any significant error.

When the species composition at the inlet and outlet gas streams are not much different, the $\Delta p_{i,LM}$ term in eqn. (4.1-2) can be replaced by Δp_i (for $y_i^{SI}=0$)
where

$$\Delta p_i = P_F y_i^F - P_S y_i^S \qquad (4.1\text{-}4)$$

The selectivity or the separation factor of the liquid membrane between

gas species i and j is given by

$$\alpha_{i,j} = Q_i/Q_j \qquad (4.1\text{-}5)$$

4.2 Modeling SO_2 transport through a liquid membrane

We are dealing here with the simultaneous mass transport of various gas species through an aqueous solution where a number of ionic and nonionic species are present. For pure water membrane, the species SO_2 and CO_2 undergo the following main ionization reactions (Roberts and Friedlander, 1980a; Abdulsattar et al., 1977):

$$SO_2 + 2H_2O \;===\; HSO_3^- + H_3O^+ \;,\; K_{eq} = 0.0140 \text{ M} \qquad (4.2\text{-}1)$$

$$CO_2 + 2H_2O \;===\; HCO_3^- + H_3O^+ \;,\; K_{eq} = 4.45 \times 10^{-7} \text{ M} \qquad (4.2\text{-}2)$$

For solutions containing SO_3^{2-} ion, one of the major reactions is (Hikita et al., 1977; 1982)

$$SO_2 + SO_3^- + H_2O \;===\; 2HSO_3^- \qquad (4.2\text{-}3)$$

As pointed out in (Roberts and Friedlander, 1980a; Roberts, 1979), a large number of chemical reactions may take place in the liquid.

Due to these complications, even an exact problem formulation becomes difficult. Here we have assumed that for our experimental conditions of parallel SO_2 and CO_2 transport, the CO_2 transport can be assumed to be physical-only (that is, no facilitation) since hydration of CO_2 is negligible.

Teramoto et al. (1978) have pointed out that, for simultaneous removal of SO_2 and CO_2, CO_2 transport will always be essentially physical, whenever, there is a finite SO_2 concentration at the gas liquid interface. For O_2 and N_2, only physical solution and diffusion are expected anyway, except when O_2 may react with the ferrous chelates. For these reasons, only the SO_2 transport and facilitation need to be studied in detail to predict SO_2 flux (and hence permeability) through the liquid membranes, and the SO_2-CO_2 selectivity.

The transport of SO_2 in water and sodium salt solutions as supported liquid membranes have been well discussed in Roberts (1979) and Roberts and Friedlander (1980). No theory is available for EDTA solution membranes. Actually a number of chemical reactions take place in the liquid phase, and a number of different chemical species exist in the membrane. The overall transport rate depends on (i) reaction equilibrium constants, (ii) gas solubility, (ii) ionic strength of the solution, (iv) effective diffusivities of the sulfur-containing species, (v) ionic activity coefficients, etc.

For the ILM, only the mass transport in the direction across the membrane needs to be considered. The general governing equation of mass transport with chemical reaction can be written as :

$$d/dx[D_{eff,i}dC_i/dx] = r_i \qquad (4.2\text{-}4)$$

where $D_{eff,i}$ is the effective diffusivity of species 'i'. Different ionic species may have different actual diffusivities, but in order to maintain electroneutrality, and the condition of no electric current across the liquid membrane; the diffusion rate of some species may be retarded, whereas that of

yet others may be accelerated. The boundary conditions on either side of the ILM would be as follows :

$$C_i = p_i H_i / \gamma_i \quad ; \; i : \text{permeants} \tag{4.2-5a}$$

$$dC_j/dx = 0 \quad ; \; j : \text{nonvolatile species} \tag{4.2-5b}$$

The net flux of SO_2 across the liquid, N_{SO_2}, is given as :

$$N_{SO_2} = (\varepsilon_M) \, D_{SO_2} \, [dC_{SO_2}/dx]_{x=0} \tag{4.2-6}$$

and the facilitation factor, F, is defined as :

$$F = \frac{N_{SO_2}}{D_{SO_2} [\Delta C_{SO_2}] \, [\varepsilon_M / t_M \tau_M]} - 1 \tag{4.2-7}$$

The values of p_i on two sides of the liquid film would be known from experimental conditions, and $D_{eff,i}$, γ_i, and H_i may be obtained from physical properties and concentrations. In an actual experiemnt, p_i of any species will change to some extent from inlet to outlet on either side of the film. In such cases, the average of inlet and outlet values would be used. Once the system of equations are solved, N_{SO_2} would be known, from which the theoretically predicted value of permeability Q_i can be evaluated.

An exact numerical solution of eqn. (4.2-4) is extremely complex. A number of chemical species and chemical reactions are involved (Roberts, 1979). The equations are nonlinear, and a number of constants used in the solution would at best be estimated values. One can demonstrate, however, that the net SO_2 flux would be given by

$$N_{SO_2} = [\sum_j D_{eff,j}\, n_j\, (C_{j,Feed} - C_{j,Sweep})/t_M]\, (\varepsilon_M/\tau_M) \qquad (4.2\text{-}8a)$$

where n_j is the number of sulfur atoms in species 'j', and $C_{j,Feed}$ and $C_{j,Sweep}$ are concentrations in liquid on the feed and the sweep side. Following (Roberts and Friedlander, 1980a), we provide brief descriptions of two of the simpler models used here. One is based on the assumption that chemical reaction equilibrium exists everywhere inside the membrane. The other is the non-equilibrium boundary layer approximation (NEBLA). The equilibrium theory would be exact if the chemical reactions involved are instantaneous; or alternately, if the reaction rates are much faster than diffusion rates.

Assuming chemical equilibrium, one may write (Roberts and Friedlander, 1980a; Roberts, 1979)

$$K_j = f_j(\bar{a}_i), \text{ and } \bar{a}_i = \gamma_i C_i \text{ ; for j-th reaction and i-th species} \qquad (4.2\text{-}8b)$$

where K_j is the reaction equilibrium constant for the j-th reaction. For example, for water as membrane, considering SO_2 ionization, one may write

$$\begin{aligned} K_{SO_2} &= (a_{HSO_3^-})(a_{H_3O^+})/(a_{SO_2(l)}) \\ &= [(\gamma_{HSO_3^-})(\gamma_{H_3O^+})/(\gamma_{SO_2})]\, [(C_{HSO_3^-})^2/C_{SO_2}] \end{aligned} \qquad (4.2\text{-}9a)$$

At the feed-membrane interface, combining eqns. (4.2-5a) and (4.2-9a), one gets

$$C_{\tilde{HSO_3^-}} = [\gamma_{\pm}]^{-1}\, [K_{SO_2}\, H_{SO_2}\, p_{SO_2}]^{1/2} \qquad (4.2\text{-}9b)$$

where $\gamma_{\pm} = [(\gamma_{HSO_3^-})(\gamma_{H_3O^+})]^{1/2}$ (4.2-9c)

Also, $C_{SO_2} = p_{SO_2} H_{SO_2} / \gamma_{SO_2}$ (4.2-9d)

Similar equations can be written for the sweep-membrane interface. Therefore, assuming that only SO_2 and HSO_3^- contribute to SO_2 transport, one can expand eqn. (4.2-8a):

$$N_{SO_2} = [D_{eff,HSO_3^-} (C_{HSO_3^-,Feed} - C_{HSO_3^-,Sweep})/t_M + D_{SO_2(l)} (C_{SO_2,Feed} - C_{SO_2,Sweep})/t_M] (\varepsilon_M/\tau_M) \quad (4.2\text{-}9e)$$

For salt solution membranes, a number of chemical reactions are possible (Roberts, 1979), and one has also to consider the electroneutrality condition, and total sodium balance,

$$\sum_i Z_i C_i = 0, \text{ and } \sum_k n'_k C_k = C_{T,Na} \quad (4.2\text{-}10)$$

The activity coefficients can be calculated as follows :

$$\log \gamma_{SO_2} = 0.076\ I,\ a_{H_2O} = 1 - 0.018 \sum_i C_i,$$

and $\log \gamma_i = A\ z_i^2\ [b_i I - I^{1/2}/(1 + Ba_i I^{1/2})]$ for other species

$$\text{where } I = \sum_i Z_i^2\ C_i \quad (4.2\text{-}11)$$

where A- and B are constants, and a_i and b_i are parameters related to the

species 'i'. The above set of equations can be solved for concentrations at the two membrane interfaces, $C_{j,Feed}$ and $C_{j,Sweep}$. The effective diffusivities may be calculated subsequently. Considering H_3O^+ and HSO_3^- to be the major ions, their effective diffusivities must be equal in order to maintain the no-current condition across the membrane, and this can be calculated as (Vinograd and McBain, 1941)

$$D_{eff,H^+} = D_{eff,HSO_3^-} = 2\ D_{H^+}\ D_{HSO_3^-} / (\ D_{H^+} + D_{HSO_3^-}) \qquad (4.2\text{-}12)$$

For multi-ion environment, more complex expressions have to be used. Knowing D_{eff} and concentrations, one can calculate N_{SO_2} using eqn. (4.2-9d).

Non-equilibrium boundary layer approximation (NEBLA) postulates the existence of two boundary layers inside the liquid membrane on either side, with a core in between which is at reaction equilibrium. It is hypothesized that only molecular diffusion takes place in the two boundary layers till the species reaches the equilibrium core where it undergoes instantaneous chemical equilibrium with the other species. According to this theory, relative characteristic times for diffusion and reaction may be of same order, and instantaneous reaction assumption really may not be valid, especially for thin liquid films. The thicknesses of the boundary layers on the feed and the sweep side (δ_f and δ_s, respectively) are given as

$$\delta_f = [D_{SO_2}/k_1]^{1/2}\ ,\quad \delta_s = [D_{HSO_3^-}/k_{-1}\ C_{H_3O^+,Sweep}]^{1/2} \qquad (4.2\text{-}13)$$

where k_1 and k_{-1} are the forward and reverse reaction rate constants for SO_2 ionization. For SO_2 system, it can be shown that $\delta_f << \delta_s$, and the effect of

feed side boundary layer can be neglected. Under steady state condition, the SO_2 flux through the equilibrium core and the sweep side boundary layer can be equated, and this enables one to calculate its concentration at their interface, from which N_{SO_2} is estimated.

4.3 Modeling NO transport through a liquid membrane

Three types of liquid membranes have been used in this study for NO separation: pure water, salt solution (with Na_2SO_3) and metal chelate solutions. For pure water, only simple permeation of NO takes place through the membrane. Therefore, for pure water membrane,

$$N_{NO} = (D_{NO}/t_M)(C_{NO,Feed} - C_{NO,Sweep})(\varepsilon_M/\tau_M) \qquad (4.3\text{-}1a)$$

Also

$$N_{NO} = (D_{NO}\, H_{NO}/t_M)(p_{NO,Feed} - p_{NO,Sweep})(\varepsilon_M/\tau_M) \qquad (4.3\text{-}1b)$$

so that the effective permeability is $D_{NO}H_{NO}\varepsilon_M/(t_M\tau_M)$. The values of D_{NO} and H_{NO} in water may be obtained from Andrew and Hanson (1961) and Takeuchi et al. (1977). For the salt solution, appropriate salting out effect on H_{NO} and correction for D_{NO} will provide the value of effective NO permeability. The permeation of NO through an aqueous solution of Fe^{2+}EDTA or Fe^{3+}EDTA is facilitated by the complex formed by the reaction (for example, for Fe^{2+}EDTA)

$$\underset{A}{NO(l)} + \underset{B}{Fe^{2+}EDTA\ (l)} \underset{k_{-1N}}{\overset{k_{1N}}{\equiv\!\equiv\!\equiv}} \underset{AB}{Fe^{2+}EDTA.NO} \qquad (4.3\text{-}2)$$

The total flux of NO resulting from the permeation of free NO (A) as well as

the complex Fe^{2+}EDTA.NO (AB) may be determined amongst others by adopting the following procedures: (1) an exact numerical solution of the governing reaction-diffusion equation; (2) obtain an equilibrium approximation of the same equation; and (3) utilize the NEBLA strategy.

Since work on an exact numerical solution of the governing reaction-diffusion equation is in progress at this time for the system of reaction (4.3-2), we focus only on the strategies (2) and (3). For equilibrium approximation, we utilize the standard approach of Ward (1970) and write the total flux of NO as

$$N_{NO} = \frac{D_A \varepsilon_M (C_{A,Feed} - C_{A,Sweep})}{t_M \tau_M} + \frac{D_{AB} \varepsilon_M (C_{AB,Feed} - C_{AB,Sweep})}{t_M \tau_M} \qquad (4.3\text{-}3)$$

where A represents NO and AB represents Fe^{2+} EDTA.NO complex. The quantity C_{AB} can be obtained from the expression

$$C_{AB} = K_{eq} C_A C_T/(1 + K_{eq} C_T) \qquad (4.3\text{-}4)$$

for feed and sweep locations by using $C_{A,Feed}$ and $C_{A,Sweep}$ respectively. Here K_{eq} is known (Chang et al., 1983) for reaction (4.3-2) and C_T is the concentration of the Fe^{2+}EDTA chelate added to the membrane (0.01M or 0.02M).

Using Roberts and Friedlander (1980a) approach for NEBLA, one can find out whether there is any feed side boundary layer resistance and/or sweep side boundary layer resistance. Calculations of Damkohler number [$Da = k_{1N} C_B (\tau_M t_M)^2/D_A$] for the feed side and [$Da = k_{-1N} (\tau_M t_M)^2/D_{AB}$] for the sweep side yield respectively 5×10^5 and 135; this means that the feed side boundary

layer resistance is negligible (since Da > 10^5). But the strip side boundary layer resistance is significant. Calculating the value of dimensionless boundary layer thickness δ_s^* on the strip side

using $$\delta_s = (D_{AB}/k_{-1N})^{1/2} \tag{4.3-5a}$$

yields $$\delta_s^* = \delta_s/(\tau_M\ t_M) \tag{4.3-5b}$$

which is thus known. Now the NO flux in the nonequilibrium core and strip side boundary layer have to be equated at the interface of the core and boundary layer (denoted by subscript i):

$$N_{NO} = \frac{D_A\ \varepsilon_M\ (C_{A,Feed} - C_{A,i})}{\tau_M\ t_M\ (1 - \delta_s^*)} + \frac{D_{AB}\ \varepsilon_M\ (C_{AB,Feed} - C_{AB,i})}{\tau_M\ t_M\ (1 - \delta_s^*)}$$

$$= \frac{D_A\ \varepsilon_M}{\tau_M\ t_M\ \delta_s^*}\ (C_{A,i} - C_{A,Sweep}) \tag{4.3-6}$$

Use now equilibrium relation (4.3-4) for the interface:

$$C_{AB,i} = K_{eq}\ C_{A,i}\ C_T/(1 + K_{eq}\ C_T) \tag{4.3-7}$$

Substituting in (4.3-6) leads to an algebraic equation for $C_{A,i}$ whose solution will provide the only unknown in N_{NO}:

$$C_{A,i} = \frac{-[1+\delta_s^* G_1 - G_2(1-\delta_s^*)K_{eq}] \pm \sqrt{[\{1+\delta_s^* G_1 - G_2(1-\delta_s^*)K_{eq}\}^2 + 4K_{eq} G_2(1-\delta_s^*)]}}{2\ K_{eq}} \tag{4.3-8}$$

where $$G_1 = D_{AB}\ K_{eq}\ C_T/D_A \tag{4.3-9a}$$

and $$G_2 = \frac{\delta_s^*}{(1 - \delta_s^*)} \left(C_{A,Feed} + \frac{D_{AB}}{D_A} C_{AB,Feed}\right) + C_{A,Sweep} \qquad (4.3\text{-}9b)$$

4.4 Mass transfer in hollow-fiber-contained liquid membrane (HFCLM) permeator

One possible fiber arrangement inside the CLM permeator shell is shown in Figure 4.4-1. It also shows a small section of the CLM between the fibers which can be considered a so-called 'unit cell' (Majumdar et al., 1988). At any cross-section of the module, there would be hundreds of such unit cells. A true concentration profile can only be obtained if one can solve the diffusion equation inside such unit cell. Even if one considers only one principal reaction (in reality, there would be a lot of side reactions, Roberts, 1979), one has to solve a boundary value problem for two simultaneous non-linear second order differential equations. Note also that the local feed and sweep compositions will change along the module (in the z-direction). The problem becomes additionally complicated because of the curved boundaries of the unit cell. Besides, there are other possible feed-sweep fiber arrangements. The exact numerical solution appears to be extremely complex. For the immediate objective of modeling the transport behavior, the problem was solved along with some justified simplifications, e.g. use of an effective membrane thickness. This has been described later.

4.5 A lumped permeation analysis for CLM

Crude estimates of the rate of mass transfer in CLM permeators can be

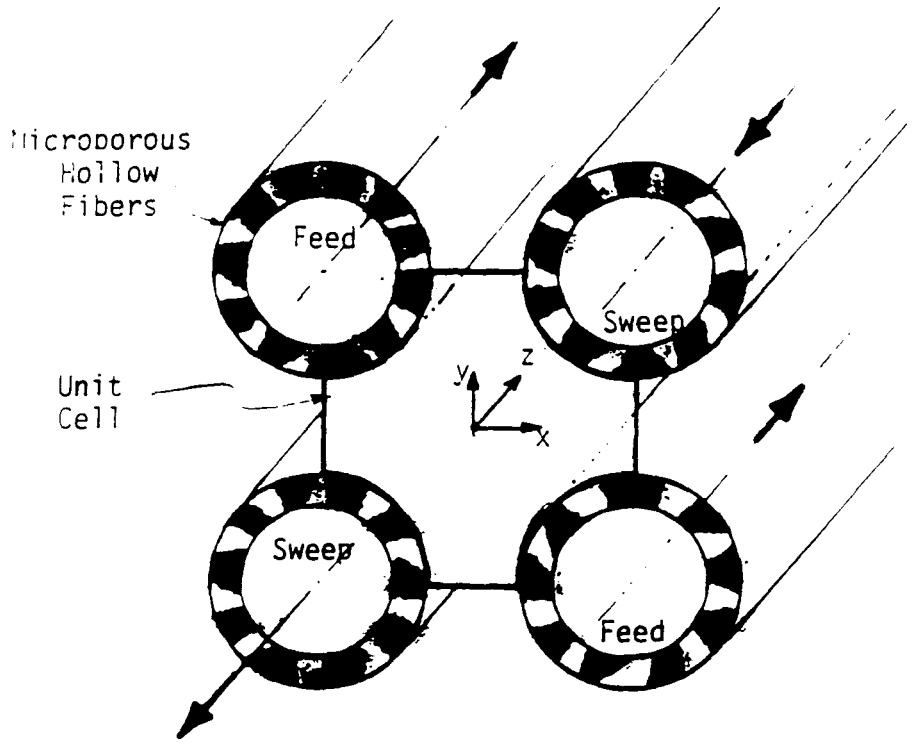

One Possible Fiber Arrangement in CLM Permeator

Principal Reaction : $SO_2 + 2H_2O \rightleftharpoons HSO_3^- + H_3O^+$

(A) (B)

Governing Equations :

$$SO_2 : D_A \left(\partial C_A/\partial x^2 + \partial C_A/\partial y^2 \right) - k_1 C_A + k_{-1} C_B^2 = 0$$

$$HSO_3^- : D_B \left(\partial C_B/\partial x^2 + \partial C_B/\partial y^2 \right) + k_1 C_A - k_{-1} C_B^2 = 0$$

Boundary Conditions : Except for SO_2 partitioning at the gas-liquid interfaces, the condition is $\partial C_i/\partial n = 0$ for all species i, where 'n' stands for normal to the unit cell envelope.

Figure 4.4-1: SO_2 Permeation in a Unit Cell of the CLM

developed theoretically if some simplifying assumptions are made. The main hypothesis here is that the overall mass transfer resistance can be expressed as the sum of individual resistances in series, as shown in Figure 4.5-1. In general one can demonstrate that the transfer resistances of the microporous hollow fiber walls are practically negligible in the present case. It can be shown that the substrate transfer coefficients are typically an order of magnitude higher than the liquid membrane transfer coefficients (calculations are available in Section 5). The overall mass transfer coefficient for each permeant K_o can therefore be expressed as

$$\frac{1}{K_o} = \frac{1}{k_F} + \frac{1}{k_S} + \frac{d}{Q} \qquad (4.5\text{-}1)$$

where k_F and k_S are the film transfer coefficients on feed and sweep side respectively, d is the effective liquid membrane thickness in the CLM module, and Q is the permeability of the permeant under consideration through the liquid membrane. The permeation flux at any point, N, is given by

$$N = K_o (p_F - p_S) \qquad (4.5\text{-}2)$$

where p_F and p_S are local permeant partial pressures on the feed and the sweep side, respectively. Although eqn. (4.5-1) is applicable locally at any cross section inside the permeator, we assume that it can be extended to the whole module with average values for the individual coefficients.

If feed and sweep (or permeate, for vacuum runs) flow rates are known, one can estimate the film transfer coefficients using available correlations.

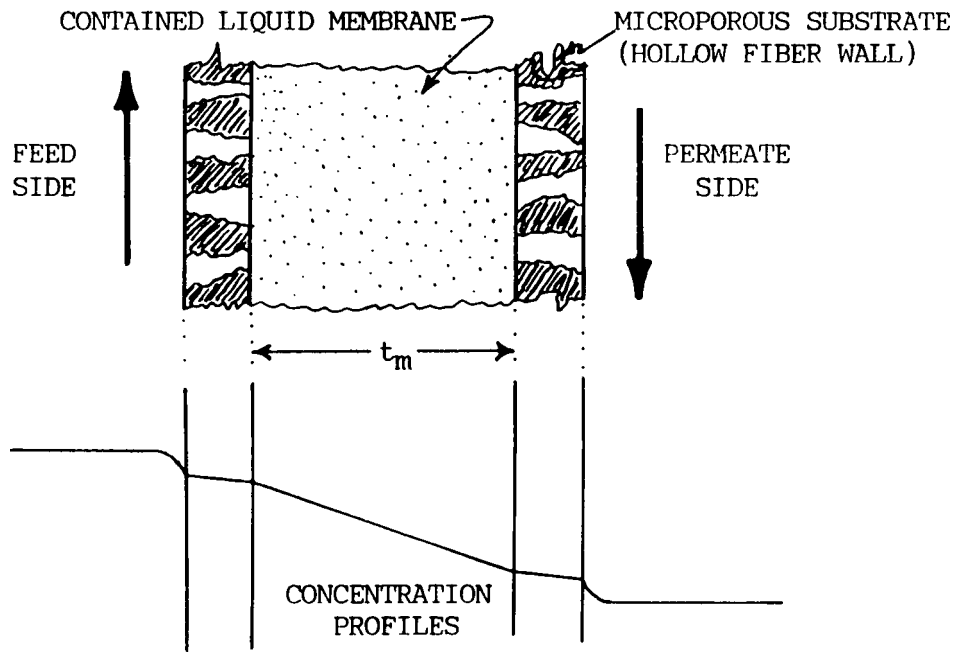

TOTAL MASS TRANSFER RESISTANCE	=	FEED SIDE GAS PHASE RESISTANCE	+	FEED SIDE SUBSTRATE RESISTANCE	+	LIQUID MEMBRANE RESISTANCE	+	PERMEATE SIDE SUBSTRATE RESISTANCE	+	PERMEATE SIDE GAS PHASE RESISTANCE

Figure 4.5-1: Individual Mass Transfer Resistances in CLM

In the present case, we may use the Graetz solution, according to which (Skelland, 1974) the average Sherwood number (Sh) can be expressed as a function of Reynolds Number (Re) and Schmidt Number (Sc):

$$Sh = (k_g\ d_i/D_g) = 0.5\ (d_i/L)\ Re\ Sc\ \phi(Re,\ Sc) \qquad (4.5\text{-}3)$$

where d_i and L are the inside diameter and the length of the hollow fiber, k_g is the gas film transfer coefficient in the fiber lumen (k_F or k_S), and D_g is the permeant diffusivity in the gas. It can be shown that for the range of flow rates employed in the present study, the quantity ϕ is almost always unity. Equation (4.5-3) can then be simplified to

$$k_g \cong 2\ V_g\ /\ (\pi\ L\ d_i\ N_T) \qquad (4.5\text{-}4)$$

where N_T is the number of hollow fibers through which the gas is passing at a flow rate of V_g. Since Q is generally known from ILM studies, and gas flow rates are experimental quantities, one can estimate K_o from eqns. (4.5-1) and (4.5-4) if d is known.

Figure 4.5-2 presents a simplified depiction of the CLM permeator module along with the relevant quantities. For sweep runs, the component material balance can be expressed as:

$$V_F\ (x^{in} - x^{out}) = V_S\ y^{out} \qquad (4.5\text{-}5)$$

The two important experimental quantities are the fractional removal F and the experimental overall mass transfer coefficient K_{expt}, expressed, respectively,

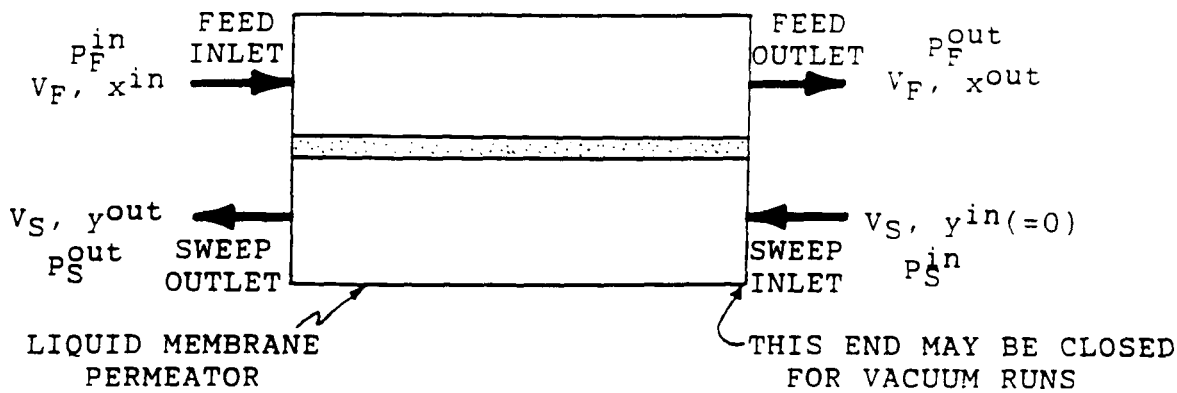

Figure 4.5-2: Material Balance in CLM Permeator

as

$$F = (x^{in} - x^{out})/ x^{in} \tag{4.5-6}$$

and $$R_T = K_{expt}\ A_T\ \Delta p_{LM} \tag{4.5-7}$$

For sweep runs, R_T and Δp_{LM} can be expressed as follows :

$$R_T = V_S\ y^{out} \tag{4.5-8}$$

$$\Delta p_{LM} = \frac{(P_F^{in}\ x^{in} - P_S^{out}\ y^{out}) - (P_F^{out}\ x^{out})}{\ln\ [(P_F^{in}\ x^{in} - P_S^{out}\ y^{out})/(P_F^{out}\ x^{out})]} \tag{4.5-9}$$

Since pressures, flow rates and compositions are all known experimentally, one can calculate K_{expt}, and this can be compared with the predicted value of K_o. Note that K_o can be calculated in this fashion only for sweep runs, since for vacuum runs y^{in} values are generally unknown.

One of the most important quantities in the above analysis is d. The best way of estimating d is by independent CLM experiemnts. A pure nonreacting gas e.g., N_2 or CO_2 is used as the feed gas, and helium can be used as a sweep gas. For a pure gas feed, the quantity k_F in eqn. (4.5-1) can be neglected. Utilizing the same analysis format as above, one can calculate d from the sweep flow rate, and sweep outlet concentration of the permeant:

$$d = Q\ [(A_T\ \Delta p_{LM}/V_S\ y^{out}) - 1/k_S] \tag{4.5-10}$$

This d may be used in calculations involving regular separation experiments using the same module, since the module property can be assumed to be constant from run to run. However, this procedure is less rigorous than that followed by Majumdar et al. (1989).

4.6 Model for multicomponent gas permeation in CLM

In the previous analysis it was considered that the change in the feed and the sweep gas flow rates within the permeator is negligible. Further, the permeation rate of a species was expressed in terms of log mean partial pressure difference. In reality, the feed and the sweep gas flow rates change from point to point within the permeator. Also, the partial pressure driving force of a species varies from point to point due to the change in the local total pressure and local species composition. The total rate of species permeation is affected by all of the above parameters.

Though not part of any task category, we have developed a model for gas permeation through HFCLM permeator, applicable to our system. The general multicomponent gas permeation model is available in Majumdar et al. (1989).

Figure 4.6-1 illustrates the separation of a gas mixture with a countercurrent sweep gas stream in a HFCLM permeator. Only one feed fiber and one sweep fiber are shown for simplicity. But the total number of fibers in feed and sweep sides may be different just as their dimensions may be different. The sweep gas stream flows countercurrent to the feed gas stream. The theoretical analysis of the permeation process is based on the following assumptions:

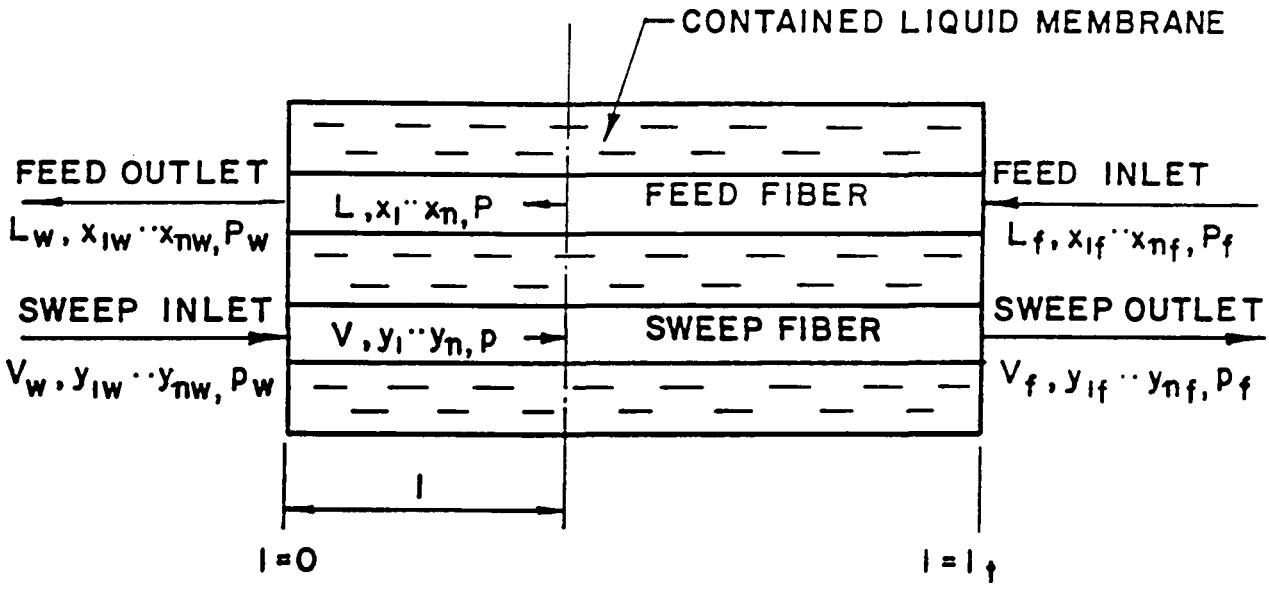

Figure 4.6-1 Schematic of a HFCLM Permeator for Modeling Sweep Gas Mode of Operation

1. The gas species permeates from one side of the liquid membrane to the other purely by solution-diffusion mechanism; no reaction occurs within the membrane.
2. The permeability coefficients of the gas components are same as those of pure gases, and are independent of pressure.
3. An effective liquid membrane thickness exists along the length of the permeator as well as all radial locations inside the fiber bundle.
4. There is no mass transfer resistance in the gas phases.
5. There is negligible diffusion along the mean gas flow path compared to the bulk gas flow.
6. Plug flow model can be used for both gas streams.
7. Pressure drop inside the fiber is governed by Hagen-Poiseuille equation.
8. Viscosity of gas mixture depends only on composition.
9. End effects in the permeator and deformation of fibers are negligible.

Assumptions 1 and 2 are really not valid due to facilitation and chemical reaction of SO_2. However this issue can only be addressed at this time by means of an effective permeability. Alternate means like equilibrium approximation will be explored in future.

An overall material balance between the feed inlet end and any location at a distance 'l' from the sweep inlet end leads to

$$N_F L - N_S V = N_F L_f - N_S V_f \qquad (4.6\text{-}1)$$

Here L -and V are local molar feed and sweep flow rates per fiber; N_F and N_S

are total number of feed and sweep fibers, respectively. The component balances can be written as

$$N_F L x_i - N_S V y_i = N_F L_f x_{if} - N_S V_f y_{if} \qquad i = 1, n \qquad (4.6\text{-}2)$$

For equal permeation areas in feed and sweep sides, one can write

$$N_F \pi D_{FO} l_t = N_S \pi D_{SO} l_t \qquad (4.6\text{-}3)$$

where D_{FO} and D_{SO} are feed and sweep fiber outside diameters, respectively, and l_t is the total effective permeation length of the permeator.

Therefore, $$N_F/N_S = D_{SO}/D_{FO} = \eta \text{ (say)} \qquad (4.6\text{-}4)$$

If the axial coordinate 'l' is positive in the direction of sweep gas flow, the governing differential equations for permeation for all species are given by

$$d(Lx_i)/dl = \pi D_{FO} (Q_i/d) [Px_i - py_i] \qquad i = 1, n \qquad (4.6\text{-}5)$$

The differential equations governing the pressure drop in the two gas streams in the two sets of fiber lumina are:

Feed side : $$dP/dl = 128 R T L \mu_F / [\pi P D_{FI}^4] \qquad (4.6\text{-}6)$$

Sweep side : $$dp/dl = - 128 R T V \mu_S / [\pi p D_{SI}^4] \qquad (4.6\text{-}7)$$

Using the following dimensionless parameters

$$S = \pi D_{FO} (Q_{ref}/d) (P_{ref}/L_{ref}) l \tag{4.6-8}$$

$$P^* = P/P_{ref}; \quad p^* = p/P_{ref} \tag{4.6-8a}$$

$$L^* = L/L_{ref}; \quad V^* = V/L_{ref} \tag{4.6-8b}$$

$$\mu_F^* = \mu_F/\mu_{ref}; \quad \mu_S^* = \mu_S/\mu_{ref} \tag{4.6-8c}$$

$$Q_i^* = Q_i/Q_{ref} \qquad i = 1, n \tag{4.6-8d}$$

$$\beta = 128 R T L_{ref}^2 \mu_{ref}/[\pi^2 D_{FI}^4 D_{FO} (Q_{ref}/d) P_{ref}^3] \tag{4.6-8e}$$

the governing differential eqns. (4.6-5) to (4.6-7) can be obtained in dimensionless form

$$d(L^* x_i)/dS = Q_i^* (P^* x_i - p^* y_i) \qquad i = 1, n \tag{4.6-9}$$

$$dP^*/dS = \beta \mu_F^* L^*/P^* \tag{4.6-10}$$

$$dp^*/dS = - \beta \theta^4 \mu_S^* V^*/p^* \tag{4.6-11}$$

where $\theta = D_{FI}/D_{SI}$ (4.6-11a)

Adding all equations represented by eqn. (4.6-9), one gets

$$dL^*/dS = \sum_{j=1}^{n} Q_j^* \, [P^* x_j - p^* y_j] \qquad (4.6\text{-}12)$$

From eqns. (4.6-1) and (4.6-2)

$$N_F \, dL = N_S \, dV \; ; \; N_F \, d(Lx_i) = N_S \, d(Vy_i)$$

which leads to

$$dV^*/dS = \eta \, dL^*/dS \; ; \; d(V^* y_i)/dS = \eta \, d(L^* x_i)/dS$$

Therefore,

$$dV^*/dS = \eta \sum_{j=1}^{n} Q_j^* \, [P^* x_j - p^* y_j] \qquad (4.6\text{-}13)$$

Now, it should be noted that

$$L^* \, dx_i/dS = d(L^* x_i)/dS - x_i \, dL^*/dS$$

$$V^* \, dy_i/dS = d(V^* y_i)/dS - y_i \, dV^*/dS$$

Combining these mathematical relations and previous equations, one gets

$$dx_i/dS = [Q_i^* \, (P^* x_i - p^* y_i) - x_i \sum_{j=1}^{n} Q_j^* \, (P^* x_j - p^* y_j)]/L^* \quad i = 1, n \qquad (4.6\text{-}14)$$

$$dy_i/dS = \eta[Q_i^* \, (P^* x_i - p^* y_i) - y_i \sum_{j=1}^{n} Q_j^* \, (P^* x_j - p^* y_j)]/V^* \quad i = 1, n \qquad (4.6\text{-}15)$$

Therefore, for n components there are 2n + 4 nonlinear coupled ordinary

differential equations in L^*, V^*, P^*, p^*, x_i and y_i which have to be solved simultaneously. Generally, it is convenient to specify the domain of the independent variable between 0 and 1. In this case, the total dimensionless area S_t (for $l = l_t$) can be made equal to unity with proper choice of reference parameters (i.e., Q_{ref}, P_{ref} and L_{ref}) in definition (4.6-8) (Majumdar, 1986). Boundary conditions for above equations can then be written as

$$S = 0 \Rightarrow V^* = V_w^*;\ P^* = P_w^*;\ y_i = y_{iw} \qquad i = 1, n \qquad (4.6\text{-}16)$$

$$S = 1 \Rightarrow L^* = L_f^*;\ p^* = p_f^*;\ x_i = x_{if} \qquad i = 1, n \qquad (4.6\text{-}17)$$

Feed and sweep side gas mixture viscosities are computed as follows (Reid et al., 1977):

$$\bar{\mu} = \sum_{i=1}^{n} \left[z_i \mu_i \Big/ \sum_{j=1}^{n} \phi_{ij} z_j \right] \qquad (4.6\text{-}18)$$

where the constants ϕ_{ij}-s are obtained as (Wilke, 1950):

$$\phi_{ij} = \left[1 + (\mu_i/\mu_j)^{1/2} (M_{wj}/M_{wi})^{1/4}\right]^2 \Big/ \left[8 (1 + M_{wi}/M_{wj})\right]^{1/2} \qquad (4.6\text{-}19)$$

Here z_i, μ_i, M_{wi} are the mole fraction, viscosity and the molecular weight of the ith species, respectively.

A computer program has been developed to solve this system of nonlinear, coupled differential equations.

Section 5

Results and Discussion

5.1 Tortuosity factor

The tortuosity factor, τ_M, of the ILM support must be known before gas permeabilities can be obtained from the experimental permeation data. Unlike porosity ε_M and film thickness t_M, τ_M can not be obtained from physical measurements. The best way to estimate τ_M is to carry out a permeation experiment using as feed a pure inert gas whose permeability through the liquid membrane is known independently. For example, for permeation of an inert gas such as N_2 through water, with no chemical reaction taking place, the permeability would be a product of the solubility and the diffusivity of N_2 in water, both of which are known quantities (available in Perry and Chilton, 1973). One can therefore estimate τ_M from experimental permeation rate. In order for the above estimate of τ_M to be applicable, however, the experimental conditions for the actual multicomponent permeation experiments, and the pure gas permeation experiments must be the same, since the value of τ_M has been found to be a function of the conditions, like pressure, nature of support, etc. (Bhave and Sirkar, 1986; Park et al., 1986).

The experimentally obtained estimates of the tortuosity factor for the liquid membrane support Celgard 2400 are presented in Table 5.1-1. Two permeants, CO_2 and N_2 were studied. Two different test cells were used to get different active permeation areas. Also in some experiments, a hydrophobic polypropylene backing (Accurel, Enka America, Inc., Asheville, NC) was used to

Table 5.1-1 : Tortuosity Factor for Celgard 2400 Under Given Experimental Conditions

Basis: i) Feed is pure CO_2 or N_2; Sweep is pure He (atmospheric)

ii) Feed / Sweep nominal flow rate = 20 cc/min

iii) Totuosity factor (τ_M) obtained from the folowing eqn.

$$\tau_M = Q_i \, (\varepsilon_M \, A_M / t_M)(\Delta p_i / R_i)$$

where

Q_i : permeability of species i in water (known)

ε_M, t_M : porosity and thickness of Celgard 2400 film, 0.38 and 25.4 microns, respectively (manufacturer's data)

A_M : active permeation area

R_i : permeation rate of species i for Δp_i partial pressure difference across the film (experimentally known)

iv) $Q_{CO_2} = 2.1 \times 10^{-7}$ (Std cc)(cm)/(sec)(cm^2)(cm Hg) (*)

v) $Q_{N_2} = 5.58 \times 10^{-9}$(Std cc)(cm)/(sec)($cm^2$)(cm Hg) (*)

Permeant	Run #	A_M (cm^2)	Feed Pressure	backing	Permeant concentration in Sweep, ppm inlet	outlet	τ_M
CO_2	1	1.27	atm.	no	0	1400	6.3
	2	1.27	atm.	no	0	790	7.5
	3	1.27	atm.	no	0	1360	6.4
N_2	1	11.4	atm.	no	258	589	7.3
	2	11.4	atm.	yes	259	569	7.4
	3	1.27	~10 psig	yes	154	247	4.1

(*) from Ward and Robb (1967), and NYSERDA Report(1987).

explore its effect on the Celgard 2400 tortuosity. As Table 5.1-1 indicates, the τ_M values for different experiments, different films, different permeants, and with or without backing, are reasonably close. Although it is difficult to decide on an exact number for τ_M, a value of 7 seemed to be appropriate. In all subsequent permeability calculations, therefore, we would use $\tau_M = 7.0$. Note that for a higher feed pressure and with a backing, a value of τ_M close to 4 was obtained, as expected from an earlier study (Bhave and Sirkar, 1986).

5.2 Preliminary studies and screening of membrane liquids for SO_2

Preliminary permeation studies indicated that the permeabilities and selectivities are generally reproducible. There were variations from run to run, but those were due to experimental error, and in spite of deviations, the trends were quite clear. The preliminary results are illustrated in Table 5.2-1. Water, 1N $NaHSO_3$ and 1N Na_2SO_3 appear to have sufficient merits to be pursued further as candidate membranes. Sulfolene solution appears to have a somewhat low selectivity under the measurement conditions. Steady state permeation behavior was observed in all three cases.

As shown in Table 5.2-2, a strongly time dependent behavior was observed when 1N Na_2SO_3 solution was utilized as a membrane. The chemistry of the absorption of SO_2 and its reactions with the salt solution are complex, particularly in presence of CO_2. Sometimes SO_2 and CO_2 may compete for the same reactions. Further, a number of different reactions may occur in the liquid phase between the various ions present, e.g. HSO_3^-, SO_3^{2-}, HCO_3^- and CO_3^{2-}. Besides, the presence of O_2 in the feed gas may alter some of the reactions. All such complicating factors may contribute to the unsteady permeation

Table 5.2-1 : Permeabilities and Selectivities

Nominal feed composition (dry): 5000 ppm SO_2, 12% CO_2, 1.8% O_2, bal. N_2

Membrane	Data No.	Permeability (Q)*		Specific Permeation Rate (Q/t_M)**		Selectivity
		SO_2	CO_2	SO_2	CO_2	SO_2-CO_2
Water	1	7.80×10^{-6}	9.30×10^{-8}	3.12×10^{-3}	3.72×10^{-5}	83.9
	2	7.17×10^{-6}	8.03×10^{-8}	2.87×10^{-3}	3.21×10^{-5}	89.3
	3	1.07×10^{-5}	1.53×10^{-7}	4.26×10^{-3}	6.11×10^{-5}	69.7
	4	6.78×10^{-6}	7.92×10^{-8}	2.71×10^{-3}	3.17×10^{-5}	85.6
	5	5.01×10^{-6}	7.02×10^{-8}	2.00×10^{-3}	2.81×10^{-5}	71.3
1N $NaHSO_3$	1	4.69×10^{-6}	3.39×10^{-8}	1.88×10^{-3}	1.36×10^{-5}	138.4
	2	3.13×10^{-6}	3.16×10^{-8}	1.25×10^{-3}	1.26×10^{-5}	98.9
	3	1.86×10^{-6}	1.84×10^{-8}	7.46×10^{-4}	7.36×10^{-6}	101.3
	4	2.30×10^{-6}	2.26×10^{-8}	9.21×10^{-4}	9.03×10^{-6}	102.0
15% Sulfolene	1	3.73×10^{-6}	8.42×10^{-8}	1.49×10^{-3}	3.37×10^{-5}	44.3
	2	2.44×10^{-6}	5.69×10^{-8}	9.76×10^{-4}	2.28×10^{-5}	42.9

* unit is (Std cc)(cm)/(sec)(cm^2)(cm Hg)

** unit is (Std cc)/(sec)(cm^2)(cm Hg)

Table 5.2-2 : Time Varying Permeation Behavior of 1N Na_2SO_3 Membrane

Nominal feed composition (dry): 5000 ppm SO_2, 12% CO_2, 1.8% O_2, bal. N_2

Data Group No.	Data at Time (hrs)	Permeability (Q)*		Specific Permeation rate** (Q/t_M)		Selectivity
		SO_2	CO_2	SO_2	CO_2	SO_2-CO_2
1	3	4.65×10^{-6}	3.46×10^{-8}	1.86×10^{-3}	1.39×10^{-5}	134.2
2	1	3.38×10^{-6}	4.94×10^{-8}	1.35×10^{-3}	1.97×10^{-5}	68.5
	2	4.78×10^{-6}	4.30×10^{-8}	1.91×10^{-3}	1.72×10^{-5}	111.1
	3	6.27×10^{-6}	3.74×10^{-8}	2.51×10^{-3}	1.50×10^{-5}	167.9
	4	7.74×10^{-6}	3.26×10^{-8}	3.10×10^{-3}	1.30×10^{-5}	237.6
	5	8.71×10^{-6}	2.81×10^{-8}	3.49×10^{-3}	1.12×10^{-5}	310.6
	6	1.17×10^{-5}	1.70×10^{-8}	4.67×10^{-3}	6.81×10^{-6}	685.6
3	1	7.85×10^{-7}	3.62×10^{-8}	3.14×10^{-4}	1.45×10^{-5}	21.7
	2	2.82×10^{-6}	3.13×10^{-8}	1.13×10^{-3}	1.25×10^{-5}	89.9
	3	3.34×10^{-6}	2.54×10^{-8}	1.34×10^{-3}	1.02×10^{-5}	131.7
	4	3.52×10^{-6}	2.51×10^{-8}	1.41×10^{-3}	1.00×10^{-5}	140.3
	5	4.10×10^{-6}	2.47×10^{-8}	1.64×10^{-3}	9.88×10^{-6}	166.1
4	1	5.22×10^{-6}	3.51×10^{-8}	2.09×10^{-3}	1.40×10^{-5}	148.9
	2	5.55×10^{-6}	2.90×10^{-8}	2.22×10^{-3}	1.16×10^{-5}	191.1
	4	7.61×10^{-6}	1.89×10^{-8}	3.05×10^{-3}	7.56×10^{-6}	402.9
	6	8.40×10^{-6}	1.60×10^{-8}	3.36×10^{-3}	6.39×10^{-6}	525.7
	8	9.11×10^{-6}	1.02×10^{-8}	3.65×10^{-3}	4.09×10^{-6}	891.3
	10	7.53×10^{-6}	5.91×10^{-9}	3.01×10^{-3}	2.36×10^{-6}	1274.8

* unit is (Std cc)(cm)/(sec)(cm^2)(cm Hg)

** unit is (Std cc)/(sec)(cm^2)(cm Hg)

behavior of the liquid film. In fact, at the end of the longest run with Na_2SO_3, when the film was opened for inspections, patches of yellow precipitates were observed on the film, indicating that there may have been irreversible alterations to the liquid membrane.

During these experiments, we faced the problem of occasional condensation of water on the active area of the film, mostly on the sweep side. This was revealed when the cell was opened at the end of each run, and the condition of the membrane inspected. The presence of this water can alter the effective behavior of the liquid film. More stringent humidity control was therefore introduced during the latter part of the investigation.

Based on further preliminary studies, a qualitative appraisal of the different membranes were made. The results are presented in Table 5.2-3. The merits of various ILM-s are decided primarily on their SO_2-CO_2 selectivities, and also on their SO_2 fluxes. Such a preliminary screening was used to eliminate some of the less promising candidate liquid membranes from further considerations at the beginning. It must be remembered, however, that some of the conclusions in Table 5.2-3 are strongly subject to the experimental conditions employed, most notably the temperature. For example, had the experiments been conducted at higher temperatures, the sulfolane and sulfolene membranes might have exhibited much better permeation properties. Also, the EDTA solubilities in water would be much higher at higher temperatures, and higher chelate concentrations could have improved their performances. Besides, the metal chelates are considered to be good candidate membranes for NO separation.

Table 5.2-3 : Preliminary Screening of Membrane Liquids

Nominal feed composition (dry): 5000 ppm SO_2, 12% CO_2, 1.8% O_2, bal. N_2

Temperature : 25^oC

Liquid	Average Permeability * (Q_i) SO_2	CO_2	Typical selectivity SO_2/CO_2	Merit as a membrane
Water	1.5×10^{-5}	2.1×10^{-7}	75	Excellent
1N $NaHSO_3$	1.5×10^{-5}	1.5×10^{-7}	100	Excellent
1N Na_2SO_3	2.0×10^{-5}	1.4×10^{-7}	140	Excellent
15% w/v Sulfolene	7.0×10^{-6}	1.6×10^{-7}	44	Tolerable**
7.5% w/v Sulfolene	1.0×10^{-5}	1.9×10^{-7}	53	Tolerable**
12% w/v Sulfolane	1.1×10^{-5}	2.0×10^{-7}	55	Tolerable**
0.02M Fe^{3+}EDTA	1.0×10^{-5}	1.8×10^{-7}	56	Tolerable
0.02M Fe^{2+}EDTA	6.8×10^{-6}	1.7×10^{-7}	40	Tolerable

* unit $(cm^3)(cm)/(sec)(cm^2)(cm\ Hg)$

** Their permeability and selectivity values are tolerable for a membrane for SO_2-CO_2 separation but the possibility of organic pollution of the atmosphere due to their finite vapor pressures disqualify them as practical membranes.

5.3 Detailed SO_2 permeability studies of selected liquid membranes

Detailed permeabilities of SO_2, CO_2, N_2 and O_2 were experimentally measured for water, solutions of $NaHSO_3$, Na_2SO_3, Fe^{2+}EDTA, and Fe^{3+}EDTA for three levels of feed concentrations. These results are compiled in Table 5.3-1. The permeability values are based on a value of $\tau_M = 7.0$. As mentioned before, there were variations in feed SO_2 concentration from day to day, and so only the ranges are reported in the table for both feed and sweep. The permeability values reported are accompanied by the number of data points on which the data are averaged. The selectivities are based on average permeabilities.

Since the O_2 and N_2 permeation rates were very low (particularly since the feed pressure was atmospheric, and the active permeation area was very small), their concentrations in the sweep outlet streams were sometimes too low to be quantified, specially for feed concentration level #3. Their permeabilities under such situations have therefore been omitted. Besides, the inlet sweep helium gas itself frequently contained O_2 and N_2 in concentrations similiar to those produced by permeation. In order to overcome this problem, one set of experiments was carried out with the best research grade helium commercially available (99.9999%, Matheson). Most of the O_2-N_2 permeability values in Table 5.3-1 are based on these experiments. The experimental data reproducibilities were generally within about $\pm$10%.

It is quite clear from the numbers in Table 5.3-1 that the SO_2 permeability varies a lot with conditions, but it seems less sensitive to the membrane- liquid, and more sensitive to the feed SO_2 concentration level. At

Table 5.3-1 : Detailed Experimental Permeablities at 25°C

SO_2 concn. range ppm		Permeabilities*/No. of data				Selectivities**		
Feed	Sweep	SO_2 x10^6	CO_2 x10^8	N_2 x10^8	O_2 x10^8	S/C	C/N	S/N
Membrane: Water								
4100-5400	100-400	15.2/13	20.5/11	1.6/4	4.9/4	74	13	962
1900-2500	15-40	14.4/5	18.3/5	1.3/3	-	79	14	1106
380-610	13-53	39.6/4	22.5/4	1.0/3	-	176	22	3872
Membrane: 1N $NaHSO_3$								
4200-4700	185-495	14.8/10	14.9/11	0.3/2	1.3/2	99	50	4950
2080-2180	100-225	14.4/3	11.3/3	0.9/3	34.5/3	128	13	1664
350-585	50-70	28.7/3	14.1/3	-	-	204	--	--
Membrane: 1N Na_2SO_3								
4440-5500	120-190	19.6/14	14.2/10	0.6/8	2.9/7	138	25	3450
1920-2015	30-110	13.3/3	11.2/3	0.9/3	21.4/2	119	13	1547
340-560	60-100	43.1/2	22.7/2	-	-	190	--	--
Membrane: 0.02M Fe^{3+}EDTA (pH = 7.2, adjusted)								
4400-5500	95-525	11.6/13	18.2/12	0.8/12	20.0/5	64	24	1536
1900-2250	150-350	27.8/3	17.7/3	0.3/2	14.0/2	157	49	7693
350-375	85-90	39.3/2	20.0/2	-	-	197	--	--
Membrane: 0.02M Fe^{3+}EDTA (pH = 1.7, unadjusted)								
4600	180	10.1/2	18.0/2	-	-	56	--	--
Membrane: 0.02M Fe^{2+}EDTA (pH = 7.1, adjusted)								
4660	110	6.8/1	16.8/1	-	-	41	--	--
2090	56	8.0/1	16.6/1	-	-	48	--	--

* average values, based on τ = 7.0; unit: $(cm)^3(cm)/(sec)(cm^2)(cm\ Hg)$
** S/C: SO_2-CO_2 ; C/N: CO_2-N_2 ; S/N: SO_2-N_2

500 ppm SO_2 level, the SO_2 permeability is 2-3 times higher than that at 5000 ppm SO_2 level, for almost all of the membranes. The SO_2 permeabilities in the middle concentration level (~2250 ppm) is, however, found to be similar (except for Fe^{3+}EDTA) to those at around 5000 ppm level.

At around 5000 ppm level, the SO_2 permeabilities through water and 1N $NaHSO_3$ show basically similar values, whereas for 1N Na_2SO_3, it is more, and for the other membranes, it is less. It is the lowest for Fe^{2+}EDTA. At 500 ppm SO_2 level, Na_2SO_3 membrane gives the highest SO_2 permeability, closely followed by water and Fe^{3+}EDTA. In case of Fe^{3+}EDTA, pH adjustment does not seem to have any appreciable effect on SO_2 permeability. Although we had observed earlier some instability in the results for Na_2SO_3 at high SO_2 concentration, at the lower SO_2 concentrations, no such instability was found.

Permeability of CO_2 decreases as one goes from water to $NaHSO_3$ or Na_2SO_3, presumably from salting out effect. For Fe^{3+} or Fe^{2+}, the permeabilities are similar to that in water since the chelate concentrations are too low. The N_2 permeability is highest for water, and it decreases for the other membranes, as expected. For O_2, however, it is very curious that as feed SO_2 concentration increased, the O_2 permeability increased significantly for at least two cases. The reasons are not clear.

In terms of SO_2-CO_2 selectivity, 1N $NaHSO_3$, 1N Na_2SO_3, and 0.02M Fe^{3+} EDTA are all excellent liquid membranes. Pure water itself is highly selective, the selectivity improves drastically as feed SO_2 concentration decreases. The CO_2-N_2 selectivities are usually around 15-20. Two values reported in Table 5.3-1 which are close to 50 may be caused by experimental

uncertainties.

The results with water are most interesting. This seems to be one of the rare situations where the solvent itself, without any carrier, constitutes a good enough membrane. Further, the solvent itself facilitates SO_2 transport significantly through HSO_3^- formation in the liquid membrane. One ought also to realize that in the HFCLM mode, the pure water membrane would eliminate the need for any humidification of the gas streams and make the process very simple.

In general, we can conclude that the SO_2 permeabilities at low feed concentrations are found to be higher for all the membranes, indicating strong facilitation. However, the trend is not very clear at the mid-level feed composition. The SO_2 permeabilities are higher for salt solutions than for pure water, although the difference is not very high. The CO_2 permeabilities are found to be reasonably constant with feed concentration and with membranes, indicating that CO_2 transport across the membrane is not facilitated. Similar conclusions were reported by Teramoto et al. (1978) for simultaneous absorption of SO_2 and CO_2 in aqueous solutions. The O_2 and N_2 permeabilities do not appear to show any trend, and indeed, as pointed out above, the experimental accuracies are sometimes questionable, especially when the sweep outlet concentrations were as low as a few hundred ppm for O_2 or N_2.

In Table 5.3-2, some of the present experimental permeabilities are compared with values for other liquid membranes reported in literature (Walker et al., 1985). The first four rows in Table 5.3-2 represent literature values, and the rest are from the present work. The SO_2 permeability, actual SO_2 flux,

Table 5.3-2 : Comparison of Present Experimental Permeabilities with Literature Values

Membrane	Temperature ^{o}C	Q_{SO_2} **	Q_{CO_2}	SO_2 flux* / driving force	Selectivity SO_2-CO_2
Cabosil, PEG and HEC on Solvinart [1]	100	-	-	3.2×10^{-3}	14
Polyvinylidene fluoride + 18% sulfolene [1]	24	4.3×10^{-8}	2.0×10^{-10}	1.7×10^{-5}	215
50% PEG in poly-acrylate on Celgard [1]	25	5.2×10^{-7}	1.3×10^{-8}	4.2×10^{-4}	40
Copolymer of poly (oxyethylene) glycol carbonate and poly-carbonate on silicone rubber [1]	--	4.0×10^{-7}	4.8×10^{-9}	--	83
Water in Celgard @ 5000 ppm SO_2	25	1.5×10^{-5}	2.1×10^{-7}	3.3×10^{-4}	74
Water in Celgard @ 500 ppm SO_2	25	4.0×10^{-5}	2.3×10^{-7}	8.5×10^{-4}	176
1N $NaHSO_3$ in Celgard @ 5000 ppm SO_2	25	1.5×10^{-5}	1.5×10^{-7}	3.2×10^{-4}	99
1N $NaHSO_3$ in Celgard @ 500 ppm SO_2	25	2.9×10^{-5}	1.4×10^{-7}	6.1×10^{-4}	204
1N Na_2SO_3 in Celgard @ 5000 ppm SO_2	25	2.0×10^{-5}	1.4×10^{-7}	4.2×10^{-4}	138
1N Na_2SO_3 in Celgard @ 500 ppm SO_2	25	4.3×10^{-5}	2.3×10^{-7}	9.2×10^{-4}	190

* unit : $(cm^3)/(sec)(cm^2)(cm\ Hg)$
** unit: $(cm^3)(cm)/(sec)(cm^2)(cm\ Hg)$
[1] : cited in Walker et al. (1985)

and SO_2-CO_2 selectivity values are shown. The table indicates that the aqueous-based liquid membranes explored here exhibit remarkably high SO_2 permeabilities and higher selectivities compared to other types of liquid and polymeric membranes. An important advantage for aqueous membranes is the facilitation at lower SO_2 concentrations. If we consider SO_2-CO_2 selectivity, we can see that its value for 1N $NaHSO_3$ @ 500 ppm SO_2 obtained here is comparable to the best literature value of 215 for PVDF with 18% sulfolene, but the former has 35-40 times more SO_2 flux. On the other hand, although the highest SO_2 flux reported in literature, 3.2×10^{-3} at 100°C, is more than the highest flux obtained in the present work (9.2×10^{-4}, at 25°C), the latter is 13-14 times more selective for SO_2. Thus the membranes explored in the present investigation have very good prospects for successful SO_2 removal, if they can be used in a stable liquid membrane structure like a HFCLM permeator.

Next, we make an attempt to compare the theoretical predictions of SO_2 flux with the experimental data. As mentioned before, two models have been used. First, we compare the predictions from the two models in Table 5.3-3. The table compiles the predicted facilitation factors for different SO_2 feed and sweep partial pressures, and for different Na^+ concentrations. For water (Na^+ concentration zero), the two models predict practically identical fluxes. As Na^+ concentration increases, however, the equilibrium approximation predicts much higher facilitation than the NEBLA. As Roberts and Friedlander (Roberts and Friedlander, 1980b) had pointed out, NEBLA may be a much better approximation for SO_2 system.

In Table 5.3-4 we present a comparison between experimental permeabilities and those predicted by NEBLA. The experimental values are

Table 5.3-3 : Predicted Facilitation Factors

Total $[Na^+]$ Normality	SO_2 concentration ppm		Facilitation factor	
	Feed	Sweep	Equilibrium approximation	NEBLA
0.0	5000	200	2.22	2.21
	2500	125	3.03	3.03
	500	75	5.84	5.83
0.1	5000	200	0.78	0.77
	2500	125	0.89	0.86
	500	75	1.98	1.92
0.5	5000	200	1.71	1.48
	2500	125	4.8	3.8
	500	75	35.1	24.3
1.0	5000	200	5.4	4.0
	2500	125	15.7	9.7
	500	75	112.	59.
3.0	5000	200	26.2	13.6
	2500	125	75.	31.
	500	75	511.	191.

Table 5.3-4 : Comparison of Experimental Permeabilities with Preliminary Predictions for SO_2

Permeability unit : $(cm^3)(cm)/(sec)(cm^2)(cm\ Hg)$

Membrane	Data		Prediction[a]	
	SO_2 conc. ppm	average SO_2 permeability	SO_2 conc. ppm	average SO_2 permeability
Water	4100-5400	15.2×10^{-6}	4750	18.7×10^{-6}
	1900-2500	14.4×10^{-6}	2200	25.5×10^{-6}
	380-610	39.6×10^{-6}	495	43.1×10^{-6}
1N Na^+ [b]	4440-5400	19.6×10^{-6}	4920	24.5×10^{-6}
	1920-2015	13.3×10^{-6}	2130	49.7×10^{-6}
	340-560	43.1×10^{-6}	470	235×10^{-6}

(a) Based on NEBLA (Roberts, 1979)
(b) Data for Na_2SO_3 membrane

Basis : SO_2 solubility : 1.21 gm mole/(lit)(atm)

SO_2 diffusivity : 1.60×10^{-5} cm^2/sec

averages over different concentration ranges, whereas the prediction is given for one typical value. The comparisons are quite good for both water as well as 1N Na^+ membrane at 5000 ppm SO_2 feed, where the facilitations are generally lower. The comparisons are reasonably good for water membrane at 500 ppm SO_2 level also (as mentioned before, we do not have an explanation for the discrepancy at the 2500 ppm level). However, the difference between NEBLA predictions and experimental values are very large for the Na^+ membranes, especially for 500 ppm SO_2 feed, when the facilitation is expected to be considerable (of the order of 100). There are two possible explanation for this : one is that NEBLA prediction may not be entirely correct, and the other is that there may be error in the experimental data itself. Since NEBLA has been shown to be reasonably accurate in low SO_2 concentrations (Roberts and Friedlander, 1980b; Roberts, 1979), our attention was focused towards the latter possibility, and that brought in an entire new dimension to our data analysis.

In liquid membrane permeation from a gaseous feed to a gaseous sweep, one always tacitly assumes that the membrane permeability can be obtained from experimental permeation rate data. An assumption, which is never mentioned explicitly, is that the gas phase mass transfer resistances are almost certainly negligible compared to that of the liquid membrane. If this were not the case, however, the experimental mass flux will always underpredict the true species permeability because of the gas phase mass transfer resistances. In the present case, since SO_2 is such a highly permeable species, and the ILM thickness is so small, gas phase resistances may become relatively important. Although in one set of experiments with 1N $NaHSO_3$ and @5000 ppm feed SO_2 concentration, a two-fold increase in feed and/or sweep flow rate did not show

any difference in experimental permeability of SO_2, we felt that we should look more closely at our system.

The first difficulty we faced was to estimate within reasonable confidence the gas phase mass transfer coefficients. The flow path in the test cell was such that the cross sectional area of flow increased from inlet to the middle of the cell, and then decreased again. The first task in estimating gas phase mass transfer coefficient would be to replace the actual geometry with a hypothetical rectangular mass transfer area with the same flow length and the same total area as the actual cell. Fixing the flow length at 1.27 cm, and equating the mass transfer areas, one can calculate the width 'w' of this hypothetical rectangular cross section from $[\pi/4\ (1.27)^2] = [w \times 1.27]$ which gives w = 1.0 cm. The depth of each half cell (H_p) was 0.08 cm.

Once this cross section is assumed, one can adopt the treatment in Skelland (1974) whereby mass transfer coefficients can be evaluated for flow through flat parallel channels. First one can calculate the Reynolds Number, Re ($= 2H_p\bar{v}\rho/\mu$) for any gas velocity $\bar{v}$, as well as the Schmidt Number Sc. Using values of ρ,μ, and diffusivity from various sources (Perry and Chilton, 1973), and using a typical gas flow rate of 20 ml/min, one can calculate Re = 4.7 and Sc = 1.0. Based on a flow length of 1.27 cm, one can calculate the gas phase mass transfer coefficient k_g for SO_2 from Figures 5.17 and 5.18 of Skelland (pg 177). It turns out we can use constant value of k_g which is about 0.1 in unit of $(cm^3)/(sec)(cm^2)(cm\ Hg)$. We must emphasize that there is no way to corroborate the applicability of this correlation to the present situation. Arguably, the assumptions inherent in the analysis (fully developed parabolic velocity- profile, and fully developed concentration profile) plus the use of

equivalent cross section may not be truly applicable in the present experimental condition. We still used the correlation, however, because we do not know of any correlation which would be more appropriate.

One can similarly use a mass transfer coefficient for the liquid membrane k_M as follows:

$$k_M = D_{SO_2} H_{SO_2} (\varepsilon_M / t_M \tau_M) (1 + F) \qquad (5.3\text{-}1)$$

where F is the facilitation factor. Knowing D_{SO_2} and H_{SO_2}, one can calculate k_M for different arbitrary values of F. This k_M can be compared to the k_g value, and one can calculate the fraction of the total mass transfer resistance which is actually offered by the liquid membrane. This last quantity, f, can be defined as

$$f = k_M^{-1} / K_0^{-1} = k_M^{-1} / [k_M^{-1} + 2k_g^{-1}] \qquad (5.3\text{-}2)$$

where K_0 is the overall mass transfer coefficient, and is the quantity that one would obtain experimentally from total SO_2 flux. The factor 2 in the above equation is based on the assumption that feed and sweep sides have the same value of k_g.

A value of f close to 1.0 points towards negligible gas phase resistance, whereas as f decreases from 1 the gas phase resistance becomes more and more important, and the apparent liquid membrane permeability obtained from experiment (proportional to K_0) will be less than the true liquid membrane permeability (proportional to k_M). Using D_{SO_2} and H_{SO_2} values

for water, and the above estimated value of k_g, one can show (Table 5.3-5) that the gas phase resistances are relatively unimportant (less than 10% error) till about F = 10 (which is the case for water membrane, and for salt membrane at high feed SO_2 concentration). On the other hand, as F increases to 50-100 (which is the case for low feed SO_2 concentration, especially for salt membrane), the value of f reduces quite substantially from 1.0, and the apparent experimental permeability of the liquid membrane would be much smaller than the true liquid membrane permeability.

In an attempt to analyze the present data, one can take the permeability value of 235×10^{-6} $(cm^3)(cm)/(sec)(cm^2)(cm\ Hg)$ from Table 5.3-4 as predicted by NEBLA. This value should be multiplied by $(\varepsilon_M/t_M\tau_M)$ to yield a value of $k_M = 5.02 \times 10^{-3}$. One can evaluate the quantity $K_0 = [k_M^{-1} + 2k_g^{-1}]^{-1}$ which comes out to be 4.53×10^{-3}, which when divided by $(\varepsilon_M/t_M\tau_M)$ yields a permeability value of 212×10^{-6}. When compared to 43×10^{-6} which is the experimentally obtained apparent permeability, this comparison is still not good. If estimates of k_g were lower, the permeability from K_0 and the apparent permeability would be closer. Before more independent studies are carried out on gas phase mass transfer coefficients under similar experimental conditions, one should probably reserve judgement on the comparison between experimental data and prediction.

We will conclude this section of SO_2 permeability studies by reporting the ILM permeability measurement experiments carried out at 75°C. We had encountered severe measurement problems due to condensation in lines, high corrosion, film liquid evaporation etc. We were able to make a few permeability measurement at 75°C through the ILM containing pure water and 1N

Table 5.3-5 : Effect of Gas Phase Mass Transfer Resistance for SO_2 Permeation through ILM

Overall mass transfer resistance	=	Feed side boundary layer resistance	+	ILM mass transfer resistance	+	Sweep side boundary layer resistance
K_0^{-1}	=	k_{gf}^{-1}	+	k_M^{-1}	+	k_{gs}^{-1}

Assuming $k_{gf} = k_{gs} = k_g$

$$K_0^{-1} = k_M^{-1} + 2\,k_g^{-1}$$

F	Percent of total resistance offered by the liquid membrane $f = k_M^{-1} / K_0^{-1}$ *
0	99.4%
3	97.6%
10	93.6%
50	76.0%
100	61.5%

* based on $k_g = 0.1\ (cm^3)/(sec)(cm^2)(cm\ Hg)$

$NaHSO_3$ solution. At high temperature, it was extremely difficult to reproduce any given set of results. Due to chemical reactions inside the humidifier prior to the test cell and elsewhere in the permeability measurement loop, even a stable feed composition was difficult to achieve. It therefore appears that the present SO_2 permeability measurement technique using ILMs is rather unsatisfactory for high temperatures.

The permeability values are reported for SO_2 and CO_2 in Table 5.3-6. Those for O_2 and N_2 are not being reported since they appeared totally out of range. Comparing the permeability values of SO_2 and CO_2 at 75°C with those obtained at 25°C (Table 5.3-1), we see that SO_2 permeability values decreased considerably at high temperature whereas CO_2 permeability increased. We think that these data are highly unsatisfactory suggesting the need for alternate measurement techniques.

5.4 Detailed NO permeability studies of selected liquid membranes

The experimental permeability values at 25°C of nitric oxide, N_2, CO_2 and O_2 for various liquids in the ILM form are presented in Table 5.4-1. As pointed out in earlier sections, there was considerable variation in permeabilities and selectivities from batch to batch. However, the NO permeabilities for such liquid membranes freshly prepared in Fe^{2+}EDTA-based liquids, particularly those not exposed to ambient atmosphere, were consistently higher. As the age of the solution increased, the permeability decreased.

In order to study the statistical nature of this variation, we stored

Table 5.3-6 : Experimental Permeabilities at 75°C

Dry feed gas composition : 5000 ppm SO_2, 12% CO_2, 1.8% O_2, balance N_2
SO_2 concentration range in feed* : 1300 - 2500 ppm
SO_2 concentration range in Sweep: 20 - 60 ppm

Membrane	Permeability x 10^{-7}		Average Permeability x 10^{-7}	
	SO_2	CO_2	SO_2	CO_2
Water	2.12	--		
	--	4.33	2.19	4.64
	2.08	3.47		
	2.37	6.13		
1 N $NaHSO_3$	1.33	3.58		
	4.36	--		
	2.18	--		
	3.06	4.13	2.64	3.59
	1.44	3.06		
	4.96	--		
	1.14	--		

* Concentration of SO_2 in feed after the humidifiers.
Permeability values are expressed in $cm^3.cm/s.cm^2.cm$ Hg
Besides SO_2 and CO_2 the feed mixture also contained O_2 and N_2. However, the concentration measurement was not dependable.

Table 5.4-1 : Nitric Oxide Permeabilities

Nominal Feed Concentration : 450 ppm Nitric Oxide (NO)

Membrane	Feed Species	Batch #	Effective Permeabilities[1] NO	N_2	CO_2	O_2	Selectivity NO/N_2	NO/CO_2
Water	NO,N_2	1	4.72×10^{-7}	2.32×10^{-7}			2.03	-
		2	4.54×10^{-7}	2.32×10^{-7}			1.96	-
		3	7.91×10^{-7}	2.63×10^{-7}			3.01	-
$Fe^{2+}EDTA$ (0.01M)	NO,N_2	1	1.14×10^{-5}	2.49×10^{-7}			45.6	-
		2	1.29×10^{-5}	2.59×10^{-7}			49.9	-
		3	1.17×10^{-5}	2.59×10^{-7}			45.1	-
		4	9.50×10^{-6}	2.70×10^{-7}			35.2	-
		5	7.12×10^{-6}	2.66×10^{-7}			26.8[2]	-
		6	7.66×10^{-6}	1.79×10^{-7}			42.9	-
		7	7.69×10^{-6}	1.66×10^{-7}			46.3	-
$Fe^{2+}EDTA$ (0.01M)	NO,N_2 CO_2	1	2.30×10^{-5}	2.39×10^{-6}	9.48×10^{-6}		9.7	2.43
		2	2.04×10^{-5}	2.30×10^{-6}	9.46×10^{-6}		8.9	2.15
$Fe^{2+}EDTA$ (0.01M)	NO,N_2 CO_2,O_2	1	1.70×10^{-5}	*	*	*		
		2	8.55×10^{-6}	*	*	*		
		3	4.88×10^{-5}	*	*	*		
		4	1.23×10^{-5}	3.65×10^{-7}	7.68×10^{-6}	*	33.9	1.6
		5	1.08×10^{-5}	2.19×10^{-6}	1.16×10^{-5}	3.75×10^{-6}	4.9	0.92
		6	1.01×10^{-5}	2.19×10^{-6}	1.16×10^{-5}	3.75×10^{-6}	4.6	0.87
		7	6.30×10^{-6}	5.75×10^{-7}	7.43×10^{-6}	*	11.0	0.85
1N Na_2SO_3	NO,N_2 CO_2,O_2	1	3.50×10^{-6}	3.98×10^{-7}	5.15×10^{-6}	1.55×10^{-6}	8.8	0.68
		2	5.07×10^{-6}	5.58×10^{-7}	6.69×10^{-6}	5.52×10^{-6}	9.1	0.76
		3	4.00×10^{-6}	4.98×10^{-7}	4.59×10^{-6}	1.59×10^{-6}	8.0	0.87
		4	4.73×10^{-6}	5.90×10^{-7}	4.85×10^{-6}	3.11×10^{-6}	8.0	0.98

[1] = (Permeation rate)/(Area)(Δp), unit $(cm^3)/(sec)(cm^2)(cm\ Hg)$.
[2] Feed Nitric Oxide Concentration is 1000 ppm.
* Concentration measurement not dependable.

the same batch of freshly prepared Fe^{2+}EDTA solution in five separate bottles under inert atmosphere, with each bottle containing three films. In general, the first film taken out of any bottle consistently showed the highest value of NO permeability (the data are presented in the first five rows for EDTA membrane). Besides, although solutions in bottles #1-5 were prepared at the same time, and each of the first films from each bottle was used at a different time, their NO permeabilities were close. This indicates that the age of the solution (as long as it is stored under inert atmosphere) had less of an effect than the exposure to atmospheric oxygen.

Quite a few NO permeability measurements were carried out with a gas mixture blend of NO, O_2, CO_2 and N_2. It is important to find out whether the presence of O_2 in the feed mixture affects the experimental results to any significant level. Oxygen is expected to affect NO permeation in two ways: firstly, the presence of O_2 may change the liquid membrane chemically, and thereby change the NO permeability. Secondly, O_2 itself may react with NO to change the NO concentration in the gas phase. Since both phenomena can occur at the same time, it may become difficult to study their effects separately.

The gas phase reaction of O_2 and NO is an irreversible one, and the extent to which NO is consumed in the process will depend strongly on the residence time of the gases inside the system before the gas stream composition is analyzed. The residence time depends on the total volume of the system (from the point O_2 and NO come in contact with each other, up to the point where the gas stream composition is monitored), including the volumes of the gas lines, the humidifiers, and the modules. It also depends obviously on the gas stream flow rate.

The reaction has been studied by various investigators. England and Corcoran (1975) have reported a reaction rate constant of 1.46×10^4 (l^2 $mole^{-2}$ s^{-1}) for a reaction which is second order in NO concentration, and first order in O_2 concentration. They also reported that moisture does not have any appreciable effect on this oxidation.

For typical NO concentration of 500 ppm ($\simeq 2 \times 10^{-5}$ mole/l) and O_2 concentration of 1.8% ($\simeq 8 \times 10^{-4}$ mole/l) the initial reaction rate would be $= (1.46 \times 10^4) \times (2 \times 10^{-5})^2 \times (8 \times 10^{-4}) = 5 \times 10^{-9}$ mole/(l)(sec). Assuming, for a rough estimate, that this rate is constant and using a residence time of 100 sec through the system, one can calculate a reduction of NO concentration due to oxidation of about 10 ppm, which is about 2% of the feed concentration. The NO permeability measurement is therefore not likely to be affected appreciably by the presence of O_2, except, of course, for the effect of O_2 on the membrane itself, e.g. Fe^{2+}EDTA.

The experimental permeability value of NO was again measured at room temperature and at a higher temperature of 76°C through various immobilized membrane liquids. Note that oxygen as well as CO_2 were not present in the feed mixture. The permeabilities, effective permeabilities and selectivities of NO and N_2 are shown in Table 5.4-2. The experiments with water and 0.01M Fe^{2+}EDTA solution at 25°C are repeated here. Except for N_2 permeability through 0.01M Fe^{2+}EDTA solution, they are generally in good agreement with the previous results.

At- higher temperature the permeability of NO through water increased

Table 5.4-2 : Nitric Oxide Permeabilities

Nominal Feed Concentration : 450 ppm Nitric Oxide (NO)

Membrane	Feed Species	Temp °C	Batch #	Effective[1] Permeability NO	Effective[1] Permeability N_2	Permeability[2] NO	Permeability[2] N_2	Selectivity NO/N_2
Water	NO,N_2	25	1	8.07×10^{-7}	2.34×10^{-7}	3.77×10^{-8}	1.10×10^{-8}	3.45
			2	7.64×10^{-7}	2.08×10^{-7}	3.57×10^{-8}	0.97×10^{-8}	3.68
		76	1	2.11×10^{-6}	-	9.85×10^{-8}	-	
			2	1.56×10^{-6}	-	7.30×10^{-8}	-	
			3	1.57×10^{-6}	4.02×10^{-7}	7.36×10^{-8}	1.88×10^{-8}	3.87
			4	1.53×10^{-6}	3.56×10^{-7}	7.15×10^{-8}	1.68×10^{-8}	4.25
$Fe^{2+}EDTA$ (0.01M)	NO,N_2	25	1	2.33×10^{-5}	-	10.90×10^{-7}	-	
			2	1.36×10^{-5}	1.55×10^{-7}	6.38×10^{-7}	7.23×10^{-9}	88.2
			3	1.36×10^{-5}	1.37×10^{-7}	6.36×10^{-7}	6.39×10^{-9}	99.4
		76	1	1.22×10^{-5}	4.96×10^{-7}	5.70×10^{-7}	2.32×10^{-8}	24.5
			2	1.93×10^{-5}	4.95×10^{-7}	9.04×10^{-7}	2.32×10^{-8}	39.0
			3	1.36×10^{-5}	-	6.38×10^{-7}	-	
$Fe^{3+}EDTA$ (0.01M)	NO,N_2	25	1	2.30×10^{-6}	2.87×10^{-7}	1.07×10^{-7}	1.34×10^{-8}	8.0
			2	1.38×10^{-6}	3.33×10^{-7}	0.65×10^{-7}	1.56×10^{-8}	4.2
		75	1	2.21×10^{-6}	10.57×10^{-7}	1.04×10^{-7}	4.95×10^{-8}	2.1
			2	1.67×10^{-6}	6.74×10^{-7}	0.78×10^{-7}	3.15×10^{-8}	2.5

[1] (Permeation rate)/(Area)(Δp), unit $(cm^3)/(sec)(cm^2)(cm\ Hg)$.

[2] calculation based on a tortuosity value of 7.0,
unit $(cm^3)(cm)/(sec)(cm^2)(cm\ Hg)$

considerably but so did the permeability of N_2. Therefore, there is virtually no change in the values of selectivity between NO and N_2 at 25°C and at 76°C. The selectivities of NO and N_2 through 0.01 M Fe^{2+}EDTA solution at 25°C are higher than those determined earlier due to the lower permeability values of N_2 in the present case. However, the permeability of NO is not affected at the higher temperature of 76°C but that of N_2 increased about 3.5 times resulting in a lower separation factor of NO and N_2 at the higher temperature. The permeability of NO through Fe^{3+}EDTA solution was in general lower than that of Fe^{2+}EDTA solution and N_2 permeability through Fe^{3+}EDTA solution was considerably higher giving rise to a lower selectivity value for NO and N_2. There is no basis for this increased N_2 permeability. Since very few experiments have been done with Fe^{3+}EDTA solution, no firm conclusion can be drawn at this time.

Table 5.4-3 compares the experimentally observed NO permeabilities with those from theoretical approaches identified in section 4.3. The simple solution-diffusion permeation model of NO through pure water (eqn. 4.3-1b) predicts a value of effective permeability to be 3.26×10^{-7}. This is somewhat lower than the experimental values which range between $4.72 - 7.64 \times 10^{-7}$. The difference may be ascribed to the uncertainties in values of D_{NO} and H_{NO} (see Bhave and Sirkar (1986) for the corresponding problem in D_{N_2} and H_{N_2}).

The situation vis-a-vis the facilitated transport of NO in Fe^{2+}EDTA solution is less satisfactory. The equilibrium approximation predicts 60 times larger permeation rate while the NEBLA predicts 4.5 times lower permeation rate. Given the uncertainties in the values of the rate constants and other physical- properties, it appears that the NEBLA strategy is not far off.

Table 5.4-3 : Nitric Oxide Permeation; Theory and Experiment

Liquid Membrane	Effective[1] Permeability		Permeation Rate[2]		
	Expt.	Theory Eqn. (4.3-1b)	Expt.	Equilibrium Approx. Eqn. (4.3-3)	NEBLA Eqn. (4.3-6)
Water	4.72×10^{-7} (Table 5.4-1) 7.64×10^{-7} (Table 5.4-2)	3.26×10^{-7}			
0.01M $Fe^{+2}EDTA$			6.34×10^{-6}	4.06×10^{-4}	1.39×10^{-6}

[1] (Permeation rate)/(Area)(Δp), unit $(cm^3)/(sec)(cm^2)(cm\ Hg)$

[2] unit cm^3/sec

Basis for theoretical calculation:

Feed : 500 ppm NO (flow rate ~ 20 cm^3/min); Sweep : 12.5 ppm (flow rate ~ 40 cm^3/min); C_T = 0.01M; τ_M = 7; ε_M = 0.38; $t_m = 25 \times 10^{-4}$ cm; A_M = 11.27 cm^2; $D_{NO} = 2.5 \times 10^{-5}$ cm^2/sec (Takeuchi et al., 1977). $H_{NO} = 1.88 \times 10^{-3}$ gmol/lit. atm. (Andrews and Hanson, 1961). $K_{eq} = 10^7$ mol^{-1}; $k_{1N} \geq 6 \times 10^7$ mol^{-1} sec^{-1}; $k_{-1N} \geq 6$ sec^{-1} (all three values from Chang et al., 1983); $D_{AB} \sim 1.1 \times 10^{-5}$ cm^2/sec.

However, an exact solution ought to be pursued before arriving at more definite conclusions regarding the usability of various facilitated transport models.

5.5 Characteristics of HFCLM permeator modules

The detailed geometrical characteristics of each HFCLM permeator module used in the present study and its experimentally estimated effective liquid membrane thickness are presented in Table 5.5-1. To determine the effectve membrane thickness experimentally, pure CO_2 and/or pure N_2 permeation studies through water as a liquid membrane were carried out. As the permeabilities of these gases through water are well known, the effective liquid membrane thickness can be calculated using eqn. (4.5-10) and from the known permeation rate of CO_2 (or N_2) obtained experimentally. As the Table shows, modules A and B show very high d values. These values can only be explained in terms of accidental separation of feed fibers from the sweep fibers during the fabrication of the module. Module C shows a much more favorable value of d, and the number is close to what can be expected by a purely theoretical prediction (Majumdar et al., 1988). For other modules, the d values are reasonably good.

5.6 Extraneous factors affecting CLM separation

Qualitatively, the following are some of the factors that may possibly affect the separation process in CLM to different extents: (1) bulk gas phase and membrane pore mass transfer resistances; (2) feed/sweep or feed/vacuum flow patterns; (3) longitudinal diffusion inside the membrane phase; (4)

Table 5.5-1 : Characteristics of Permeator Modules

Module #	Effective Length	Fiber Diameter Inside/Outside	No.of Fibers Feed/Sweep	Mass Transfer Area	Effective Membrane Thickness	Area per Volume
	cm	cm x 10^{-4}		cm^2	cm	cm^2/cm^3
A	68.6	100/150	300/300	970	0.2591	48.5
B	36.0	200/250	90/90	254	0.2267	24.2
C	157.5	100/150	300/300	2227	0.0258	48.5
D*	157.5	100/150	300/300	2227	--	48.5
E	43.2	100/150	300/300	610	0.0123**	48.5
F	44.5	100/150	300/300	628	0.0719	48.5
G	63.5	240/290	120/120	694	0.0175	37.5

Area per Volume indicates the ratio of active membrane surface area to equipment volume

* This module was not well characterized; only two runs were made with this module.

**Value obtained from Guha (1989)

position of the membrane replenishment port; (5) the nature of the membrane pressurizing gas; (6) extent of water condensation in the gas lines; (7) for sweep mode, the amount of sweep gas permeated into the feed side. Item (1) will be considered later in detail. Item (2) is generally important in most membrane gas separation processes. Usually countercurrent flow pattern gives better separation.

At the gas-liquid interfaces, the membrane liquid may be considered to be at equilibrium with the gas it is in contact with at every location inside the permeator. The concentration in the membrane phase, therefore, will change not only across from feed fiber to the sweep fiber, but also along the module. For countercurrent operation, the permeant concentration in the membrane liquid phase is expected to be the highest in the feed inlet side of the module, and the lowest in the feed outlet side. For highly soluble SO_2, back diffusion along the module length may not be totally ruled out. For the same reason, the position of the membrane replenishment port may affect separation to some extent.

Another point to note is the possible diffusion of the dissolved gases in the shell liquid into the liquid reservoir. Pressurization of the membrane liquid reservoir with the feed gas itself will equilibrate the reservoir liquid with the feed composition, and the effect of this already equilibrated liquid entering the permeator module (to replenish lost membrane) will be different from the situation when the reservoir is pressurized with, for example, the sweep gas, or any other gas. (Ideally, therefore, it is desirable to pressurize membrane liquid in the reservoir and deliver it to the permeator by alternate means.)

The amount of water that is collected at the water separators at the feed/sweep outlets gradually increase with time. This water may act as a sink by continuously absorbing some gas species from the gases passing over it. The extent of this effect is not known at this time.

5.7 SO_2 separation by HFCLM permeator

We will first provide the preliminary SO_2 separation data. We will then speculate on the reasons behind the observed transfer coefficients. Since these speculations did not resolve the problem, alternate strategies were adopted by making better permeators and developing a complete numerical solution.

Preliminary SO_2 separation data

Preliminary separation results obtained with permeator module A and water CLM are shown in Table 5.7-1. Different sets of data indicate different configurations, e.g. changing the water entry point to the shell, vacuum runs with or without the moisture trap, exchanging the feed/sweep fiber sets, etc. The results show that excellent SO_2 removal rates can be achieved under high sweep to feed flow rate ratios. Note also that the actual transfer rates are much higher for higher feed flow rates, although the corresponding percent removal rates are low. There are two reasons for this. Firstly, for higher feed flow rates, the feed composition levels remain high, and hence the partial pressure driving force will be high. Secondly, higher flow rates through the given module reduce the fiber lumen mass transfer resistance, if

Table 5.7-1 : Preliminary SO_2 Separation Results for Water CLM

CLM permeator module A
Nominal feed SO_2 concentration = 5000 ppm
Temperature = 25°C
In sweep mode, flow pattern is countercurrent
In vacuum mode, vacuum is pulled from both ends

Set No.*	Run No.	Mode	Nominal flow rates (ml/min) Feed	Sweep	Vacuum (" Hg)	Percent SO_2 removed from feed
1	1	Sweep	40	80	-	50
2	1	Vacuum	20	--	29	78
3	1	Sweep	20	100	-	86
4	1	Vacuum	20	--	29	70
	2		20	--	29	60
5	1	Sweep	20	100	--	94
	2		40	100	--	79
	3		100	100	--	53
6	1	Sweep	40	100	--	78
	2		20	100	--	92
7	1	Sweep	20	100	--	90

* Different sets of runs mostly indicate different configurations

any, which should improve mass transfer rates. Run set numbers 4,5 and 6 were conducted with only enough interruption to change the configuration in between the sets. Total run time was about fourteen (14) days for these three sets. They demonstrate an exceptionally stable performance. For vacuum runs, vacuum was pulled from both ends, and the best removal rate was about 78%.

Some typical SO_2 separation data obtained with three different modules are presented in Table 5.7-2. Range of fractional removal is shown for both sweep and vacuum runs. The numbers indicate that excellent recoveries are possible in sweep mode if sufficient membrane area is available. For vacuum runs using the same modules, the recoveries are in general lower.

We have also studied the SO_2 transport through water CLM for various combinations of feed/sweep flow rates. As shown in Table 5.7-3, increase in gas flow rates increase the experimental mass transfer coefficients. One possible explanation is that the SO_2 transport is strongly affected by gas phase film transfer resistances. Note also that by increasing the flow rates, K_{expt} could be enhanced 5 to 6 times. The experiments shown in Table 5.7-3 were repeated once again. The results were found to be highly reproducible.

Preliminary speculations on SO_2 transfer rate in a CLM permeator

In a CLM permeator, gases flow through the hollow fiber lumina. The porous hollow fiber walls (called here the substrate) are also filled with stagnant gas phases (Majumdar et al., 1988). As a crude approximation, the overall mass transfer resistance can be expressed as the sum of the individual resistances as shown at the beginning of Table 5.7-4. The table also shows the

Table 5.7-2 : Typical CLM Results for SO_2 Separation

Temperature : 25°C
Feed Gas Composition (dry basis) : 5000 ppm SO_2, 1.8% O_2, 12% CO_2, bal N_2
Liquid Membrane : Water

Module	Membrane Area cm^2	Mode	Feed Flow Rate Range cc/min	Typical SO_2 Removal Rate
A	970	Sweep	20-100	60-90%
		Vacuum		50-70%
B	254	Sweep	20-40	55-65%
		Vacuum		25-35%
C	2227	Sweep	40-150	80-95%

Table 5.7-3 : Effect of Gas Phase Flow Rate on SO_2 Transport across HFCLM

Liquid membrane : Water
Module : C (length 157.5 cm, total contact area 2227 cm^2)
Nominal Feed concentration (dry) : 5000 ppm SO_2, 12% CO_2, 1.8% O_2, bal. N_2.
Temperature: 24°C

Flow rates Feed/Sweep cc/min	Flux $cm^3/(sec)(cm^2)$	Δp_{LM} cm Hg	K_{expt} $cm^3/(sec)(cm^2)(cm\ Hg)$	Percent SO_2 removed from
38.5/42.9	1.09×10^{-6}	0.1686	6.43×10^{-6}	75.3%
75.0/45.1	2.04×10^{-6}	0.1328	1.54×10^{-5}	72.6%
75.0/139.5	2.56×10^{-6}	0.1579	1.62×10^{-5}	91.1%
146.3/142.9	4.76×10^{-6}	0.1775	2.68×10^{-5}	86.9%

Table 5.7-4 : Correlations for Gas Phase Film Transfer Coefficients for CLM Permeators

Overall mass transfer resistance	=	Feed + Sweep boundary layer resistances	+	Feed + Sweep substrate resistance	+	CLM transfer resistance

Basis : Module C, length 157.5 cm, 300 fibers, 100 micron ID fibers.

Typical liquid membrane (water) transfer coefficient for SO_2 [1]
$= 1.36 \times 10^{-3}$ (cc)/(sec)(cm^2)(cm Hg)

Typical substrate coefficient = 6.50×10^{-3} (cc)/(sec)(cm^2)(cm Hg)[2]

Schmidt Number for SO_2-N_2 system = 1.02 [3]

Total gas flow rate cc/min V_g	Average gas velocity cm/sec v_g	Reynolds Number	k_g, cm^3/(sec)(cm^2)(cm Hg) Solution #1 [4]	Solution #2 [5]	Solution #3 [6]
20	14.15	0.122	1.36×10^{-5}	2.551	4.40×10^{-2}
40	28.30	0.244	2.72×10^{-5}	2.551	5.54×10^{-2}
100	70.74	0.609	6.78×10^{-5}	2.551	7.52×10^{-2}
1000	707.4	6.094	6.78×10^{-4}	2.551	1.62×10^{-1}

[1] based on ILM experimental value;

[2] based on slip flow regime, Rangarajan et al. (1984);

[3] system properties calculated from Perry and Chilton (1973);

[4] series type Graetz solution* : $k_g = 2V_g/(\pi L d_i N_T)$

[5] asymptotic Graetz solution* : $k_g = 3.656\ (D_g/d_i)$

[6] Sieder-Tate correlation : $k_g d_i/D_g = 1.86\ [d_i^2 v_g/LD_g]^{1/3}$ **

* Skelland (1974)

** Sieder and Tate (1936)

transfer coefficient values. The substrate transfer coefficients, which do not depend on the lumen flow rates, were obtained by first calculating the mean free path of SO_2 under the given conditions. It was found that 'slip flow' regime prevails. The corresponding transfer coefficient was calculated using the appropriate equations (Rangarajan et al., 1984).

There are various correlations available to predict film transfer coefficients for flow through tubes. Since the Reynolds numbers for the given situations are always low, laminar flow can be assumed. Values of k_g for three different correlations are shown in Table 5.7-4.

The k_g values in column 4 of Table 5.7-4 calculated using the series-type Graetz solution (Skelland, 1974):

$$Sh\ [= k_g d_i/D_g] = 0.5\ (d_i/L)\ Re\ Sc\ \Phi \qquad (5.7\text{-}1)$$

(where Sh, Re and Sc are Sherwood, Reynolds, and Schmidt Numbers, d_i and L are fiber inside diameter and length, respectively, D_g is gas phase diffusivity of SO_2) has a series type term Φ whose value for the given conditions is practically 1.0. The numbers reported in Table 5.7-4 clearly indicate that the lumen boundary layer coefficients from series-type Graetz solution are almost two orders smaller than the CLM transfer coefficient, and hence may control the mass transfer rates in the permeator. This, of course, assumes that the liquid membrane thickness is small and no other complications exist. For the given module dimensions, it can be shown, theoretically, that solution 1 should not be applicable. However, k_g values predicted from the other two correlations are too large (two to five orders of magnitude), and strangely,

only solution 1 can predict the experimental SO_2 separation data of Table 5.7-3 within the same order of magnitude (Table 5.7-5). The other two correlations would overpredict K_{expt} by orders of magnitude.

Some alternative explanations are as follows. The permeability of SO_2 is very high according to the ILM studies. In case of HFCLM, for a low gas flow rate, most of the SO_2 quickly disappears from feed at the entry region of the module. For the rest of the permeator length, the driving force for SO_2 transfer (Δp_{SO_2}) is quite small. Therefore, the amount of SO_2 transfer is little in the rest of the permeator length. However, K_{expt} is determined over the whole permeator length with overall $\Delta p_{SO_2,LM}$, and is therefore low. With a higher gas flow rate, more SO_2 can permeate through a larger length of permeator for essentially similar $\Delta p_{SO_2,LM}$ leading to higher K_{expt} (column 4, Table 5.7-3).

There is an additional possibility. Modules A and B have large values of effective membrane thickness, an order of magnitude larger than that of module C. Thus in modules A and B the values of K_{expt} should have been much lower if the membrane resistance was important. However, K_{expt} for all three modules are somewhat comparable. The reasons may lie in the structure of the contained liquid membrane in module C vis-a-vis that in modules A and B.

Permeator C had a large reservoir of liquid around the fiber bundle all along the permeator length. Along the length of a HFCLM permeator, there would be gradients in SO_2 and HSO_3^- ion concentrations. Inside the fiber bundle, the radial gradient is orders of magnitude larger than the longitudinal gradient - thus the longitudinal gradient may not be disturbed. However, the large pool

Table 5.7-5 : CLM SO_2 Separation : Experimental Data vs Prediction

Temperature : 25^oC
Feed Gas Composition (dry basis) : 5000 ppm SO_2, 1.8% O_2, 12% CO_2, bal N_2
Liquid Membrane : Water

Module	Permeant	Overall Mass Transfer Coefficients*	
		K_{expt}	K_o
A	SO_2	1.01×10^{-5}	9.76×10^{-6}
	CO_2	7.03×10^{-7}	7.58×10^{-7}
B	SO_2	3.12×10^{-5}	2.64×10^{-5}
	CO_2	7.11×10^{-7}	9.07×10^{-7}
C	SO_2	2.67×10^{-5}	2.06×10^{-5}
	CO_2	7.60×10^{-6}	5.89×10^{-6}

* Unit is $(cm^3)/(sec)(cm^2)(cm\ Hg)$

of liquid outside the fiber bundle will have its longitudinal gradient smeared easily. This would affect the concentration profiles in the membrane liquid inside the fiber bundle, reducing the mass transfer rate considerably. This is equivalent to considerable backmixing in the membrane liquid. The solution to the problem may be to have a module like C with low effective membrane thickness, but without any reservoir of membrane liquid around the fiber bundle in the permeator.

Additional SO_2 separation data with new permeators

Further separation experiments for SO_2-CO_2-N_2-O_2 mixtures were, therefore, carried out with two short permeators having very small amount of membrane liquid in the shell side. Experiments were made with only one of these permeator modules as well as with two modules in a series configuration. In the series configuration, the exit feed gas stream from one permeator was introduced as fresh feed to the other. However, pure helium sweep gas (for sweep mode of operation) or vacuum (for vacuum mode of operation) was applied to each permeator separately. It was anticipated that this would increase the partial pressure driving force of SO_2 across the contained liquid membrane and thereby increase the SO_2 removal efficiency. The series configurations are shown schematically in Figure 5.7-1.

Sulfur dioxide separation results from a feed mixture of SO_2-CO_2-N_2-O_2 under sweep mode of operation are presented in Table 5.7-6. Here, we have studied the separation behavior by varying the feed and the sweep gas flow rates. All the experiments have been carried out with pure water membrane in two short permeators in a series configuration. Note that these modules are

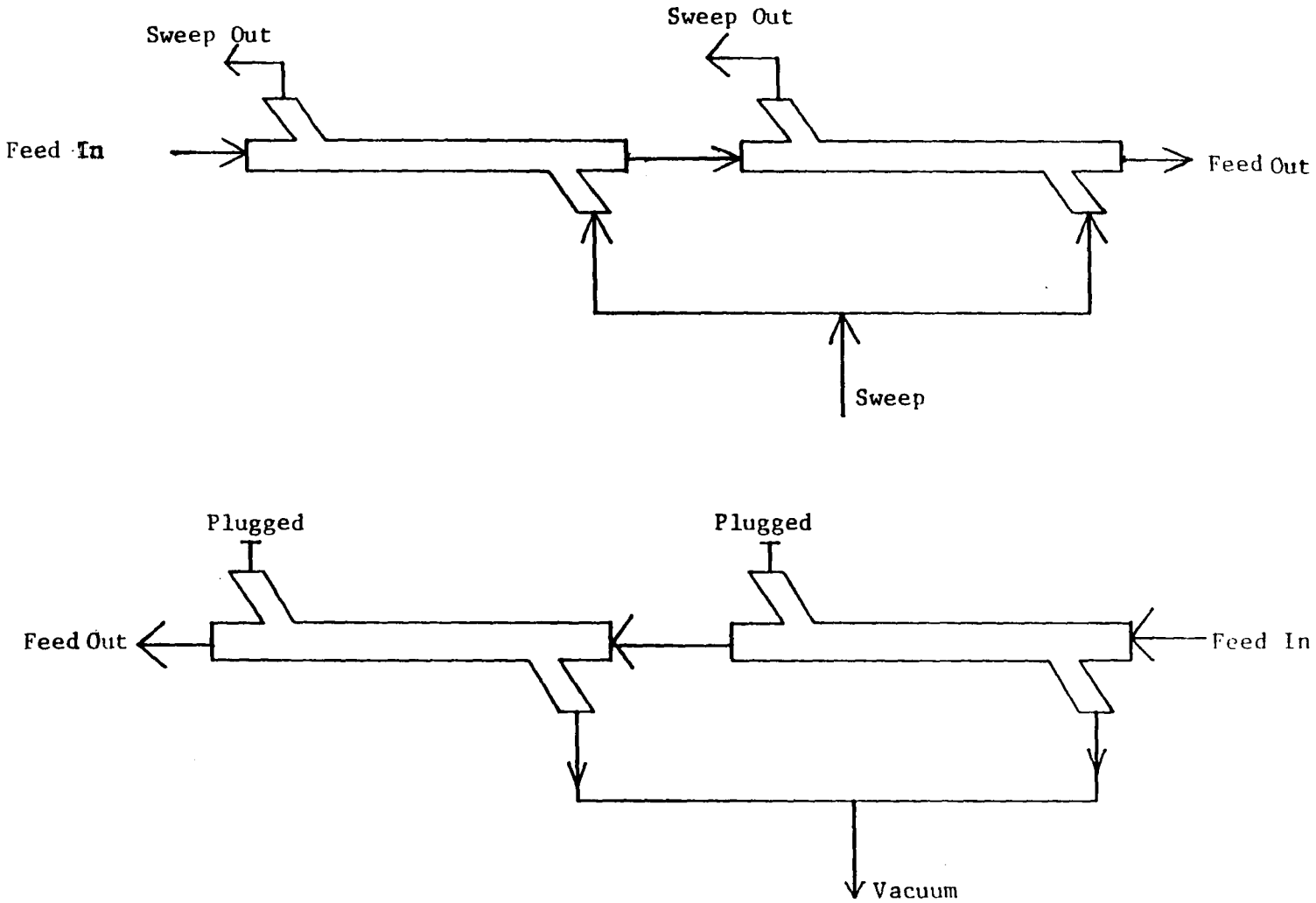

Figure 5.7-1: Sweep and Vacuum Modes of Operation with Two Short Permeators in Series

Table 5.7-6 : Separation of SO_2 with Two HFCLM Permeators Under Sweep Mode

Liquid membrane : Water

Module : E (no of fibers in each side: 300; length: 43.2 cm;
fiber od: 150×10^{-4} cm; total contact area 610 cm^2)

F (no of fibers in each side: 300; length 44.5 cm;
fiber od: 150×10^{-4} cm; total contact area 628 cm^2)

Nominal Feed concentration (dry) : 5000 ppm SO_2, 12% CO_2, 1.8% O_2, bal. N_2.

Temperature: 24°C

Flow rates Feed/Sweep* cc/min	Flux x 10^6 $cm^3/(s.cm^2)$ #E	#F	Δp_{LM} cm Hg #E	#F	K_{expt} x 10^5 $cm^3/(s.cm^2.cm\ Hg)$ #E	#F	Percent SO_2 removed #E	#E & F
72.7/114.9	7.21	1.69	0.2096	0.0616	3.44	2.75	72.6	90.2
72.7/225.8	8.35	1.10	0.2126	0.0381	3.93	2.89	84.1	95.5
72.2/290.3	8.89	0.97	0.2092	**	4.25	**	89.8	~100
144.8/223.9	14.49	3.57	0.2719	0.0873	5.33	4.09	69.4	88.1
201.3/223.9	15.74	5.07	0.3223	0.1280	4.88	3.96	58.4	77.8

* sweep flow rates are reported as total flow rates through modules E & F

** no SO_2 was detected in the purified stream by the GC column therefore, Δp_{LM} and K_{expt} calculations were not possible

substantially smaller than module C used in our earlier studies. For example, the membrane surface area of module E is only 27.4% of module C. The combined membrane area of modules E and F is about 55% of that of module C.

For each module we have calculated the SO_2 flux and the value of K_{expt} separately. As Table 5.7-6 shows, increase in gas flow rates increases the mass transfer coefficient. Very high removal of SO_2 was obtained in two small permeators. Interestingly, the percent removal of SO_2 is much higher in the first permeator compared to the second one even though the available membrane areas in both are similar. This shows that the second permeator is being grossly underutilized here. The first small permeator was able to reduce the SO_2 composition to a sufficiently low level which in turn drastically decreased the driving force for SO_2 permeation in the second permeator. Next set of sweep runs were made with a single short permeator (module F) only. The results are reported in Table 5.7-7. Note that, the mass transfer coefficient values are very high (in the order of $1x10^{-4}$ $cm^3/s.cm^2.cm$ Hg).

SO_2 separation experiments under vacuum mode of operation were made with a single short module as well as with two short modules in a series configuration. The results are reported in Table 5.7-8. The separation behavior for both cases are shown in Figure 5.7-2 where SO_2 concentration in the purified stream and the total percent SO_2 removal is plotted against the feed gas mixture flow rate. The removal rate increases considerably with a decrease in the feed gas flow rate. The performance of two permeators in series (modules E and F combined) is obviously better than a single permeator (module E). However, we do not see a dramatic increase in performance when two modules are used instead of one due to the reasons given earlier (i.e.,

Table 5.7-7 : Separation of SO_2 in a Short HFCLM Permeator

Liquid membrane : Water
Module : F (no of fibers in each side: 300; length 44.5 cm;
fiber od: 150×10^{-4} cm; total contact area 628 cm^2)
Nominal Feed concentration (dry) : 5000 ppm SO_2, 12.0% CO_2, 1.8% O_2, bal N_2
Temperature: 24°C

Mode (Run time in days)	Flow rate Feed/Sweep (cc/min)	SO_2 flux ($cc/s.cm^2$)	$K_{expt} \times 10^4$ ($cm^3/s.cm^2.cmHg$)	percent SO_2 removed from feed
Sweep (2)	60.1/166.2	5.21×10^{-6}	1.03	65.4
Sweep (2)	60.1/288.5	5.26×10^{-6}	1.05	66.0
Sweep (2)	103.6/288.5	6.95×10^{-6}	1.17	50.6

Table 5.7-8 : Separation of SO_2 in HFCLM Permeator Under Vacuum Mode

Liquid membrane : Water
Module : E (no of fibers in each side: 300; length: 43.2 cm;
fiber od: 150×10^{-4} cm; total contact area 610 cm^2)
F (no of fibers in each side: 300; length 44.5 cm;
fiber od: 150×10^{-4} cm; total contact area 628 cm^2)
Nominal Feed concentration (dry) : 5000 ppm SO_2, 12% CO_2, 1.8% O_2, bal. N_2.
Temperature: 24°C

Module #	Feed Flow rate cc/min	Vacuum inch Hg	SO_2 flux cc/(sec)(cm^2)	percent SO_2 removed from feed
E	46.3	27.9	4.80×10^{-6}	77.4
	77.5	26.7	7.91×10^{-6}	74.3
	146.6	26.7	10.22×10^{-6}	51.1
	204.8	27.1	13.24×10^{-6}	47.3
E & F	46.3	27.6	2.91×10^{-6}	93.3
	77.5	26.6	4.45×10^{-6}	85.3
	145.6	27.3	6.40×10^{-6}	65.4
	204.8	26.8	8.30×10^{-6}	60.3

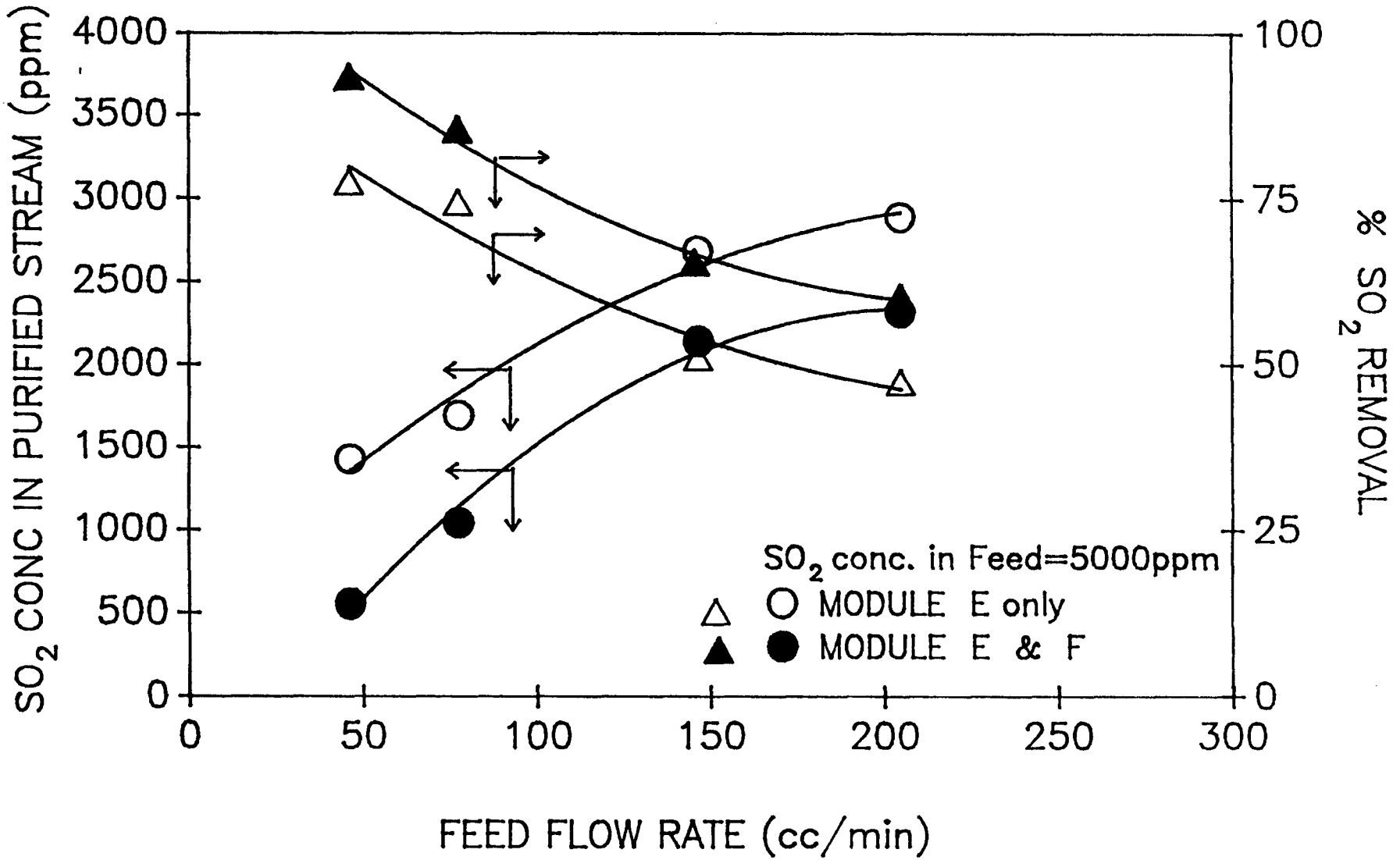

Figure 5.7-2: Performance in Vacuum Mode of Operation: Single Permeator and Two Permeators in Series Configuration.

the driving force in the second permeator is considerably lower). With two permeators, as much as 93% feed SO_2 was removed when 46 sccm feed was introduced through modules E and F. In general, higher fractional removal of SO_2 was achieved with a lower feed flow rate.

Finally, we present the experimental data obtained with 1N $NaHSO_3$ solution as a liquid membrane in Table 5.7-9. These experiments were carried out at room temperature in module G having larger diameter hollow fibers (240 micron ID). Excellent fractional removal of SO_2 was obtained in both sweep and vacuum modes. These particular experiments with 1N $NaHSO_3$ solution were stopped when steady state was achieved. Therefore, we do not know the effect of prolonged exposure of SO_2 on the CLM, if any, under such conditions.

Gas flow pressure drop

Flow pressure drop calculations were made for different fiber sizes and for various gas flow rates using Hagen-Poiseuille equation. The calculations are shown in Table 5.7-10. The pressure drop is considerably lower for larger diameter hollow fibers. We had also observed a major reduction in gas stream pressure drop when module G with larger diameter hollow fibers (240 micron ID) was utilized for experiments. The pressure drop can be lowered even further if hollow fibers of 400 micron ID are used since pressure drop is inversely proportional to the fourth power of the fiber inside diameter. This will allow the use of much higher flow rate of gases in the permeator.

Numerical simulation results

Table 5.7-9 : Separation of SO_2 with 1N $NaHSO_3$ Solution as a Liquid Membrane

Liquid membrane : 1N $NaHSO_3$ in water
Module : G (no of fibers in each side: 120; length 63.5 cm; fiber od: 290×10^{-4} cm; total contact area 694 cm^2)
Nominal Feed concentration (dry) : 6764 ppm SO_2, 13.2% CO_2, 1.8% O_2, bal N_2
Temperature: 24^oC

Mode (Run time in days)	Flow rate Feed/Sweep (cc/min)	Vacuum (in Hg)	SO_2 flux ($cc/s.cm^2$)	$K_{expt} \times 10^5$ ($cm^3/s.cm^2.cmHg$)	percent SO_2 removed from feed
Sweep (2)	41.5/78.3	-	6.61×10^{-6}	5.71	98.0
Vacuum (2)	41.5/ -	27.8	5.60×10^{-6}	-	83.1

Table 5.7-10 : Typical Gas Pressure Drop Calculations

Basis: Hagen-Poiseuille equation; N_2 flow through module

Viscosity : 1.75×10^{-4} poise; Number of fibers in the module = 300

Flow Rate cc/min	Pressure Drop Per Foot Length of Module					
	Fiber ID = 100 µM		Fiber ID = 240 µM		Fiber ID = 400 µM	
	psi	ft. water	psi	ft. water	psi	ft. water
20	0.35	0.81	0.01	0.02	0.0014	0.003
50	0.87	2.01	0.03	0.07	0.0034	0.008
100	1.75	4.05	0.05	0.12	0.0068	0.016
200	3.50	8.09	0.11	0.25	0.0137	0.032

Based on the mathematical model presented in section 4.3, a computer program was developed to predict the multicomponent gas mixture separation behavior in a hollow-fiber-contained liquid membrane permeator. The model is based on solution-diffusion mechanism and valid for gas/liquid systems in which the permeability coefficients of gases do not change with the applied pressure. Strictly, the model is not valid for SO_2 due to facilitation and chemical reaction. However, for water membrane, we can try to predict the behavior considering an effective permeability for SO_2.

The experimental separation data and numerical simulation results are compared in Table 5.7-11. The data were obtained with permeator C for SO_2-CO_2-N_2-O_2 mixture separation through water CLM with a pure helium sweep stream. The effective SO_2 permeability was assumed to be 15×10^{-6} scc.cm/ s.cm^2.cm Hg (Table 5.3-1). We have shown the SO_2 composition in the sweep outlet stream and CO_2 composition in the feed outlet stream (no SO_2 was found at the feed outlet) in Table 5.7-11. The model predicts the results quite well. Note that, the gas permeabilities of other gas species were obtained by multiplying the diffusivity and solubility values. Further, there are no gas phase boundary layers in this analysis suggesting that the lumped analysis in section 5.7 is inappropriate.

5.8 NO separation in HFCLM permeators

Earlier in section 5.4 we have discussed the problems associated with NO oxidation in presence of oxygen. They are probably more important for CLM runs, which involve longer gas lines and larger system volumes. Minimization of the residence time should be one of the goals in designing an apparatus. An

Table 5.7-11 : Comparison of Experimental Separation Data with Numerical Simulation Results

Permeator : C
Membrane : Water
Membrane Thickness : 0.0258 cm
Feed : 5000 ppm SO_2 ,12% CO_2 , 1.8% O_2, balance: N_2
Sweep : Pure Helium

Flow Rate Feed/Sweep cc/min	SO2 Composition in Sweep outlet stream (ppm)		CO2 composition in Feed outlet stream (%)	
	Data	Simulation	Data	Simulation
73.7/143.9	2423	2500	2.76	4.13
73.7/45.1	6167	6738	5.39	5.90
43.8/45.1	4848	4636	3.64	3.54

Basis: SO_2 Permeability : 1.5×10^{-5} scc.cm/s.cm^2.cm Hg
CO_2 Permeability : 2.1×10^{-7} scc.cm/s.cm^2.cm Hg
N_2 Permeability : 5.57×10^{-9} scc.cm/s.cm^2.cm Hg
O_2 Permeability : 9.01×10^{-9} scc.cm/s.cm^2.cm Hg
He Permeability : 9.74×10^{-9} scc.cm/s.cm^2.cm Hg

additional complication is the possibility of oxidation of NO in the liquid water phase (inside the humidifier) by the dissolved oxygen, the mechanism of which is not well known. Because of all these uncertainties, a number of runs were carried out in duplicate, with and without oxygen. For CLM runs involving NO, the true NO-concentration entering the permeator module was found out by an independent experiment, where the gas stream coming out of the humidifier was passed directly through the membrane dryer (bypassing the CLM module), and the NO concentration measured by the the MSA analyzer.

Some preliminary nitric oxide separation data using CLM modules, as well as some experimental mass transfer coefficient data are shown in Table 5.8-1. One very important point to note is the drastic drop in NO concentration from the dry feed gas mixture to the gas stream actually entering the permeator module. The recoveries in Runs #5-7 are quite encouraging, showing that a very substantial amount of NO can be removed from the feed using Fe^{2+}EDTA. Runs #5-7 were actually continuation of the same run, with only a short pause in between Run #5 and #6 in order to start the oxygen flow in the feed. The total run time was about ten days, which shows excellent performance stability of these CLM modules. It is important to note, however, that these are preliminary results, and all the runs were carried out in sweep mode only.

The detailed studies of nitric oxide separation by HFCLM were carried out in module C with Fe^{2+}EDTA solution as a liquid membrane. The experimental results are presented in Table 5.8-2. Different batches of liquid membrane were used. Generally, freshly prepared liquid membranes almost always showed better performance. It is believed that in presence of oxygen, the membrane liquid probably degraded slowly with time. The results are presented in Table

Table 5.8-1 : Preliminary Nitric Oxide Separation Results Using CLM

Run #	Module	Membrane Liquid	Oxygen in Feed	Feed Inlet Concentration	NO Recovery From Feed	K_{expt}* for NO
1	A	Water	yes	190 ppm NO 8.8%CO_2, 1.65% O_2 bal N_2	4%	6.82×10^{-7}
2	A	Fe^{2+}EDTA (0.01M)	yes	246 ppm NO 8.8% CO_2, 1.65% O_2 bal N_2	6%	7.09×10^{-7}
3	D**	0.01M Fe^{2+}EDTA 0.25N Na_2SO_3	no	448 ppm NO 11.0% CO_2, bal N_2	33%	2.13×10^{-7}
4	D	-Do-	no	454 ppm NO 9.1% CO_2, bal N_2	23%	3.11×10^{-7}
5	C	Fe^{2+}EDTA (0.01M)	no	458 ppm NO 10.8% CO_2, bal N_2	81%	2.62×10^{-6}
6	C	-Do-	yes	235 ppm NO 8.4% CO_2, 1.87% O_2 bal N_2	84%	4.67×10^{-6}
7***	C	-Do-	yes	- Do -	84%	4.53×10^{-6}

* unit $(cm^3)/(sec)(cm^2)(cm\ Hg)$.

** This module has not been used previously, and is not well characterized, but the dimensions are same as that of module C.

*** Runs 6 and 7 are for different sweep flow rates.

Table 5.8-2 : Separation of Nitric Oxide in HFCLM Permeator

Liquid membrane : 0.01M Fe^{2+}EDTA in water
Module : C (length 157.5 cm, total contact area 2227 cm^2)
Nominal Feed concentration (dry) : 450 ppm NO, 8% CO_2, 2% O_2, balance N_2
Temperature: 24°C

Membrane liquid batch	Mode (Run time in days)	Flow rate Feed/Sweep cc/min	Vacuum inch Hg	NO flux **	K_{expt} ***	percent NO removed from feed
#1[1]	Sweep (6)	22.4/199.7	--	2.39×10^{-8}	1.31×10^{-6}	52.3%
#1	Vac(2)* (2)	13.4/-	27.7	7.02×10^{-9}	-	31.8%
#1	Vac(2) (2)	14.3/-	25.3	4.28×10^{-9}	-	18.2%
#2[1]	Vac(1)* (4)	25.0/-	25.8	2.75×10^{-8}	-	32.7%
#3[2]	Vac(1) (3)	14.0/-	25.4	2.85×10^{-8}	-	62.2%
#3	Vac(2) (1)	14.3/-	25.0	2.54×10^{-8}	-	54.2%
#3	Sweep (4)	26.4/193.5	--	6.76×10^{-8}	3.39×10^{-6}	75.7%

* Vac(2) means vacuum pulled from both sides of module, whereas Vac(1) means vacuum is pulled from one side while the other side is plugged, with a net countercurrent flow.
** unit $cm^3/(sec)(cm^2)$
*** unit $(cm^3)/(sec)(cm^2)(cm\ Hg)$
[1] used from a previous batch.
[2] freshly prepared.

5.8-2 in the same order that the experiments were carried out. The flux of NO and the percentage of NO removed from the feed gas are also reported in the same table. A removal rate as high as 75% was obtained in the sweep mode of operation.

For vacuum runs, the experimental mass transfer coefficients, K_{expt}, can not be calculated directly, since the permeate composition at the closed end of the permeator is unknown, and hence the partial pressure driving force of permeant across the liquid membrane can not be calculated. As the table shows, the nitric oxide removal from feed was quite good, although as the age of liquid membrane increased, the separation performance fell steadily.

More experiments were carried out for separation of nitric oxide with a 0.01 M Fe^{2+}EDTA solution as a liquid membrane under vacuum mode of operation. All the possible variations of the vacuum mode (e.g., cocurrent, countercurrent and cocurrent-countercurrent) have been covered in this study. Also, we repeated a sweep run in order to check the reproducibility. The results are reported in Table 5.8-3 in the same sequence as they were carried out.

In general the nitric oxide removal rate was quite good. However, the first set of data under vacuum mode with countercurrent flow show that the separation performance decreased steadily with time. The flux of NO was reduced to about 50% of the original value as the experimental run was continued for over 4 days. We have seen earlier that such a deterioration occurs with the age of the liquid membrane solution. Note further that the liquid membrane solution was always exposed to the feed gas mixture containing 2% oxygen. This suggests that membrane regeneration efforts by creeping

Table 5.8-3 : Separation of Nitric Oxide in HFCLM Permeator

Liquid membrane : 0.01M Fe^{2+}EDTA in water
Module : C (length 157.5 cm, total contact area 2227 cm^2)
Nominal Feed concentration (dry) : 450 ppm NO, 8% CO_2, 2% O_2, balance N_2
Temperature: 24°C

Mode (Run time in days)	Flow Mode	Flow rate Feed/Sweep cc/min	Vacuum inch Hg	NO flux cc/(s.cm^2)	percent NO removed from feed
Vacuum (4)	Counter-current	16.6/-	25.8	3.03×10^{-8}	71.8[1]
				2.34×10^{-8}	59.4[2]
				1.62×10^{-8}	47.4[3]
				1.43×10^{-8}	44.3[4]
Vacuum (2)	Counter-current	16.6/-	26.2	3.08×10^{-8}	71.7[5]
Vacuum (3)	Cocurrent	17.1/-	27.4	1.47×10^{-8}	42.6
Vacuum (2)	Cocurrent-Countercurrent	16.6/-	27.8	1.37×10^{-8}	43.3
Sweep (5)	Counter-current	27.4/191.1	-	7.22×10^{-8}	78.8
Sweep (4)	Counter-current	26.4/193.5	-	6.76×10^{-8}	75.7[6]

[1] after 30 hrs. of operation
[2] after 58 hrs. of operation
[3] after 70 hrs. of operation
[4] after 105 hrs. of operation
[5] fresh membrane solution
[6] data from Table 5.8-2

recirculation outside the permeator would be needed to ensure a stable high flux with Fe^{2+}EDTA as a carrier.

In the next experiment freshly prepared solution was introduced in the permeator as liquid membrane. An increase in the flux of NO was readily observed. After evaluating all data collected in the vacuum mode, one can conclude that the flow pattern has little or no effect on the separation of nitric oxide under the conditions used in this study. The experimental data obtained under sweep mode show that the permeator behavior is highly reproducible. For comparison we have also included the previous data obtained under similar conditions (from Table 5.8-2).

Finally, the data for separation of NO with a Fe^{3+}EDTA solution as liquid membrane are presented in Table 5.8-4. The experiments were carried out in a short module under both vaccum and sweep modes of operation. However, the feed gas mixture did not contain any oxygen. High NO fluxes and NO removal rates were observed in both cases. The flux of NO obtained with module F is about one order of magnitude higher than that obtained with module C (Table 5.8-3). This shows that a large section of the module C was being underutilized. The composition of NO in the feed gas is low to start with and most of the NO probably permeated at the entry region of the module C. This resulted in a very low driving force and the amount of NO transfer in the rest of the permeator length was negligible. The results reported in Table 5.8-3 are highly encouraging because it is anticipated that the problem of flux deterioration (as observed with Fe^{2+}EDTA liquid membrane) would not be present when Fe^{3+}EDTA solution is the liquid membrane. The prime cause of flux reduction with Fe^{2+}EDTA in presence of O_2 is oxidation of Fe^{2+}EDTA. If the

Table 5.8-4 : Separation of NO in HFCLM Permeator with Fe^{3+}EDTA Membrane

Liquid membrane : 0.01M Fe^{3+}EDTA in water
Module : F (length 44.5 cm, total contact area 628 cm^2)
Nominal Feed concentration (dry) : 490 ppm NO, balance N_2
Temperature: 24^oC

Mode (Run time in days	Flow Mode	Flow rate Feed/Sweep (cc/min)	Vacuum (in Hg)	NO flux ($cc/s.cm^2$)	$K_{expt} x10^5$ ($cc/s.cm^2$. cmHg)	percent NO removed from feed
Sweep (2)	Counter-current	39.6/78.3	-	$3.74x10^{-7}$	2.36	72.7
Vacuum (2)	Cocurrent-counter current	39.6/ -	27.5	$3.63x10^{-7}$	-	70.5

carrier to start with is $Fe^{3+}EDTA$, no such flux reduction is expected. Further, at 25°C, more concentrated $Fe^{3+}EDTA$ solution can be used leading to high facilitation. More experiments are, therefore, necessary.

5.9 Combined SO_2 - NO separation by HFCLM permeator

The separation results for simultaneous separation of SO_2 and NO from a feed mixture of SO_2-NO-CO_2-O_2-N_2 at 24°C are presented in Table 5.9-1. As the table indicates, the separations were very respectable. For SO_2, the feed outlet SO_2 concentration was below the detection limit of the GC used (Varian 3700), which was about 200 ppm. The fact that a HFCLM permeator module can effect 90+% removal of SO_2 and typically 60-70% removal of nitric oxide simultaneously is highly encouraging. These data were obtained with permeator C.

We should mention that the sweep mode runs in this table showed some material balance problems. The SO_2 flux calculated based on sweep outlet concentrations (which is how the fluxes were calculated in Table 5.9-1 for sweep runs) was found to be less than that calculated based on the difference between feed inlet and outlet. It is possible that some SO_2 reacted irreversibly in presence of NO and $Fe^{2+}EDTA$ to form various side products.

Next the combined SO_2 - NO separation runs were carried out in short permeators (module E and module G, respectively) both in sweep and vacuum modes with 0.01M $Fe^{2+}EDTA$ solution as a liquid membrane. The steady state separation results are reported in Tables 5.9-2 and 5.9-3 for modules E and G, respectively. Excellent separation results were achieved in both modes. With a high sweep flow rate (three times that of feed gas flow rate), greater than

Table 5.9-1 : Simultaneous Separation of SO_2 and NO in HFCLM Permeator

Liquid membrane : 0.01M Fe^{2+}EDTA in water (only one batch used)
Module : C (no of fibers in each side: 300; length: 157.5 cm;
fiber od: 150×10^{-4} cm; total contact area: 2227 cm^2)
Nominal Feed concentration (dry) : 2750 ppm SO_2, 450 ppm NO, 6.6% CO_2, 1.1% O_2, balance N_2.
Temperature: 24°C

Mode (Run time in days)	Flow rate Feed/Sweep cc/min	Vacuum inch of Hg	Permeant flux (**) SO_2	Permeant flux (**) NO	K_{expt} (***) SO_2	K_{expt} (***) NO	percent removed from feed SO_2	percent removed from feed NO
Sweep (6)	24.2/54.5	-	3.94×10^{-7}	6.85×10^{-8}	5.76×10^{-6}	4.91×10^{-6}	>93%	73.2%
Sweep (1)	26.4/194.2	-	2.91×10^{-7}	6.10×10^{-8}	3.40×10^{-6}	3.54×10^{-6}	>93%	75.3%
Sweep (3)	24.0/42.0	-	3.37×10^{-7}	5.94×10^{-8}	4.98×10^{-6}	3.66×10^{-6}	>93%	59.7%
Vac(2) (1)	17.5/-	25.7	1.64×10^{-8}	3.44×10^{-7}	-	-	>93%	32.5%
Vac(2) (1)	72.3/-	25.4	1.03×10^{-6}	?	-	-	68.6%	?
Vac(2) (1)	75.9/-	25.3	9.64×10^{-7}	3.52×10^{-8}	-	-	61.2%	13.2%

Note : Vac(2) means vacuum pulled from both sides of module, whereas Vac(1) means vacuum is pulled from one side while the other side is plugged, with a net countercurrent flow.
** unit $cm^3/(sec)(cm^2)$
*** unit $(cm^3)/(sec)(cm^2)(cm\ Hg)$

Table 5.9-2 : Simultaneous Separation of SO_2 and NO in a Short HFCLM Permeator

Liquid membrane : 0.01M Fe^{2+}EDTA in water

Module : E (no of fibers in each side: 300; length: 43.2 cm; fiber od: 150×10^{-4} cm; total contact area: 610 cm^2)

Nominal Feed concentration (dry) : 6764 ppm SO_2, 490 ppm NO, 13.2% CO_2, 1.8% O_2, balance N_2.

Temperature: 24°C

Mode (Run time in days)	Flow rate Feed/Sweep (cc/min.)	Vacuum (in Hg)	Permeant flux ($cc/s.cm^2$) SO_2 ($\times 10^{-6}$)	Permeant flux ($cc/s.cm^2$) NO ($\times 10^{-7}$)	$K_{expt} \times 10^5$ ($cc/s.cm^2.cmHg$) SO_2	$K_{expt} \times 10^5$ ($cc/s.cm^2.cmHg$) NO	percent removal SO_2	percent removal NO
Sweep (3)	41.5/78.3	-	6.48	2.84	3.86	1.51	84.6	51.1
Sweep (2)	41.5/118.2	-	7.18	3.50	5.10	2.16	99.4	63.1
Vacuum (1)	41.4/ -	27.5	4.89	3.06	-	-	70.0	73.3*
Vacuum (1)	60.1/ -	27.5	10.66	5.59	-	-	98.6	75.7+

* nominal feed concentration: 6188 ppm SO_2, 370 ppm NO, 1.8% O_2, bal N_2

+ nominal feed concentration: 6588 ppm SO_2, 450 ppm NO, 1.8% O_2, bal N_2

Table 5.9-3 : Simultaneous Separation of SO_2 and NO in HFCLM permeator

Liquid membrane : 0.01M Fe^{2+} EDTA in water
Module : G (no of fibers in each side: 120; length: 63.5 cm;
fiber od: 290×10^{-4} cm; total contact area: 694 cm^2)
Nominal Feed concentration (dry) : 6764 ppm SO_2, 490 ppm NO, 13.2% CO_2, 1.8% O_2, balance N_2
Temperature: 24°C

Mode (Run time in days)	Flow rates Feed/Sweep (cc/min)	Vacuum (in Hg)	Flux ($cc/s.cm^2$) SO_2 ($\times 10^{-6}$)	Flux ($cc/s.cm^2$) NO ($\times 10^{-7}$)	$K_{expt} \times 10^5$ ($cc/s.cm^2.cmHg$) SO_2	$K_{expt} \times 10^5$ ($cc/s.cm^2.cmHg$) NO	percent removal SO_2	percent removal NO
Sweep (3)	41.5/78.3	-	5.89	2.09	2.71	0.73	87.4	42.8
Vacuum (2)	41.5/ -	27.5	5.87	3.13	-	-	87.2	64.1

95% of the feed SO_2 was removed (Table 5.9-2). Note that, the permeator E is only 43 cm long. Comparing the results of both modes, it seems that vacuum mode is more effective in removing NO. Due to evaporation of water at a high rate, the permeate side partial pressure of NO is probably reduced more in the vacuum mode than in the sweep mode. This will lead to better facilitation and higher flux. The permeant fluxes obtained in these two permeators are about one order of magnitude higher than those of permeator C. As expected, the pressure drop in module G was much lower than that of module E.

Finally, we carried out combined SO_2 - NO separation runs in module F at a higher temperature of 70^oC. A solution of 0.01M Fe^{2+}EDTA chelate was utilized at first as a liquid membrane. Experiments were carried out in both sweep and vacuum modes. Compared to high temperature ILM experiments, these experiments with HFCLM permeator are orders of magnitude simpler. The steady state performances are shown in Table 5.9-4. Although these preliminary findings show a small decrease in performance at the high temperature compared to those in Table 5.9-3, the results are very encouraging. Note that only a 0.01M Fe^{2+}EDTA solution was used. At this temperature of 70^oC, higher chelate concentration can be used; that would increase NO removal without affecting SO_2 removal (due to salting out). Further, since we have observed excellent and almost equivalent performances with Fe^{3+}EDTA membrane (Table 5.8-4), we can reasonably expect a stable liquid membrane for combined SO_2/NO separation at 70^oC in the presence of O_2.

With that idea in mind, we carried out another experiment with a solution of 0.04M Fe^{3+}EDTA chelate solution at 70^oC. The performances are shown in Table 5.9-5. A continuous run was made for 6 days with a feed gas

Table 5.9-4 : Simultaneous Separation of SO_2 and NO at High Temperature

Liquid membrane : 0.01M Fe^{2+}EDTA in water
Module : F (no of fibers in each side: 300; length: 44.5 cm;
fiber od: 150×10^{-4} cm; total contact area: 628 cm^2)
Nominal Feed concentration (dry) : 6764 ppm SO_2, 490 ppm NO, 13.2% CO_2,
1.8% O_2, balance N_2
Temperature: 70°C

Mode (Run time in days)	Flowrates Feed/Sweep (cc/min)	Vacuum (in Hg)	Flux (cc/s.min.) SO_2 $(\times 10^{-6})$	Flux (cc/s.min.) NO $(\times 10^{-7})$	$K_{expt} \times 10^5$ (cc/s.cm^2.cmHg) SO_2	$K_{expt} \times 10^5$ (cc/s.cm^2.cmHg) NO	percent removal SO_2	percent removal NO
Sweep (2)	41.5/78.3	-	5.18	2.53	1.68	0.92	70.0	46.9
Vacuum (4)	41.5/ -	27.8	6.62	3.20	-	-	89.0	59.4

Table 5.9-5 : Simultaneous Separation of SO_2 and NO in HFCLM Permeator at High Temperature

Liquid membrane : 0.04M Fe^{3+}EDTA in water
Module : F (no of fibers in each side: 300; length: 44.5 cm; fiber od: 150×10^{-4} cm; total contact area: 628 cm^2)
Nominal Feed concentration (dry) : 5000 ppm SO_2, 500 ppm NO, 12.0% CO_2, 1.8% O_2, balance N_2
Temperature: 70°C

Mode (Run time in days)	Elapsed time (hr)	Flow rate (cc/min) F/I	F/O	Vacuum (inHg)	Flux x 10^6 (cc/s.cm^2) SO_2	NO	% removed from feed SO_2	NO
Vacuum (6)	24	40.3	27.6	27.3	5.32	0.24	92.2	58.7
	48		27.4	27.5	4.55	0.24	79.0	60.0
	72		26.8	27.3	4.20	0.24	72.9	59.4
	96		26.1	27.8	3.73	0.24	64.7	59.1
	120		26.8	28.0	3.46	0.24	60.1	58.0
	144		25.5	27.8	3.13	0.25	54.3	59.7

F/I : Feed In; F/O : Feed Out

mixture containing SO_2, NO, CO_2, N_2 and O_2 under vacuum mode of operation. The results demonstrate the absence of liquid membrane degradation in the presence of O_2 when Fe^{3+}EDTA solution instead of Fe^{2+}EDTA solution is used instead of Fe^{2+}EDTA solution is used as a membrane.

Note that, the flux of SO_2 dropped quite a bit from its initial value but that of NO remained constant for the entire period. The reasons are following. During the experiment, the feed gas mixture was humidified at the room temperature before it was introduced into the module kept in another bath at $70^{o}C$. The gas mixture inside the module, not being saturated, naturally picked up moisture from the membrane liquid solution and thereby increased the solution concentration. This should decrease the removal rate of both SO_2 and NO due to any salting out effect. However, we do not see any substantial change in NO removal rate as the reaction rate of NO and the chelate increases at higher chelate concentration produced by evaporation. In actual practice, this increasing chelate concentration can be easily avoided by very slow recirculation of membrane liquid outside and addition of moisture.

Section 6

Conclusions

Excellent SO_2 permeabilities and extremely high selectivities for SO_2/CO_2 (~ 70-200) and SO_2/N_2 (~ 1500 - 3000) were obtained from simulated flue gases with aqueous immobilized liquid membranes such as water and solutions of $NaHSO_3$ or Na_2SO_3 at 25°C. For aqueous liquid membranes of 0.02M Fe^{2+}EDTA or 0.02M Fe^{3+}EDTA, the SO_2 permeabilities at 25°C are marginally lower and the SO_2/CO_2 selectivities are somewhat smaller (~ 50 - 200). A 0.01M aqueous solution of Fe^{2+}EDTA had a high selectivity for NO/N_2 (~ 40 - 50). Equilibrium approximation and NEBLA strategy describe SO_2 facilitation through the pure water membranes adequately. Similar theories for NO facilitated transport through chelate solutions have poorer predictive capabilities. At a high temperature of 75°C, the SO_2 permeabilities appear to be significantly lower.

The excellent aqueous liquid membranes selected via ILM studies were found to perform efficiently when used as liquid membranes in the novel hollow-fiber-contained liquid membrane (HFCLM) permeators of small dimensions. Depending on the permeator length which varied between 17 to 62 inches and the gas flow rates, 60 to 95%+ of SO_2 were easily removed from a 5000 ppm SO_2 containing feed flue gas by an aqueous membrane into the permeate which either had a sweep gas or was subjected to vacuum. The SO_2 flux level at 25°C in a small permeator was found to be around 1.1×10^{-4} $cm^3/sec\text{-}cm^2\text{-}cm$ Hg. Aqueous membranes of Fe^{2+}EDTA or Fe^{3+}EDTA removed 50 - 85% of NO from 250-500 ppm NO containing feed gas.

Using an aqueous solution of 0.01M Fe^{2+}EDTA and a feed flue gas containing both SO_2 and NO, 70 - 90%+ of feed SO_2 and 50 - 75% of feed NO were simultaneously removed at 25°C in a small HFCLM permeator. In flue gases containing O_2 and no SO_2, the Fe^{2+}EDTA membrane showed a significant decrease in NO recovery with time. However, Fe^{3+}EDTA membranes, which are not affected by O_2, showed a performance in HFCLM permeator almost equivalent to that of fresh Fe^{2+}EDTA solution in removing NO suggesting resolution of the problem.

The HFCLM purification run at 70°C with a feed containing SO_2 and NO showed a performance only slightly inferior to the 25°C run. Much more experimentation at 70°C is desirable to draw firmer conclusions. These 70°C runs used only 0.01M chelate solutions. Much higher solubilities of chelates at this temperature suggest possibilities for even better NO separation. By using a permeator built of 240 micron ID hollow fibers, the pressure drop in feed flue gas was drastically reduced from those built with 100 micron ID fibers. A permeator with 400 micron ID hollow fibers is expected to provide even lower pressure drops at higher gas flow rates.

Section 7

Recommendations

The following recommendations are being made for future work in flue gas cleanup by hollow-fiber-contained liquid membrane technique.

1. More experiments are desirable with iron-EDTA salts, especially with Fe^{3+}EDTA salt solution. Testing of other new chemicals such as EDTA salt of zinc etc. as membranes should also be considered.
2. Experiments should be carried out with two permeators in series with the first permeator containing a membrane selective only to SO_2 while the second one containing another liquid membrane selective only to NO. This will lead to better separation chemistry and easier recovery of gaseous byproducts.
3. It is expected that very slow membrane regeneration or circulation would produce much better results in terms of stability.
4. Dimethylaniline (DMA) or oligomers of DMA have very high solubility for SO_2 gas. They should be used as a sweep liquid for SO_2 separation in a HFCLM permeator under sweep organic liquid mode. Such a sweep liquid may be regenerated easily in a separate vessel by stripping.
5. The ILM permeability apparatus used in the current study was not very effective for high temperature SO_2 or NO_x permeability measurements. A better design or an entirely new arrangement should be considered.
6. Further work is necessary in the model development for facilitated transport of SO_2 in a HFCLM permeator. A better model is also desirable for NO facilitation through immobilized liquid membrane containing Fe^{2+}EDTA.

7. Study HFCLM permeator operation with 400 μm ID hollow fibers for feed gas to reduce the flue gas pressure drop drastically and increase volumetric throughput. To reduce liquid membrane thickness, use smaller fiber diameter in the permeate side in mixed fiber permeators.

8. The current project was undertaken to study the feasibility of SO_2 and NO separation from a flue gas mixture by the new hollow-fiber-contained liquid membrane technique. No attempt was made to evaluate the process from an economic point of view. A separate study should be made in that direction. Economic comparison of various modes of operation should also be considered in that study to identify the optimum mode of operation.

Section 8

Notation

The general units are given below. Frequently more common units are used for clarity. The actual units used at any place are clearly stated in the text.

$\bar{a}_i$	activity of species i in liquid membrane
a_i, b_i	parameters, eqn. (4.2-11)
A,B	constants, eqn. (4.2-11)
A_M	total membrane permeation area in the test cell, m^2
A_T	total membrane permeation area in lumped CLM analysis, m^2
C_i	concentration of species i in the liquid membrane, $mole/m^3$
$C_{T,Na}$	total sodium concentration in the liquid membrane, $mole/m^3$
d	liquid membrane thickness in HFCLM, m
Da	Damkohler number
D_i	diffusivity of species i, m^2/sec
$D_{eff,i}$	effective diffusivity of i, m^2/sec
D_{FI}, D_{FO}	inside and outside diameters of feed fibers, m
D_{SI}, D_{SO}	inside and outside diameters of sweep fibers, m
f	variable, eqn. (4.2-15)
F	facilitation factor, eqn. (4.2-7)
G_1	parameter defined in eqn. (4.3-9a)
G_2	quantity defined by eqn. (4.3-9b)
H_i	Henry's constant for species i, $mole/m^3$-Pa
H_p	height of flow channel in the flat test cell, m
I	ionic strength of liquid membrane, g ion/m^3
k_1, k_{-1}	forward and reverse reaction rate constants for SO_2 ionization
k_{1N}, k_{-1N}	forward and reverse reaction rate constants for NO complexation

k_g	gas phase film transfer coefficient, m/sec
k_M	liquid membrane mass transfer coefficient, m/sec
K_0	Overall mass transfer coefficient, m/sec
K_{eq}	equilibrium constant of a chemical reaction
K_j	equilibrium constant for reaction j
l	distance of any permeator location, starting from sweep inlet end, m
l_t	total length of permeation in a permeator, m
L, L_f, L_w	feed side gas flow rate per fiber at any location, at the feed inlet end and outlet end of the permeator, respectively, mole/sec
L_{ref}	reference flow rate per fiber, mole/sec
L^*, L_f^*, L_w^*	dimensionless feed side gas flow rate per fiber at any location, at the feed inlet end and outlet end of the permeator, respectively
M_{wi}	molecular weight of gas species i, g/mole
n_j	number of sulfur atoms in j-th species
n'_j	number of sodium atoms in j-th species
N_i	flux of species i across the liquid membrane, mole/m^2-sec
N_F, N_S	total number of feed and sweep fibers, respectively
N_T	total number of hollow fibers, used in lumped CLM analysis
p_i	partial pressure of species i in gas phase, Pa
Δp_i	partial pressure difference across membrane for species i, Pa
p, p_f, p_w	sweep side pressure at any location, at the sweep outlet end and inlet end of the permeator, respectively, Pa
P, P_f, P_w	feed side pressure at any location, at the feed inlet end and outlet end of the permeator, respectively, Pa
P_{ref}	reference pressure, Pa
p^*, P^*	dimensionless sweep and feed pressure, respectively, defined by eqn. (4.6-8a)
p_f^*, p_w^*	dimensionless pressures at sweep outlet and inlet, respectively
P_f^*, P_w^*	dimensionless pressures at feed inlet and outlet, respectively

P_F, P_S	pressures on the feed and the sweep side of the liquid membrane, Pa
Q_i	permeability of species i, mole-m/m^2-sec-Pa
Q_{ref}	reference permeability, mole-m/m^2-sec-Pa
Q_i^*	dimensionless permeability of species i
r_i	rate of reaction of species i
R	universal gas constant, m^3-Pa/mole-^oK
R_i	rate of mass transfer of species i across the membrane, scc/sec
Re	gas phase Reynolds number ($=2H_p\bar{v}\rho/\mu$)
S	dimensionless area, defined by eqn. (4.6-8)
S_t	total dimensionless area
Sc	gas phase Schmidt number
Sh	gas phase Sherwood number
t_M	microporous support membrane thickness in ILM, m
T	absolute temperature, ^oK
$\bar{v}$	average gas velocity in the test cell, m/sec
V_F	total flow rate of feed gas, m^3/sec
V_S	total flow rate of sweep gas, m^3/sec
V, V_f, V_w	sweep side gas flow rate per fiber at any location, at the sweep outlet end and inlet end of the permeator, respectively, mole/sec
V^*, V_f^*, V_w^*	dimensionless sweep side gas flow rate per fiber at any location, at the sweep outlet end and inlet end of the permeator, respectively
w	effective width of flow channel in test cell, m
x	direction of permeation along the liquid membrane thickness
x_i, x_{if}, x_{iw}	mole fraction of species i in the feed side gas mixture at any location, at the feed inlet end and outlet end of the permeator, respectively
y_i -	mole fraction of species i in gas streams in ILM and lumped CLM analysis

y_i, y_{if}, y_{iw} mole fraction of species i in the sweep side gas mixture at any location, at the sweep outlet end and inlet end of the permeator, respectively

z_i local mole fraction of species i in a multicomponent gas mixture, is equal to either x_i or y_i

Z_i number of charge on species i

Greek symbols

$\alpha_{i,j}$ selectivity between gas species i and j

β dimensionless parameter, defined in eqn. (4.6-8e)

γ_i activity coefficient of species i

δ_f, δ_s feed and sweep side boundary layer thickness in NEBLA theory

δ_f^*, δ_s^* dimensionless feed and sweep side boundary layer thickness

ε_M porosity of liquid membrane support in ILM studies

η dimensionless parameter, defined in eqn. (4.6-4)

θ dimensionless parameter, defined in eqn. (4.6-11a)

μ gas viscosity, Pa-sec

μ_i viscosity of gas species i, Pa-sec

μ_F, μ_S viscosity of feed and sweep side gas mixture, respectively, at any location of the permeator, Pa-sec

μ_{ref} reference viscosity, Pa-sec

μ_F^*, μ_S^* dimensionless viscosity of feed and sweep side gas mixture, respectively, at any location of the permeator, defined in eqn. (4.6-8c)

$\bar{\mu}$ viscosity of multicomponent gas mixture, defined by eqn. (4.6-18), Pa-sec

π 3.14159...

ρ gas density, Kg/m^3

τ_M tortuosity factor of the liquid membrane support in ILM studies

ϕ_{ij} constants arising in gas mixture viscosity estimation, defined in eqn. (4.6-19)

Superscripts/Subscripts

expt	experimental value
Feed,Sweep	pertaining to local values on the feed and the sweep side, respectively
LM	logarithmic mean
FI,FO	feed inlet and feed outlet, respectively
SI,SO	sweep inlet and sweep outlet, respectively
*	pertaining to dimensionless quantity

Section 9

References

Abdulsattar, A.H., S. Sridhar and L.A. Bromley, Thermodynamics of the sulfur dioxide - seawater system, AIChE Journal, 23, 62 (1977).

Andrew, S.P.S., and D. Hanson, The dynamics of nitrous gas absorption, Chem Eng. Sci., 14, 105 (1961).

Bhave, R.R., and K.K. Sirkar, Gas permeation and separation by aqueous membranes immobilized across the whole thickness or in a thin section of hydrophobic microporous Celgard films, J. Membrane Sci., 27, 41 (1986).

Chang, S.G., D. Littlejohn and S. Lynn, Effects of metal chelates on wet flue gas scrubbing chemistry, Environ. Sci. Technol., 17, 649 (1983).

Drummond, C.J., and D.F. Gyorke, Research strategy for the development of flue gas treatment technology, ACS Symposium Series No. 319, 146 (1986).

England, C., and W.H. Corcoran, The rate and mechanism of the air oxidation of parts-per-million concentrations of nitric oxide in the presence of water vapor, Ind. Eng. Chem. Fund., 14, 55 (1975).

Guha, A.K., Studies on different gas separation modes with hollow fiber contained liquid membrane, Ph.D. Dissertation, Stevens Inst. of Technol. (1989).

Hikita, H., S. Asai and T. Tsiji, Absorption of sulfur dioxide into aqueous sodium hydroxide and sodium sulfite solutions, AIChE Journal, 23, 538 (1977).

Hikita, H., S. Asai, A. Yano and H. Nose, Kinetics of absorption of carbon dioxide into aqueous sodium sulfite solutions, AIChE Journal, 28, 1009 (1982).

Majumdar, S., A new liquid membrane technique for gas separation, Ph.D. Dissertation, Stevens Inst. of Technol. (1986).

Majumdar, S., A.K. Guha and K.K. Sirkar, A new liquid membrane technique for gas separation, AIChE Journal, 34, 1135 (1988).

Majumdar, S., A. K. Guha, Y. T. Lee and K. K. Sirkar, A two-dimensional analysis of membrane thickness in a hollow fiber contained liquid membrane permeator, J. Membrane Sci., 43, 259 (1989).

New York State Energy Research and Development Authority (NYSERDA) Report No. 87-10 (1987).

Park, J.K., H.N. Chang, J.H. Park and Y.Y. Earmme, Direction-dependent flux anomalies in asymmetric reverse osmosis membranes. A theoretical analysis, Ind. Eng. Chem. Fundam., 25, 189 (1986).

Perry, R.H., and C.H. Chilton (Eds.), Chemical Engineers' Handbook, 5th

Edition, McGraw-Hill (1973).

Rangarajan, R., M.A. Majid, T. Matsuura and S. Sourirajan, Permeation of pure gases under pressure through asymmetric porous membranes. Membrane characterization and prediction of performance, Ind. Eng. Chem. Process Des. Dev., 23, 79 (1984).

Reid, R. C., J. M. Prausnitz and T. K. Sherwood, The Properties of Gases and Liquids, McGraw-Hill, New York, NY, (1977).

Roberts, D.L., Sulfur dioxide transport through aqueous solutions, PhD Dissertation, Calif. Inst. of Technol. (1979).

Roberts, D.L., and S.K. Friedlander, Sulfur dioxide transport across aqueous solutions : part I. theory, AIChE Journal, 26, 593 (1980a).

Roberts, D.L., and S.K. Friedlander, Sulfur dioxide transport across aqueous solutions : part II. experimental results and comparison with theory, AIChE Journal, 26, 602 (1980b).

Sada, E., and H. Kumazawa, Individual and Simultaneous absorption of dilute NO and SO_2 in aqueous slurries of $MgSO_3$ with Fe^{II}-EDTA, Ind. Eng. Chem. Process Des. Develop., 19, 377 (1980).

Sada, E., and H. Kumazawa, Absorption of NO in aqueous solution of Fe^{III}-EDTA chelate and aqueous slurries of $MgSO_3$ with Fe^{III}-EDTA chelate, Ind. Eng. Chem. Process Des. Develop., 20, 46 (1981).

Sieder, E.N. and G.E. Tate, Heat transfer and pressure drop of liquids in tubes, Ind. Eng. Chem., 28, 1429 (1936).

Sengupta, A., and K.K. Sirkar, Membrane gas separation, in Progress in Filtration and Separation, Vol. 4, R.J. Wakeman, Ed., 289 (1986).

Skelland, A.H.P., Diffusional Mass Transfer, John Wiley and Sons, New York (1974).

Takeuchi, H., M. Ando and N. Kizawa, Absorption of nitrogen oxides in aqueous sodium sulfite and bisulfite solution, I&EC Proc. Des. Dev., 16, 303 (1977).

Teramoto, M., M. Nagamochi, S. Hiramine, N. Fujii and H. Teranishi, Simultaneous absorption of SO_2 and CO_2 in aqueous Na_2SO_3 solution, International Chemical Engineering, 18, 250 (1978).

Vinograd, J.R., and J.W. McBain, Diffusion of electrolytes and of the ions in their mixtures, J. Amer. Chem. Soc., 63, 2008 (1941).

Walker, R.J., C.J. Drummond and J.M. Ekmann, Evaluation of advanced separation techniques for applications to flue gas cleanup processes for the simultaneous removal of sulfur dioxide and nitrogen oxides, Report DOE/PETC/TR-85/7, Department of Energy, Pittsburgh (1985).

Ward, W.J., Analytical and experimental studies of facilitated transport, AIChE Journal, 16, 405 (1970).

Ward III, W.J., and W.L. Robb, Carbon dioxide - oxygen separation: facilitated transport of carbon dioxide across a liquid film, Science, 156, 1481 (1967).

Wilke, C. R., A viscosity equation for gas mixtures, J. Chem. Phys., 18, 517 (1950).